Université de Montréal

Contribution à l'étude du mécanisme de
sécrétion d'ATP par des cellules épithéliales pulmonaires
et des fibroblastes soumis à un choc hypotonique

par
Francis Boudreault

Institut de génie biomédical
Faculté de médecine

Thèse présentée à la Faculté des études supérieures
en vue de l'obtention du grade de
Ph.D. en génie biomédical

Octobre, 2004

Université de Montréal

Université de Montréal
Faculté des études supérieures

Cette thèse intitulée:

Contribution à l'étude du mécanisme de
sécrétion d'ATP par des cellules épithéliales pulmonaires
et des fibroblastes soumis à un choc hypotonique

présentée par:

Francis Boudreault

a été évaluée par un jury composé des personnes suivantes:

Yves Berthiaume
président-rapporteur

Ryszard Grygorczyk
directeur de recherche

Jean-Yves Lapointe
codirecteur

Sergei Orlov
membre du jury

John Hanrahan
examinateur externe

Rémy Sauvé
représentant du doyen de la FES

RÉSUMÉ ET MOTS CLÉS

En réponse à un choc hypotonique les cellules sécrétent de l'ATP par un mécanisme encore inconnu. La proposition que ce nucléotide accélère le transport mucociliaire au niveau des bronches et favorise la sécrétion de fluide au sein des alvéoles a déclenché une série d'études à la recherche du passage qu'emprunte l'ATP. Au cours des cinq dernières années, on favorisait un modèle basé sur un canal activé par l'étirement de la membrane plasmique, parce que le gadolinium, l'inhibiteur de choix de cette famille de canaux, abolissait la sécrétion par hypotonicité d'ATP mesurée par la réaction de bioluminescence de la luciférase. Nous avons démontré qu'en fait, aux concentrations nécessaires pour bloquer ces canaux mécanosensibles, cet inhibiteur amplifiait la quantité d'ATP sécrétée par des fibroblastes (NIH/3T3) et une dose bien supérieure était nécessaire pour inhiber complètement la libération d'ATP des fibroblastes et des cellules épitheliales pulmonaires A549 et 16HBE14o⁻. Cette pharmacologie ambiguë et variable d'une cellule à l'autre indiquait un mécanisme de sécrétion par exocytose. Dans le but de vérifier cette hypothèse, nous avons analysé, pour ces mêmes cellules, la cinétique de sécrétion d'ATP conjointement avec la variation de calcium intracellulaire. Les variations de volume de ces cellules adhérentes ont également été analysées à l'aide d'une technique de reconstruction 3D basée sur des vues de profil et de dessous obtenues à l'aide d'une chambre spécialement conçue. Ces expériences ont révélé, que la sécrétion d'ATP par hypotonicité ne corrélait ni avec l'accroissement de volume cellulaire et l'activation attendue des canaux mécanosensibles, et ni avec l'ouverture des canaux activés durant le retour au volume original et inhibés par le NPPB. En revanche, la sécrétion d'ATP était parfaitement synchronisée avec l'augmentation de calcium intracellulaire. De plus, une brusque augmentation de calcium intracellulaire a provoqué la libération d'ATP sans gonflement cellulaire alors que cette libération était fortement atténuée par l'utilisation d'un chelateur de calcium ou en abaissant la température à 10°C. L'ensemble de ces résultats indiquent que la sécrétion d'ATP causée par un choc hypotonique s'effectue par un mécanisme exocytotique qui dépend étroitement du calcium intracellulaire.

Mots-clés: gadolinium, exocytose, volume cellulaire, calcium intracellulaire, NPPB

SUMMARY AND KEYWORDS

Hypotonic shock releases ATP from a variety of cells by a poorly defined mechanism(s). The suggestion that extracellular ATP might be involved in mucociliary clearance and alveoli fluid secretion prompted many studies aimed at discovering the nature of the ATP release pathway in lung and elsewhere. A mechano-sensitive ATP channel has been implicated during the past five years because Gd^{3+}, an inhibitor of stretch-activated channels, suppressed cell swelling-induced ATP efflux monitored by luciferase bioluminescence. We found that concentrations typically used to block mechanosensitive channels, actually stimulated hypotonically-induced ATP release from fibroblasts (NIH/3T3) and inhibition of ATP release required dosages much higher for fibroblasts, lung epithelial A549 and 16HBE14o⁻ cells. Such cell-specific effects of Gd^{3+} were most consistent with its action on membrane lipids and membrane-dependent processes such as exocytosis. To further investigate this preliminary finding, we evaluated for those previous cells, the kinetics of cell swelling-induced ATP secretion and intracellular calcium changes. The concomitant volume changes of substrate-attached cells were also analyzed with a three-dimensional cell shape reconstruction method based on images acquired from 2-perpendicular directions with the use of a custom-designed flow-through chamber. These experiments revealed, that cell swelling-induced ATP release neither correlate with cell volume expansion and the expected activation of stretch-sensitive channels, nor with the activation of volume-sensitive, NPPB-inhibitable anion channels during RVD. By contrast, ATP release was synchronized, in all three cell types, with cytosolic calcium elevations. Furthermore, a calcium ionophore triggered ATP release in the absence of cell swelling, while it was significantly diminished by loading cells with a calcium chelator or by lowering the temperature to 10°C. These results strongly support the involvement of a calcium-dependent exocytosis in cell swelling-induced ATP release.

Keywords: gadolinium, exocytosis, cell volume, intracellular calcium, NPPB

TABLE DES MATIÈRES

LISTE DES SIGLES ET ABRÉVIATIONS

μ	Viscosité absolue
ADP	Adenosine 5'-diphosphate
ARN	Acide ribonucléique
ATP	Adenosine 5'-triphosphate
BAPTA	1,2-bis(2-aminophenoxy)ethane-N,N,N',N'-tetraacetic acid
CFTR	Cystic fibrosis transmembrane regulator
EC_{50}	Concentration de l'agoniste pour stimuler à 50% de l'effet maximal
EDTA	Ethylenediaminetetraacetic acid
EGTA	Ethyleneglycol-bis(2-aminoethyleether)-N,N,N',N'-tetraacetic acid
IC_{50}	Concentration de l'antagoniste pour inhiber 50% de l'effet maximal
MDR	Multidrug-resistance protein
NANC	Non-adrénergique et non-cholinergique
NMDA	N-methyl-D-aspartate
NPPB	5-nitro-2-(3-phenylpropylamino)benzoic acid
Pa	Pascal (N/m^2)
RVD	Retour au volume de départ
SAC	Stretch-activated channel
SH2	Src homology regions 2
UTP	Uridine 5'-triphosphate
VDAC	Voltage dependant anion channel

REMERCIEMENTS

Je tiens à remercier Hélène Chabot, attachée de recherche, pour ses précieux enseignements et conseils sur la méthode en laboratoire. Ainsi que Marie-Claude Tessier et Chantal Massé, également attachées de recherche, qui ont toujours su répondre avec amabilité à mes nombreuses interrogations. Et aussi les chercheurs Yves Berthiaume et André Dagenais ainsi que mon codirecteur de recherche, Jean-Yves Lapointe pour les précieux conseils qu'ils m'ont prodigués. Je ne saurais oublier Ryszard Grygorczyk, un directeur de recherche affable, compétent, toujours disponible et qui s'est avéré être, par dessus tout, un formidable collègue de travail.

Finalement, je désire aussi remercier la Fondation Canadienne de la Fibrose Kystique pour leur support financier durant ce doctorat.

AVANT-PROPOS

Cette thèse de doctorat se situe aux confins de deux champs d'étude: la mécanotransduction et la signalisation extracellulaire. Le premier domaine, en pleine émergence, s'intéresse à la réponse physiologique aux forces mécaniques. Le second, englobe la communication entre cellules qui peut être divisée en trois catégories générales selon l'éloignement qui sépare l'émetteur du récepteur: à grande distance, à proximité et très rapprochée, soit dans ce dernier cas par l'entremise d'une fente synaptique. A chacune de ces catégories est associée un type de messager moléculaire: hormone, cytokine et neurotransmetteur, selon l'ordre précédent.

On savait déjà que l'ATP, substance fondamentale dans le transport d'énergie, pouvait aussi jouer un rôle de neurotransmetteur. Or, de récentes observations suggèrent que son champ d'action ne serait pas seulement limité à l'étroitesse d'une synapse mais s'étendrait à plusieurs cellules; l'ATP agirait ainsi comme une cytokine. Moduler le transport mucociliaire bronchique, contrôler le niveau de liquide de surface tapissant les alvéoles, ajuster le tonus vasculaire, promouvoir la sécrétion de lait, voilà quelques uns des rôles possibles qu'on attribue à la cytokine ATP. La multitude de mécanismes régulés par l'entremise de l'ATP extracellulaire est étonnament diverse. Et, en général, repose sur l'idée qu'un stimulus mécanique, une force ou une pression par exemple, est responsable de la sécrétion d'ATP. Cependant tous ces modèles, qui pourtant s'accordent si bien sur le rôle de la signalisation autocrine/paracrine par ATP, ne parviennent pas à faire consensus sur la manière dont cette ATP est sécrétée par les cellules en réponse à l'effort. Même constat quand on se limite à un effort unique comme un gonflement cellulaire causé par un choc hypotonique. Bien qu'à ce type de stimulus s'ajoute de nombreux effets secondaires engendrés par la dilution du milieu intracellulaire, celui-ci demeure le plus utilisé à ce jour pour simuler une charge mécanique. Et c'est justement la résolution de ce cas particulier du mécanisme de sécrétion d'ATP par hypotonicité qui constitue l'objectif de cette recherche.

Une recherche ardue où il a fallu commencer par tester la validité du modèle dominant basé sur un canal perméable à l'ATP et activé par l'étirement de la membrane plasmique, pour le rejeter du même souffle, en raison du comportement ambiguë et contradictoire de l'unique inhibiteur utilisé pour supporter ce modèle. Ensuite, il a fallu

innover en améliorant d'une part, la résolution de la mesure de sécrétion d'ATP par hypotonicité et en inventant d'autre part, une technique d'évaluation du volume d'une cellule en expansion rapide. Dans les deux cas, des chambres de perfusion furent entièrement conçues et fabriquées par le thésard, qui développa également une technique mathématique de reconstruction 3D basée sur une vue de profil et de plan d'une cellule adhérente. En combinant les résultats obtenus grâce à ces innovations avec ceux provenant de techniques de mesure plus conventionnelles comme l'électrophysiologie (patch-clamp) et la microscopie épifluorescente; il fut possible pour la première fois de déterminer que la sécrétion d'ATP par hypotonicité est: transitoire, indépendante des variations de volume cellulaire mais fortement dépendante du calcium intracellulaire et, en toute probabilité, de nature exocytotique.

Les trois articles scientifiques qui ont permis d'aboutir à cette conclusion originale constitue le corps du présent document. On retrouve également, en supplément à ces textes et en guise de conclusion, une discussion inédite qui questionne le bien-fondé du rôle de l'ATP comme cytokine et qui souligne que les cellules non-neuronales sont équipées pour envoyer et recevoir des messages par ATP mais, peut-être, uniquement entre proches voisines.

Cette thèse a été déposée à la Faculté des études supérieures le 17 août 2004.

INTRODUCTION

L'ATP source d'énergie

L'ATP sert comme source d'énergie pour les besoins de la cellule et, par extension, de l'organisme. D'un poids moléculaire d'environ 503, l'anion ATP^{4-} ($C_{10}H_{12}N_5O_{13}P_3$) consiste (voir Figure 1) en un groupement adénine de la famille des purines - bicyclique et riche en azote – lié par une N-glycolysation à un sucre à 5 carbones, le ribose, complété par une chaîne de trois phosphastes attachés entre eux par des ponts acide-anhydres et fusionnés au ribose en 5'. Ce nucléotide forme, presque toujours, un complexe avec le Mg^{2+}, un cation essentiel pour son hydrolyse.
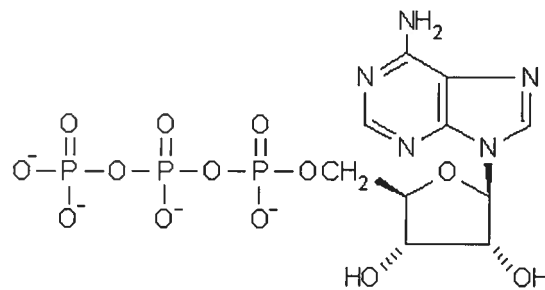
Figure 1 -   Structure atomique de l'ATP^{4+} (modifiée du catalogue 2004 de SIGMA, St-Louis, USA)

L'ATP est produite en partie dans le cytosol par glycolyse mais surtout à l'intérieur des mitochondries par les réactions du *cycle de Krebs* et la respiration cellulaire aérobie. Fraîchement synthétisée à partir de l'ADP, elle retourne au cytosol en franchissant la double membrane mitochondriale par le complexe formé du pore anionique VDAC et de l'échangeur ADP/ATP. L'hydrolyse de ce nucléotide est très favorable énergétiquement (ΔG=-12 Kcal/mole) et sert à procurer l'énergie nécessaire à de nombreuses réactions physiologiques comme la contraction musculaire, le transport vectoriel de nutriments de l'intestin vers le sang ou leur réabsorption au niveau du rein.

Une molécule polyvalente

En plus de son rôle dans le transport d'énergie, l'ATP occupe les fonctions les plus diverses, comme fournir un ion phosphate dans la phosphorylation du glucose, un monosaccharide qui est aussi essentiel dans la synthèse d'ATP; ce qui permet de stocker ce sucre sous la forme compacte du glycogène. La phosphorylation d'un substrat sert aussi comme mode de signalisation cellulaire. Ce mécanisme permet, entre autres, la reconnaissance entre protéines. Par exemple, la phosphorylation de certains résidus tyrosine sur un récepteur à activité tyrosine kinase, comme le récepteur à l'insuline, permet aux protéines munies d'un domaine SH2 de s'y associer et d'enclencher ainsi une cascade de signalisation aboutissant au noyau cellulaire et à la transcription d'ARN messager.

Certains canaux ioniques sont aussi modulés intracellulairement par une liaison directe à l'ATP. C'est le cas du K_{ATP}, un canal potassique - inhibé par les composés sulfonylurés à action hypoglycémique - que l'on retrouve entre autres chez les cellules pancréatiques et qui sert dans la sécrétion d'insuline et aussi chez les cellules alvéolaires de type II où il jouerait, tel que récemment découvert, un rôle dans le transport vectoriel des fluides (Leroy *et al.*, 2004).

L'ATP participe également à la communication intercellulaire comme neurotransmetteur mais aussi comme cytokine comme on le verra aux sections suivantes.

Un nucléotide comme neurotransmetteur

Le système nerveux autonome, reponsable de la préparation de l'organisme face à l'agression et au repos, utilise 2 principaux types de neurotransmetteurs post-ganglionnaires: la noradrénaline et l'acétylcholine. Cependant, ces neurotransmetteurs sont absents de certaines synapses autonomiques associées aux muscles lisses de l'intestin et de la vessie. Au début des années 1970, Burnstock et coll. ont identifié le neurotransmetteur de ces synapses non-adrénergiques et non-cholinergiques: l'ATP (Burnstock *et al.*, 1970; Burnstock *et al.*, 1972), qui a également été identifiée comme co-transmetteur à la jonction neuromusculaire avec l'acétylcholine (Unsworth & Johnson, 1990). On a aussi ultérieurement découvert des synapses purinergiques dans le système nerveux central.

Les récepteurs purinergiques qui ont pour principal ligand l'ATP, mais aussi l'UTP (une pyrimidine), se répartissent en deux familles: les $P2X_{1-7}$, ionotropiques, à 2 segments transmembranaires (TM) qui peuvent former des multimères, sont sélectifs aux cations et rectifient vers l'intérieur; et les $P2Y_{1,2,4,6,11,12}$, métabotropiques, structurés en 7 TM et qui se lient principalement aux protéines G_q.

Quand l'ATP prend la clef des champs

A la fin des années 1970, l'analyse de surnageant de cellules endothéliales a démontré la présence d'ATP en concentration significative et sa continuelle dégradation, donc sa libération en continu (Nees *et al.*, 1979). Ce qui était une curiosité alors, est devenu du plus grand intérêt lorsque l'on a découvert le rôle possible de l'ATP comme messager extracellulaire dans la synthèse des prostaglandines (Pearson *et al.*, 1983). Cela suggérait, entre autres, que les cellules endothéliales n'étaient pas de simples acteurs passifs durant la réponse immunitaire mais pouvaient y participer activement, en compagnie des cellules sanguines, à l'aide d'une signalisation autocrine et paracrine par ATP. On y reviendra plus loin.

Mais c'est surtout la nature mécanosensible de la sécrétion d'ATP qui nous intéresse ici. Les cellules endothéliales, on le sait, sont continuellement exposées à des efforts en cisaillement dû à l'écoulement du fluide légèrement visqueux qu'est le sang (μ_{sang}= 3,63 mPa·s à 37°C et, pour référence: $\mu_{huile\ à\ moteur-SAE\ 30}$ = 290 mPa·s à 20°C). Le sang, en effet, peut générer des contraintes de l'ordre de 1 à 2 Pa dans la circulation artérielle mais 10 fois moindre dans les veines (Guo *et al.*, 2000), une amplitude que les systèmes de perfusion de cultures cellulaires peuvent aisément générer; même si la viscosité d'une solution physiologique standard est moindre (μ_{eau}= 0,7 mPa·s à 37°C) parce que les conditions géométriques et de vitesse d'écoulement sont différentes. On a découvert ainsi que, dans ces systèmes, les cellules endothéliales sécrétent de l'ATP (Milner *et al.*, 1990) en réponse à ces efforts de cisaillement.

Bien que d'autre mécanismes comme l'hypoxie (Burnstock, 1987), povoque la sécrétion d'ATP, un stress mécanique s'est rapidement imposé comme stimulus prépondérant dans la sécrétion d'ATP. Et, rapidement, on a découvert une variété de chargements mécaniques capables de libérer de l'ATP des cellules: la flexion du substrat (Grygorczyk & Hanrahan, 1997), la compression (Sauer *et al.*, 2000), la stimulation par

une micropipette (Stout *et al.*, 2002) et le choc hypotonique (Hazama *et al.*, 1999; Mitchell *et al.*, 1998; Van der Wijk *et al.*, 1999; Hisadome *et al.*, 2002). Ce dernier type d'effort, bien que à certains égards moins physiologique, est le plus couramment utilisé dû à sa simplicité.

L'ATP une cytokine en émergence

Tel que déjà mentionné, la sécrétion d'ATP dans le milieu extracellulaire ne devait pas rester longtemps une simple curiosité et rapidement ce phénomène fut intégré dans quelques modèles physiologiques. Par exemple, un des premiers qui a été suggéré, propose que l'ATP une fois libérée des cellules endothéliales et/ou des erythrocytes, réajuste localement la pression vasculaire en activant les récepteurs purinergiques des cellules environnantes des muscles lisses (Burnstock, 1987). Un mécanisme d'action où l'ATP extracellulaire agit sur une assez grande distance à la manière d'une cytokine.

Mais c'est surtout l'alliance de cette notion de cytokine ATP et de la nature mécanosensible de sa sécrétion qui allait donner naissance au plus grand nombre de modèles. Au niveau endothélial, par exemple, on croit que la sécrétion d'ATP en réponse aux contraintes de cisaillement est augmentée lors de l'inflammation (Bodin & Burnstock, 1998). On avance également que ce type de mécanisme local de rétroaction biologique sert aussi dans la sensation d'une vessie pleine (Ferguson *et al.*, 1997; Birder *et al.*, 2003) ou dans la sécrétion de lait par les glandes mammaires (Blaug *et al.*, 2003). Une pléthore de modèles qui, de par leur nombre, semble indiquer que la cytokine ATP se voue presque entièrement à la mécanotransduction.

Le rôle possible de la cytokine ATP dans le poumon

Au niveau du poumon, moduler le transport mucociliaire et contrôler le niveau de liquide de surface tapissant les alvéoles sont deux mécanismes également réputés pour recourir à l'ATP comme cytokine. En effet, l'ATP est connue pour être sécrétée par les cellules épithéliales pulmonaires en réponse à des chargements mécaniques (Grygorczyk & Hanrahan, 1997) et pour augmenter la fréquence des battements ciliés des cellules bronchiales. Elle est aussi impliquée dans la sécrétion de mucus et la sécrétion de fluide par les cellules alvéolaires (Stutts *et al.*, 1992; Chen *et al.*, 2001; Morse *et al.*, 2001) en interagissant avec plusieurs récepteurs métabotropiques P2Y, largement exprimés au niveau du poumon (Communi *et al.*, 1999).

L'ATP s'évade-t-elle par un canal?

Bien que l'exocytose soit le mécanisme généralement reconnu de sécrétion d'ATP dans le cas des synapses NANC, la nature du mécanisme de sécrétion mécanosensible ou régulée d'ATP par des cellules non-neuronales demeure, encore aujourd'hui, sujet à controverse. Les hypothèses sont nombreuses et dans la majorité des cas on a proposé un canal commme mécanisme de perméation.

Certains candidats comme le CFTR et le MDR (Prat *et al.*, 1996;Abraham *et al.*, 1993) n'ont pas résisté devant les observations contradictoires (Grygorczyk & Hanrahan, 1997; Li *et al.*, 1996). La liste des hypothèses continue de s'allonger sans que l'on ne soit encore capable de discerner le véritable mécanisme. Cette liste comporte présentement des canaux anioniques membres du groupe des SAC (Taylor *et al.*, 1998), des canaux responsables du RVD (Hisadome *et al.*, 2002), des pores à haute conductance tels les VDAC (Sabirov *et al.*, 2001) et les demi-connexines (Cotrina *et al.*, 1998), des canaux anioniques sensibles à différents inhibiteurs, principalement le NPPB, propres à la famille des canaux chlorure (Sauer *et al.*, 2000; Hazama *et al.*, 1999; Mitchell *et al.*, 1998). D'autres hypothèses plus hardies, comme par exemple l'ectoATPase CD39 (Bodas *et al.*, 2000) qui aurait un double rôle d'ATPase et de canal perméable à l'ATP, ont également été avancées.

L'ATP se répand-t-elle par exocytose?

D'autres observations indiquent plutôt une sécrétion mécanosensible d'ATP par exocytose. En effet, la libération basale et mécanosensible d'ATP est fortement atténuée par des substances qui perturbent la machinerie exocytotique, tel le brefeldin A qui abolit la sécrétion d'ATP d'oeufs de grenouilles de *Xenopus* (Maroto & Hamill, 2001), ou encore, les composés monensine et N-ethylmaleimide qui diminue la quantité d'ATP libérée par des cellules endothéliales (Bodin & Burnstock, 2001).

Plusieurs hypothèses se bousculent pour expliquer la sécrétion mécanosensible d'ATP et nous expliquerons au prochain chapitre la démarche que nous avons suivie pour tenter d'y mettre un peu d'ordre dans le cadre de cette thèse.

DÉMARCHE EXPÉRIMENTALE ET RÉSUMÉ DES ARTICLES

Réexaminer le modèle dominant (article 1)

Au début des années 2000, de nombreux modèles de sécrétion d'ATP suite à des chocs hypotoniques se concurrençaient (voir INTRODUCTION). Cette discordance suggérait que le véritable mécanisme restait encore à trouver. Cependant il y avait un modèle, favori parmi les autres, qui semblait indiquer la voie à suivre. Principalement basé sur la découverte que le gadolinium, un lanthanide et inhibiteur de choix des SAC, abolissait la libération d'ATP causée par un choc hypotonique, ce modèle annonçait, à tout le moins, les caractéristiques fondamentales de ce mécanisme soit un canal ionique perméable à l'ATP et activé par l'étirement de la membrane plasmique.

Une hypothèse mise à mal par la démonstration exposée dans cette thèse que le Gd^{3+} inhibe également la réaction de bioluminescence utilisée pour doser l'ATP, et que la dose de Gd^{3+} utilisée normalement pour supprimer la sécrétion d'ATP par hypotonicité est bien supérieure à celle normalement suffisante pour bloquer un SAC. De surcroît, cet «inhibiteur» pouvait même, dans certains cas, «accroître» la libération d'ATP.

A l'origine de ce réexamen, il y a l'observation que le Gd^{3+} avait un effet inhibiteur sur l'émission de luminescence de la réaction luciférase/luciférine à des concentrations micromolaires, soit le même ordre de grandeur utilisé pour l'inhibition des canaux appartenant à la famille des SAC. De plus, cet effet était dépendant du temps d'incubation en présence d'ATP et de la présence dans la préparation d'agent chelateur de calcium tel l'EDTA. Malgré cela, il continuait d'être possible que le Gd^{3+} ait un réel effet inhibiteur sur la sécrétion d'ATP; après tout il était fort logique de s'attendre à ce qu'un SAC soit impliqué dans la sécrétion mécanosensible d'ATP. Comment alors discerner le vrai du faux?

Notre approche consista à déterminer premièrement la nature du mécanisme d'inhibition de la réaction de luminescence. Cette inhibition résultait de la substitution de l'ion Mg^{2+}, cation essentiel pour permettre l'hydrolyse d'ATP, par le Gd^{3+} pour former une paire Gd-ATP non-hydrolysable. Ce mécanisme de substitution repose, semble-t-il, sur une plus grande affinité de l'anion ATP^{4-} pour le Gd^{3+} que pour le Mg^{2+}. Pour réaliser

le dosage d'ATP, il fallait donc séparer le Gd^{3+} de la paire Gd-ATP. Pour y parvenir, on a utilisé un chelateur ayant une très forte affinité pour le Gd^{3+}, l'EGTA, mais très peu pour le Mg^{2+}, et ce, en présence d'une concentration élevé de $MgSO_4$ afin d'immédiatement remplacer le Gd^{3+} chelaté par un cation Mg^{2+} et ainsi reformer un duo Mg-ATP hydrolysable. Il était alors possible d'effectuer un choc hypotonique en présence d'une concentration élevée de Gd^{3+} extracellulaire tout en évitant d'inhiber la réaction de luminescence utilisée pour mesurer la quantité d'ATP libérée. En effet, bien que ce lanthanide s'associe aussitôt à l'ATP fraîchement secrétée, on pouvait réaliser la substitution des cations une fois l'échantillon prélevé, en mélangeant à celui-ci une solution d'EGTA et de $MgSO_4$ et, après une période d'incubation, doser l'ATP.

Un dosage qui a révélé que le Gd^{3+} inhibait, à la fois, et la réaction de bioluminescence, et la libération d'ATP! Mais cette observation dans notre cas, au lieu de raffermir l'hypothèse des SAC dans la sécrétion d'ATP, l'affaiblissait parce que la concentration du lanthanide nécessaire pour 50% d'inhibition (IC_{50}) atteignait 150 μM pour une lignée de cellules épithéliales alvéolaires (A549) et 50 μM pour une lignée dérivée d'épithélium bronchique (16HBE14o-). Il s'agit de concentrations bien supérieures à 10 μM, soit la dose suffisante de Gd^{3+} pour abolir 90% de l'activité d'un SAC: il était donc improbable que cet hypothétique canal fasse partie de cette catégorie. De plus, et contre toute attente, sur des lignées de fibroblates (NIH/3T3), on a observé qu'une concentration de Gd^{3+} de l'ordre de 10 à 250 μM augmentait la quantité totale d'ATP libérée par rapport à celle sécrétée en absence de cet ion. Dans l'ensemble, ces résultats indiquaient donc un effet différent du Gd^{3+} pour chacune des lignées cellulaires ce qui est incompatible avec l'hypothèse d'un canal unique perméable à l'ATP.

Par quel mécanisme agit le Gd^{3+}? Il est difficile de répondre à cette question tant les effets non spécifiques de cet ion «malicieux» sont nombreux. Cependant, puisque le Gd^{3+} présente une affinité pour les phospholipides semblable à celle qu'il a pour les phosphates de l'ATP et puisqu'il a été démontré qu'une concentration micromolaire de ce lanthanide suffisait à déplacer les ions calcium normalement lié au feuillet externe de la membrane plasmique, nous avons fait l'hypothèse que l'ATP pouvait utiliser un mécanisme de sécrétion par exocytose, un procédé qui repose sur une fusion complexe de phospholipides membranaires. Ce mode d'action expliquerait la différence observée

entre les 3 types cellullaires, chacun exprimant probablement une mosaïque différente de phospholides avec une affinité différente pour le gadolinium.

Le détail de ces méthodes expérimentales, l'ensemble des résultats et une discussion plus élaborée figurent dans l'article 1: *Cell swelling-induced atp release and gadolinium-sensitive channels*.

Développer une mesure de variation rapide de volume cellulaire (article 2)

Rejeter l'hypothèse d'un SAC perméable à l'ATP contribuait peu à préciser la nature du mécanisme de sécrétion mécanosensible d'ATP. En effet, il existait encore trop d'alternatives à ce modèle dans la littérature. Il fallait donc défricher et surtout évaluer plus en profondeur le mécanisme d'exocytose suggéré par les résultats de l'article 1.

Afin d'y voir plus clair, il est apparu important de pouvoir déterminer la cinétique exacte de la sécrétion d'ATP par hypotonicité. Du plus haut intérêt était alors de savoir quand l'ATP était sécrétée: durant le gonflement ou durant le retour au volume de départ. Si la majorité de l'ATP est libérée durant le gonflement cela indiquera un mécanisme sensible à l'étirement de la membrane c-à-d soit un SAC ou une exocytose favorisée par l'augmentation de la tension membranaire. Au contraire, si la majorité de l'ATP est sécrétée durant le RVD, ces modèles seront infirmés et l'on penchera pour les candidatures des canaux perméables aux anions. Ainsi, il serait possible d'éliminer des candidats par l'analyse combinée de la cinétique de sécrétion d'ATP et de variation de volume cellulaire et ce, en évitant le recours aux inhibiteurs pharmacologiques et leurs inévitables «dommages collatéraux» (voir article 1).

Or, aucune technique disponible ne permettait d'évaluer adéquatement le changement rapide de volume d'une cellule adhérente c-à-d attachée à son substrat de verre ou de plastique, en réponse à un choc hypotonique. Pour réaliser cette mesure, plusieurs possibilités s'offraient à nous. Premièrement, les cellules pouvaient être séparées de leur substrat, une situation inacceptable dans notre cas. Alternativement, on pouvait mesurer un seul paramètre, par exemple le changement de hauteur cellulaire. Finalement, on pouvait utiliser une corrélation capricieuse entre la concentration intracellulaire d'un fluorophore et le volume cellulaire. Aucune de ces techniques ne pouvait satisfaire à nos exigences en terme de résolution. Une méthode fut alors inventée pour permettre de mesurer avec une précision suffisante le changement rapide de volume

d'un cellule adhérente. Une chambre de perfusion fut fabriquée qui permet de photographier le profil en expansion d'une cellule attachée à son substrat. A partir d'une vue de profil combinée à une vue de plan de cette même cellule, il a été possible de reconstruire en 3D la morphologie de la cellule, et ainsi permettre de mesurer la cinétique de variation de volume avec une résolution supérieure aux méthodes couramment utilisées.

Non seulement cette technique offre-t-elle une meilleure précision de mesure mais aussi elle permet de mieux saisir la nature d'un choc osmotique en visualisant directement le film du gonflement cellulaire. Cette nouvelle méthode a notamment permis de découvrir une phase plateau (volume constant) inconnue jusqu'alors et qui précède le RVD. Une phase pendant laquelle la majorité de l'ATP est sécrétée tel qu'expliqué à la prochaine section. Tous les détails techniques de la chambre, les calculs mathématiques et les résultats de validation de la technique de reconstruction 3D sont inclus dans l'article 2: *Conventional microscopy 3D imaging technique to evaluate rapid volume changes of substrate-adherent cells.*

Améliorer la résolution de la mesure de sécrétion d'ATP et corréler volume cellulaire, sécrétion d'ATP et calcium intracellulaire (article 3)

Les techniques de mesure utilisées dans l'article 1 ne possédait ni la précision, ni la résolution temporelle nécessaire pour une analyse fine de la cinétique de sécrétion d'ATP. Une méthode par perfusion s'imposait alors, et une chambre fermée à écoulement laminaire fut conçue avec un rapport optimal entre le volume de la chambre et le nombre de cellules afin de maximiser la sensibilité de la mesure. Des contraintes supplémentaires étaient imposées par la sensibilité de la réaction luciférase/luciferine, par la nécessité de réduire au minimum les volumes morts et par l'obligation de limiter le plus possible le cisaillement dû à l'écoulement du fluide.

Grâce à cette chambre de perfusion, il fut possible d'observer, pour la première fois, avec une résolution et une précision inégalée, la nature transitoire de la sécrétion d'ATP par hypotonicité. Ces résultats montrèrent que l'ATP est sécrétée en majorité durant une phase de plateau: une phase qui était inconnue à ce jour et qui précède le RVD. Ceci démontrait la nature indépendante au changement de volume du mécanisme de sécrétion d'ATP. Par contre, en accord avec une théorie exocytotique, l'augmentation

de la concentration de calcium cytosolique était parfaitement synchronisée avec l'augmentation du taux de sécrétion d'ATP en réponse au choc hypotonique.

Pour mettre en lumière le peu de rapport direct entre l'étirement de la membrane plasmique et la libération d'ATP, on a provoqué sa libération en absence de choc hypotonique par l'augmentation soudaine de la concentration cytosolique de calcium en perméabilisant la membrane plasmique avec un ionophore (ionomycine). De plus, il a également été possible d'inhiber la sécrétion d'ATP par hypotonicité soit en maintenant le calcium intracellulaire très bas à l'aide d'un chelateur de calcium (BAPTA), soit en refroidissant à 10°C la solution de perfusion. Dans les deux cas, une inhibition significative de la quantité d'ATP excrétée a été observée malgré un accroissement du volume de la cellule semblable à celui mesuré en condition contrôle.

L'ensemble de ces résultats présenté dans l'article 3: *Cell swelling-induced ATP release is synchronized with intracellular calcium elevations*, a permis de renforcer l'hypothèse avancée dans l'article 1 qui suggère que le mécanisme de sécrétion mécanosensible d'ATP par hypotonicité procède par exocytose de vésicules remplies d'ATP. L'étude de la cinétique de sécrétion d'ATP a permis aussi de démontrer que la variation de calcium intracellulaire régule étroitement ce mécanisme mais que, contrairement à l'opinion couramment admise, l'étirement de la membrane plasmique durant l'accroissement de volume de la cellule ne commande pas directement la libération d'ATP.

LISTE DES ARTICLES

Chacun des articles, listés ci-dessous, est présenté sous la forme d'un manuscrit standard et se divise dans cet ordre: le corps du texte, les figures suivi de leurs légendes, les tableaux, les remerciements, les références et, le cas échéant, le texte des annexes. A noter qu'en réponse aux commentaires du jury, de légères modifications ont été apportées aux textes des articles. Par conséquent, le contenu des articles 1 et 2 diffère de celui paru dans la revue scientifique.

Article 1 – Cell swelling-induced ATP release and gadolinium-sensitive channels (F. Boudreault et R. Grygorczyk)

Paru dans le *American Journal of Physiology Cell Physiology* en janvier 2002.

Article 2 – Conventional microscopy 3D imaging technique to evaluate rapid volume changes of substrate-adherent cells (F. Boudreault et R. Grygorczyk)

A paraître dans le *Journal of Microscopy* en septembre 2004.

Article 3 – Cell swelling-induced ATP release is synchronized with intracellular calcium elevations (F. Boudreault et R. Grygorczyk)

Soumis au *Journal of Physiology* le 20 juillet 2004.

Cell swelling-induced ATP release and gadolinium-sensitive channels

Francis Boudreault and Ryszard Grygorczyk

Centre hospitalier de l'Université de Montréal and Department of Medicine,
Université de Montréal, Montréal, Québec, Canada

ACCORD DES COAUTEURS

Identification

Francis Boudreault
Ph.D. en Génie Biomédical

Description de l'article

Francis Boudreault et Ryszard Grygorczyk
Cell swelling-induced ATP release and gadolinium-sensitive channels
American Journal of Physiology Cell Physiology, janvier 2002

Déclaration de tous les coauteurs autres que l'étudiant

À titre de coauteur de l'article identifié ci-dessus, je suis d'accord pour que *Francis Boudreault* inclue cet article dans sa thèse de doctorat qui a pour titre: *Contribution à l'étude du mécanisme de sécrétion d'ATP par des cellules épithéliales pulmonaires et des fibroblastes soumis à un choc hypotonique.*

Ryszard Grygorczyk   13 Aug. 2004
Coauteur   Signature   Date

ABSTRACT

ATP release induced by hypotonic swelling is an ubiquitous phenomenon in eukaryotic cells, but its underlying mechanisms are poorly defined. A mechano-sensitive ATP channel has been implicated because Gd^{3+}, an inhibitor of stretch-activated channels, suppressed ATP efflux monitored by luciferase bioluminescence. We examined the effect of Gd^{3+} on luciferase bioluminescence and on ATP efflux from hypotonically-swollen cells. We found that luciferase was inhibited by $\leq 10\ \mu M$ Gd^{3+}, and this may have contributed to the previously-reported inhibition of ATP release. In ATP efflux experiments, luciferase inhibition could be prevented by chelating Gd^{3+} with EGTA before luminometric ATP determinations. Using this approach, we found that $10\ \mu M$ to $100\ \mu M\ Gd^{3+}$, i.e. concentrations typically used to block mechano-sensitive channels, actually stimulated hypotonically-induced ATP release from fibroblasts. Inhibition of ATP release required at least $500\ \mu M$, $200\ \mu M$ and $100\ \mu M\ Gd^{3+}$ for fibroblasts, A549 and 16HBE14o⁻ cells, respectively. Such biphasic and cell-specific effects of Gd^{3+} are most consistent with its action on membrane lipids and membrane-dependent processes such as exocytosis.

INTRODUCTION

ATP release induced by mechanical stimuli, such as hypotonic swelling, shear stress or mechanical strain, has been observed in all eukaryotic cells examined (4,16,20-22,27,29,31). Extracellular ATP and other nucleotides then interact with purinergic P2Y and P2X receptors to regulate a broad range of physiological responses, including vascular tone, muscle contraction, cell proliferation, mucociliary clearance, synaptic transmission and platelet aggregation (5,7,12). The mechanism of mechanosensitive (MS) ATP release is not known, and several have been proposed including the fusion of ATP-enriched protein transport vesicles, ATP transporters and MS ATP channels (6,20),(23,28,29). The latter hypothesis was based on the observation that Gd^{3+}, an inhibitor of stretch-activated cation channels, inhibited swelling-induced ATP efflux when it was monitored by luciferase bioluminescence. In particular, for epithelial cells, it was proposed that the cystic fibrosis transmembrane conductance regulator (CFTR) facilitates swelling-induced ATP release through a separate ATP-permeable channel and contributes to cell volume regulation. A MS channel was implicated because ATP release was blocked by Gd^{3+} (6).

ATP-dependent luciferase bioluminescence allows the detection of femtomoles of ATP, however, light output from the reaction depends on a number of factors, including ionic strength, pH, temperature and the concentration of divalent cations (25), all of which may vary during the experiment. For example, experimental manipulations aimed at modulating ATP efflux from cells, such as application of hypotonic media or putative inhibitors, may directly interfere with the bioluminescence reaction and hinder accurate ATP detection. The trivalent lanthanide Gd^{3+} blocks mechano-gated channels and has diverse, often nonspecific effects that include blockage of other channel types, induction of liposome fusion and pore formation in erythrocytes (2,9),(14,18,19),(32). Many of these actions may originate from binding of Gd^{3+} to phospholipids and alteration of physical properties of the cell membranes (13). In addition to direct and indirect inhibition of ion channels, lanthanides have been reported to inhibit several enzymes, including calcium ATPases, proteinases and kinases (14,15,33). Use of Gd^{3+} is further complicated by

its strong binding to certain anions often present in physiological and cell culture solutions such as phosphate, carbonate, sulfate, EDTA, albumin and ATP (8,14). Thus, the concentration of free Gd^{3+} in the presence of these anions could be significantly overestimated, leading to erroneous conclusions (8).

In this study, we sought to examine the effect of Gd^{3+} on ATP detection by luciferase-luciferin bioluminescence and on ATP efflux from hypotonically-swollen cells. We found that ATP-dependent luciferase bioluminescence was directly inhibited by ≤10 μM of free Gd^{3+} and may have contributed to the previously-reported apparent inhibition of ATP efflux from several cell types. When luciferase inhibition was prevented by chelating any Gd^{3+} before luminometric ATP determinations, we found that Gd^{3+} at 10-100 μM stimulated ATP efflux from hypotonically- swollen 3T3 fibroblasts. Inhibition of ATP efflux from fibroblasts and lung epithelial A549 cells by Gd^{3+} was observed at 200-500 μM, i.e. concentrations significantly higher than those used typically to directly block MS ion channels. Our results do not support the view that Gd^{3+}-sensitive channels are involved in ATP release and suggest that indirect and nonspecific effects of Gd^{3+} on lipid membrane and membrane-dependent processes should be considered.

METHODS

Cell culture. Adult human lung carcinoma A549 cells and NIH 3T3 fibroblasts (American Type Culture Collection) were grown in DMEM media supplemented with 10% FBS, 20 mM L-glutamine, penicillin-G 60 μg/ml and streptomycin 100 μg/ml. Human bronchial epithelial 16HBE14o⁻ cells, a generous gift from Dr. D. Gruenert, were cultured as described (10). All constituents of the culture media were from GIBCO-BRL (Burlington, ON). Cell monolayers were grown to near confluency on culture-treated plastic in 12-well plates with an area of 3.14 cm^2/well.

ATP efflux experiments. Before the experiments, culture media was removed from the wells, and the cell monolayers were washed two times with physiological NaCl solution. Due to massive ATP release during the wash, the cells were allowed to equilibrate for approximately 1 hr at 37°C and to reduce ATP to its basal level (16).

In addition, repeated gentle replacement of half of the extracellular solution allows the extracellular ATP concentration to be quickly reduced close to the basal level. ATP efflux experiments were performed at 37°C on a rotating platform (30 RPM) to ensure mixing and to minimize the unstirred layer above the cells. Each well with cells contained 500 µl of solution, and hypotonic shock was applied by adding the appropriate volume of distilled water or solution containing only divalent cations (see below). Samples (25 or 50 µl) of the medium covering the cells were taken at various time points, and ATP content determined immediately by luciferin/luciferase bioluminescence assay.

Luciferin/luciferase luminometric assay. To measure ATP content in the samples, we used glycine-buffered firefly luciferase with added luciferin (Sigma, cat. # L3641) at a concentration of 1 mg/ml of the total reagent. In some experiments, we employed a custom-made mix of EDTA-free luciferin and luciferase. It contained 150 µM luciferin (cat. # L6882), approximately 2 µM luciferase (cat. # L9506), 50 mM glycine, 0.1 mM Tris, 10 mM $MgSO_4$, and 1 mg/ml BSA, all purchased from Sigma. During the assay, 50 µl of the medium was mixed in the cuvette with 50 µl of luciferin/luciferase reagent, and the average light signal was measured for 10 s with a TD20/20 luminometer (Turner Design, Sunnyvale, CA). ATP content was determined using [ATP] versus luminescence standard curves which were made for each experimental solution and each luciferase reagent preparation. In experiments where gadolinium was used to block ATP efflux from the cells, samples of extracellular media were first treated with EGTA + $MgSO_4$ to chelate any gadolinium before luminometric measurements, as described in more detail in the Results section. For experiments requiring prolonged luminescence measurement, the luminometer was connected to a computer and the luminescence signal was recorded and displayed in real time with software provided by the luminometer manufacturer and Microsoft Excel.

Cell viability test. The uptake of ethidium bromide, a nuclei marker, was monitored in selected experiments to evaluate cell viability and the possible contribution of cell lysis to ATP release. Cell monolayers were incubated in the presence of 0.15 to 0.3

μg/ml of ethidium bromide, and red-stained dead cells were counted by epifluorescence microscopy.

Solutions and chemicals. Physiological NaCl solution contained (in mM): 140 NaCl, 5 KCl, 1 $MgCl_2$, 1 $CaCl_2$, 10 Hepes, 10 glucose, pH 7.4, adjusted with NaOH. For hypotonic cell swelling, tonicity of the NaCl solution was reduced by adding an appropriate volume of distilled water or, in the majority of experiments, a solution that contained 1 mM $MgCl_2$ and 1 mM $CaCl_2$ to preserve the concentration of divalent cations during hypotonic shock. $GdCl_3$ hexahydrate (Sigma) was prepared as a 100 mM stock solution in distilled water.

Statistical analysis. Statistical significance was assessed at P<0.05 by ANOVA.

RESULTS

Gadolinium directly inhibits luciferase bioluminescence. Hypotonicity-induced ATP release experiments are often performed by adding luciferase reagent directly to the cell's extracellular media and measuring ATP-dependent bioluminescence in real time. However, change in salt concentration during hypotonic shock as well as the addition of putative ATP-release blockers could have a direct effect on the luciferase bioluminescence reaction. This is illustrated in Figure 1 A, where we simulated typical hypotonicity-induced ATP efflux in the absence of cells. The bioluminescence reaction was initiated in a test tube containing physiological extracellular saline with the luciferase reagent, by adding 10 nM or 100 nM ATP. Approximately 10 min later, when ATP-dependent luciferase bioluminescence reached a relatively stable level, the NaCl was diluted by 30% with distilled water containing the luciferase reagent to mimic the hypotonic shock applied to cells without diluting the luciferase reagent. This resulted in a step-like enhancement of light output despite concurrent dilution of ATP. Subsequent application of 50 μM $GdCl_3$ caused ~50% inhibition of bioluminescence. These results demonstrate that Gd^{3+} and changes in NaCl concentration have a direct effect on luciferase bioluminescence and may contribute to an apparent modulation of ATP efflux observed with cells. It is noteworthy that the enhancement and inhibition of bioluminescence were smaller when 10 nM ATP was used instead of 100 nM (Fig. 1 A, trace labeled *low ATP* and *high ATP* respectively).

These effects, therefore, may go unnoticed in experiments when ATP concentration in the media is low. The direct inhibitory effect of Gd^{3+} on luciferase bioluminescence was dose-dependent and, under our experimental conditions, required relatively high concentrations similar to those reported previously to inhibit ATP efflux from cells, typically ≥ 100 μM (Fig. 1 B).

The extent of bioluminescence inhibition by Gd^{3+} may vary with time and, to some extent, it also depends on the exact experimental protocol used. For example, somewhat different inhibition was observed when Gd^{3+} was first incubated with luciferase and bioluminescence recorded upon the subsequent addition of ATP compared to the protocol in which Gd^{3+} was pre-incubated with ATP before addition of the luciferase reagent. This latter case is illustrated in Figure 1 C, where the dose-inhibition curves of luciferase luminescence were determined at different time points after mixing $GdCl_3$ with ATP. It shows that the $GdCl_3$ concentration required to produce 50% inhibition of bioluminescence was approximately 300 μM at 0.5 min, but decreased significantly to 50 μM at 150 min. Longer incubation of ATP with Gd^{3+} for up to 24 h did not significantly change this inhibition (not shown). Time-dependent inhibition may be relevant in ATP efflux assays, when aliquots of extracellular media are taken at different time points, but their ATP content is measured later, after all the samples are collected.

Several commercially-available luciferase reagents contain EDTA. In the experiments shown in Figure 1, we used glycine-buffered firefly extract with added luciferin (Sigma, cat. # F3641), which contains approximately 0.5 mM EDTA when dissolved at a concentration of 1 mg/ml. Due to strong binding of Gd^{3+} to EDTA (14), the actual concentration of free Gd^{3+} responsible for the observed inhibition of the luciferase reaction could be significantly lower. Indeed, this was confirmed in the experiment illustrated in Figure 2. When nominally EDTA-free luciferase-luciferin reagent was used, 10 μM Gd^{3+} was sufficient to inhibit luciferase activity by more than 50% (Fig.2 A). Addition of 250 μM EDTA abolished the inhibition by 10 μM of Gd^{3+} (Fig. 2 A, trace labeled + *EDTA*) and shifted the dose-response inhibition curve to the right, consistent with the chelation of Gd^{3+} by added EDTA (Fig.2 B).

Chelation of Gd^{3+} by EGTA prevents inhibition of luciferase in ATP efflux experiments. Strong binding of Gd^{3+} by EDTA or EGTA may be used to remove Gd^{3+} from aliquots of extracellular media before determining ATP content by luminometry. This could allow studies of Gd^{3+} effects on ATP efflux from cells while avoiding its inhibitory action on luciferase bioluminescence. Figure 3 shows that incubation of Gd^{3+}-containing media with 25 mM EGTA + 5 mM $MgSO_4$ for 30 min chelated any Gd^{3+} and almost completely removed inhibition of bioluminescence. We used this method in subsequent studies of swelling-induced ATP efflux from cells.

Re-examination of the effect of Gd^{3+} on ATP release from hypotonically-swollen cells. Figure 4 shows the accumulation of ATP in extracellular media bathing NIH 3T3 fibroblasts, human lung carcinoma A549 cells and human bronchial epithelial 16HBE14o⁻ cells, determined 25 min after hypotonic shock. Hypotonic shock was applied in the absence or presence of increasing concentrations of Gd^{3+}, from 0 to 500 μM. After chelating Gd^{3+} with EGTA+$MgSO_4$, ATP content in aliquots of extracellular media was determined by luminometry. Figure 4 A demonstrates that in response to 50% hypotonic shock the fibroblasts released approximately 6-fold more ATP in the presence of 10 μM to 200 μM Gd^{3+} compared to the hypotonic shock applied in the absence of Gd^{3+}. At 500 μM Gd^{3+}, the amount of released ATP declined and was similar to that observed in the absence of Gd^{3+}. Qualitatively similar behavior was observed with A549 cells (Fig. 4 B), the amount of ATP released in the presence of 30 μM Gd^{3+}, was reproducibly, although statistically not significantly, increased and it was inhibited approximately 80% by 200 μM Gd^{3+}. For 16HBE14o⁻ cells, slight inhibition of hypotonically-induced ATP release could be noticed already with 30 μM Gd^{3+} but statistically significant inhibition required ≥100 μM (Fig. 4 C). Hypotonic shock and Gd^{3+} did not cause any detectable cell lysis during these experiments, as evaluated by ethidium bromide uptake and fluorescence microscopy (see Methods). Under control conditions, typically 3 to 10 cells per 1,000 were found to be stained. The number of dead cells, however, did not increase during 25-min exposure to 50% hypotonic shock.

DISCUSSION

The mechanisms underlying cell swelling-induced ATP release remain poorly defined. In this study, we have tested the hypothesis that Gd^{3+}-inhibitable channels are involved by evaluating the direct effect of Gd^{3+} on luciferase bioluminescence and on ATP efflux from cells. We have also taken into account the tight binding of Gd^{3+} to ATP and to other anions, such as EDTA, that are often present in luciferase reagent.

In cell-free experiments, we found that the luciferase bioluminescent reaction is directly blocked by less than 10 μM Gd^{3+} and enhanced in hypotonic solution. Reduction of the luciferase assay sensitivity by Gd^{3+} and its increase in hypotonic solution were also noticed in a recent study on MS ATP release from *Xenopus* oocytes (23). Block of luciferase bioluminescence by Gd^{3+} may be responsible, at least in part, for the reported inhibition of ATP efflux from cells. Lanthanides have been previously reported to inhibit several enzymes, including proteinase, phosphoglycerate kinase, hexokinase, pyruvate kinase, calcium ATPase and malic enzyme (14,15,33). It has been suggested that the mechanism of inhibition of several kinases involves competitive replacement of Mg^{2+} by lanthanides in the biologically-active Mg-ATP complex (14),(15). A similar mechanism may be responsible for the inhibition of luciferase bioluminescence observed in our study. Negatively-charged phosphates on ATP bind more tightly to Gd^{3+} than to Mg^{2+} or Ca^{2+}. The logarithm of the association constant (pK_a) for the ATP-metal ion complex is 7.1 for Gd^{3+} at pH 8 (14), compared to 5.8 for Mg^{2+} and 3.8 for Ca^{2+} (24). This favors competitive displacement of Mg^{2+} by Gd^{3+} in the Mg-ATP complex. Inhibition of luciferase activity by the formation of biologically-inactive Gd-ATP complex rather than direct binding of Gd^{3+} to the luciferase enzyme would agree with our observation that after inhibition of bioluminescence by Gd^{3+}, the addition of fresh Mg-ATP to the reaction mixture produced a strong luminescence signal (data not shown).

Inhibition of bioluminescence required high concentrations of Gd^{3+} (100 μM to 200 μM) when the luciferase reagent contained EDTA. However, when a nominally EDTA-free luciferase reagent was used, we observed a 50% block of bioluminescence by only 10 - 17 μM Gd^{3+} (Fig. 2 A and 2 B respectively). This is

because Gd^{3+} strongly binds to EDTA and EGTA, with affinities even higher than for ATP (pK_a of 17.4 and 17.5 respectively) (24). The presence of these molecules, or other anions of high affinity for Gd^{3+}, in the luciferase reaction solution will affect the concentration of free Gd^{3+} available to form the Gd-ATP complex and shift the threshold of inhibition to apparently higher $GdCl_3$ concentrations. This is demonstrated in Figure 2 B, where the addition of 250 µM EDTA shifted the dose-inhibition curve to the right, a result consistent with approximately 1:1 binding of EDTA and Gd^{3+}. Chelation of Gd^{3+} may explain why inhibition of luciferase bioluminescence was not detected in cell-free tests in some studies. Furthermore, because $GdCl_3$ is typically more than 1,000-fold in excess of ATP (10 µM versus 10 nM), it could be estimated that even when 95% of Gd^{3+} is chelated by anions, essentially 100% of ATP will be bound in a Gd-ATP complex, leading to complete inhibition of the luciferase reaction. This may account for the very steep dose-dependence of inhibition seen in Figure 2 B. As a consequence, minor differences in Gd^{3+} binding capacities of solutions used in experiments with and without cells may lead to entirely different results, depending on whether any Gd^{3+} was available to form the Gd-ATP complex. In some studies, 200-500 µM Gd^{3+} was required to produce noticeable inhibition of bioluminescence, while in others it was blocked by 10-30 µM Gd^{3+}, the concentrations typically used to block mechano-gated channels and luciferase bioluminescence in our experiments (20,28-30). These differences may reflect the varying composition of experimental solutions and their different capacity to bind Gd^{3+}. Although we have observed luciferase inhibition by as low as 10 µM $GdCl_3$, the concentration of free Gd^{3+} in these experiments was certainly lower than that of total added $GdCl_3$ due to binding by other anions present in this luciferase reagent, such as sulfate, Tris, albumin, glycine (see Methods) and traces of EDTA, which were left from the luciferase purification step (~100 nM according to the manufacturer).

To examine the effect of Gd^{3+} on ATP efflux from cells, while avoiding its inhibitory influence on the luciferase reaction, the samples of extracellular media containing Gd^{3+} in this study were treated with EGTA + $MgSO_4$ to chelate any Gd^{3+} before the luminometry determinations of ATP content. Usually, to properly

determine ATP content in extracellular solutions of different compositions, it is sufficient to make luminescence-ATP calibration curves for each experimental solution tested. This approach, however, will not work reliably for solutions containing Gd^{3+} because it binds directly to ATP and often leads to complete loss of the bioluminescence signal. This is further complicated by the fact that inhibition is time-dependent (Fig. 1 C). This time-dependence may be due to slow equilibration/redistribution of Gd^{3+} between ATP and other Gd-binding anions such as phosphate, sulfate, carbonate or EDTA often present in the reaction solution.

The present study revealed that the effect of Gd^{3+} on cell swelling-induced ATP release was cell type specific and showed biphasic dependence for some cells. ATP released by fibroblasts was enhanced by low concentrations of Gd^{3+}, but was inhibited by higher concentrations, although differently for different cell types. Our results vary from those of earlier studies, which did not detect stimulation of ATP release, but reported 50% to 70% inhibition by ~200 μM Gd^{3+} regardless of the cell type tested including, fibroblasts, human bronchial epithelial 16HBE14o⁻ cells, rat hepatocytes and cholangiocytes (28,30). We believe that these differences could be attributed to direct inhibition of luciferase bioluminescence combined with partial chelation of the Gd^{3+} added in those studies.

One possible mechanism of the enhanced ATP accumulation that we observed in the presence of Gd^{3+} could be inhibition of ATP hydrolysis by ecto-nucleotidases. This mechanism, however, is unlikely to contribute significantly, since ATP hydrolysis by cell ecto-nucleotidases is relatively slow at the ATP concentrations observed in our experiments (16). Thus, an increased rate of ATP release in the presence of Gd^{3+} is likely responsible for the enhanced ATP accumulation. This phenomenon may be related to the reported fusogenic effects of low concentrations of lanthanides (2), which could facilitate fusion of ATP-containing vesicles with the plasma membrane. Such a mechanism would, however, require extracellularly-applied Gd^{3+} to have access to the cytosolic side of the membrane. Although cell membranes are considered to be impermeable to lanthanides (14), a recent study suggests that La^{3+}, and to some extent Gd^{3+}, could be rapidly taken up into the cytosol of Chinese hamster ovary cells (17).

ATP release is clearly inhibited at higher Gd^{3+} concentrations of 200 μM to 500 μM. While 10 μM Gd^{3+} is often sufficient to block mechano-gated channels (19), the effects of higher Gd^{3+} concentrations may be explained in terms of Gd^{3+} interaction with the outer surface of cell membranes. Lanthanides have a high affinity for cellular membrane phospholipids, with K_d values in the micromolar range (14). Binding of lanthanides to the outer surface of cell membranes not only decreases its negative surface charge, but also produces structural changes in the membrane/water interface, lipid packing and phase equilibrium (13). Membrane-stiffening caused by Gd^{3+} could decrease a cell's osmotic sensitivity. For example, lanthanides have been reported to decrease osmotic fragility of erythrocytes, thus protecting them from hypotonic hemolysis (14).

The present data do not entirely exclude the possibility that stretch-activated channels may contribute to MS ATP release from some cell types. Although Gd^{3+} and other lanthanides were often found to have biphasic stimulator/inhibitory effects on exocytotic release of various neurotransmitters (1,14), it should be noted that small stimulation of MS channel activity by low concentrations and inhibition by higher concentrations of Gd^{3+} were reported in *E. coli* protoplasts (11). However, in *Xenopus* oocytes, which also possess MS and Gd^{3+}-sensitive channels, electrophysiological studies have demonstrated that mechanical stimuli much stronger than that required to cause ATP release failed to activate an increase in membrane conductance, ruling out the involvement of such channels in these cells (23,27,34). Further investigations are required to verify whether similar responses could be seen in cell lines tested in this study. Besides Gd^{3+}, certain anion channel blockers, such as NPPB and DIDS, were also reported to inhibit ATP release (6,20,26,29). However, our preliminary experiments showed that 100 μM NPPB caused ~20% inhibition of the luciferase bioluminescnce (data not shown). Furthermore, DIDS was also recently reported to directly interfere with luciferase activity (3). It may be desirable, therefore, to systematically re-examine the effect of various Cl channel blockers on luciferase bioluminescence before any firm conclusions can be drawn regarding their block of ATP release.

In summary, our data showing cell-specific and, for some cells, biphasic effects of Gd^{3+} on swelling-induced ATP release do not support the view that channels directly inhibitable by Gd^{3+} are involved. Rather, they are consistent with indirect effects of Gd^{3+} on lipid membranes. Therefore, other mechanisms should also be considered, such as the recently-proposed exocytotic release due to fusion of ATP-enriched vesicles involved in transporting proteins from the Golgi complex to the cell surface (23).
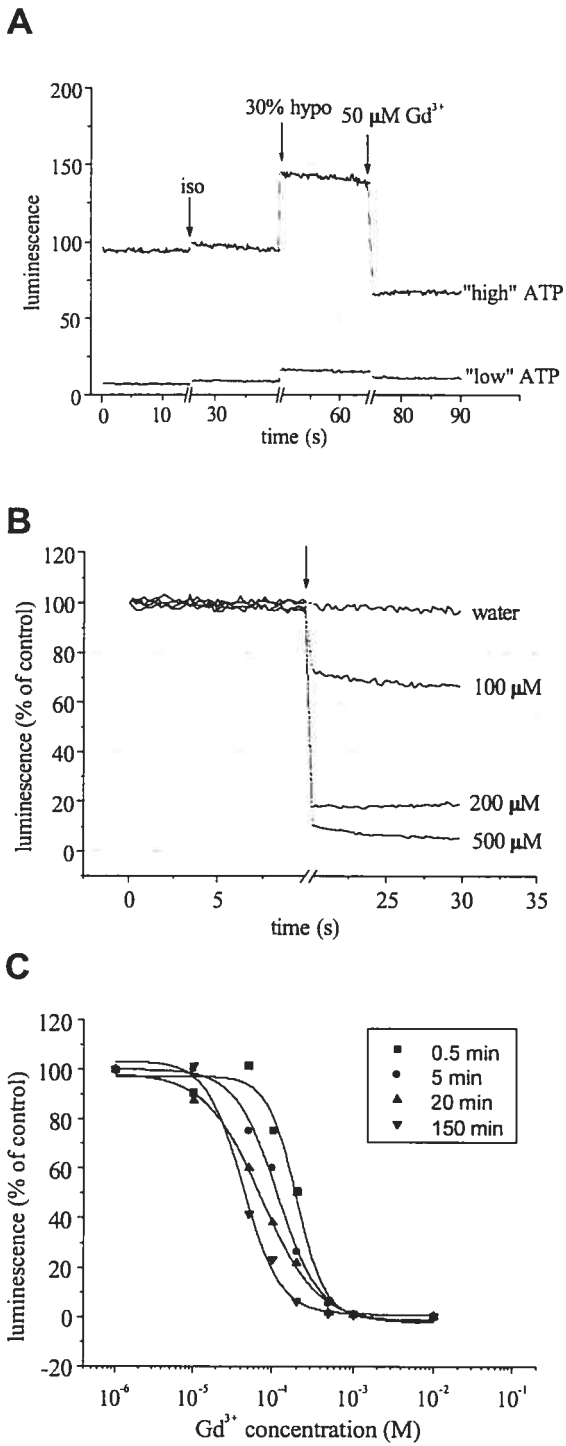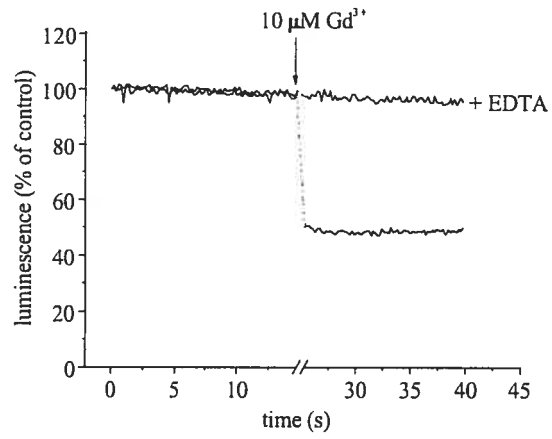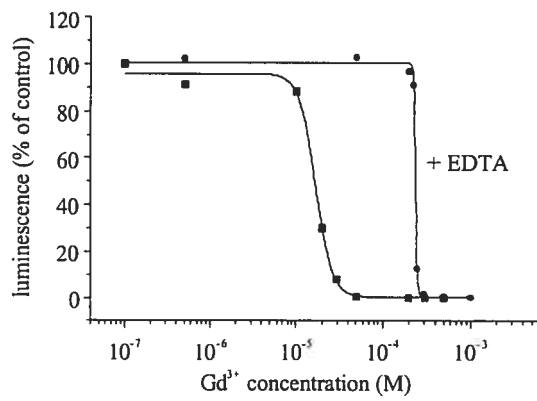
A

B

C

Figure 1

A

B

Figure 2

Figure 3

A

B

C
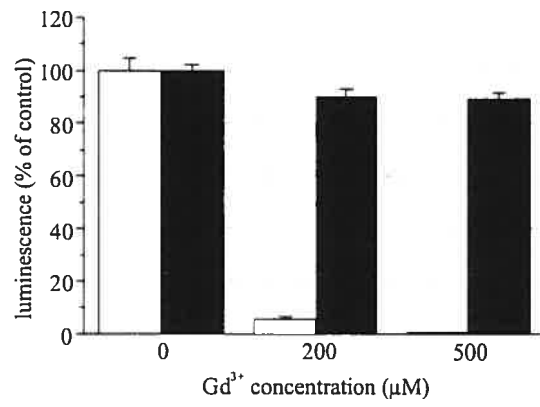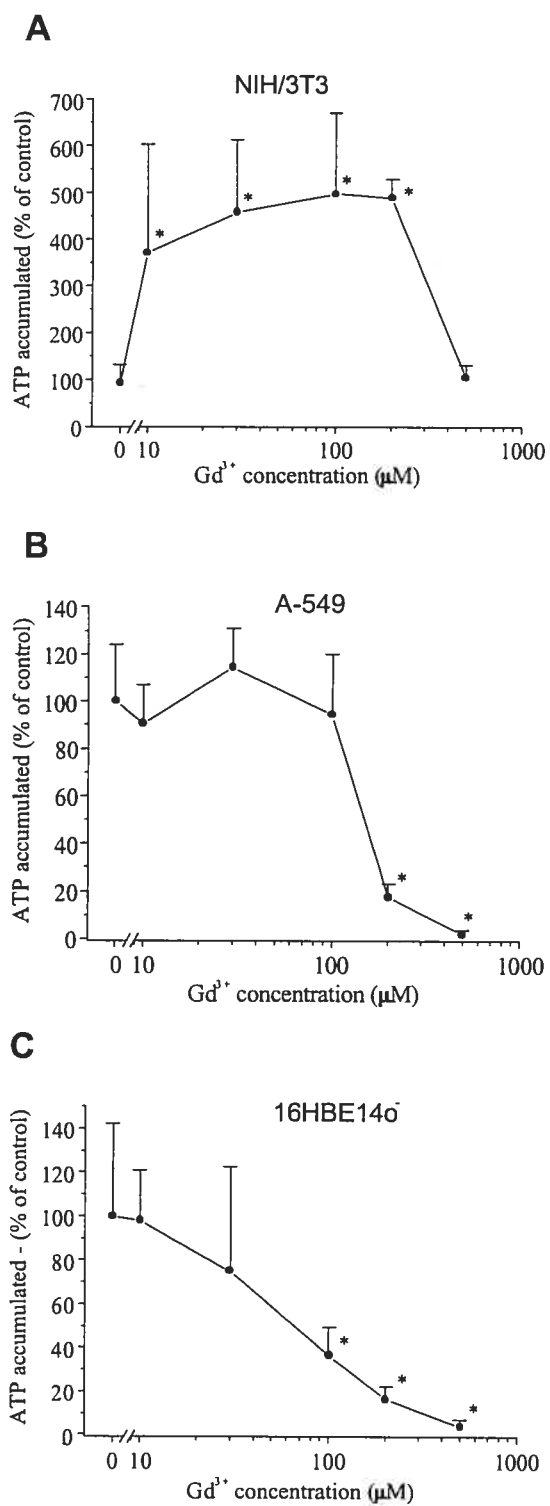

Figure 4

FIGURE LEGENDS

Figure 1.Gadolinium inhibits luciferase bioluminescence.

A. Luciferase bioluminescence is rapidly enhanced by reducing salt concentration in the sample (arrow marked *30% hypo*), while 50 μM Gd^{3+} causes rapid inhibition by ~50%. In this cell-free experiment, a test tube contained 500 μl of physiological extracellular saline and 0.1 mg/ml of commercially-available EDTA-containing luciferase reagent (see Methods for details). To reduce salt concentration in the sample, an appropriate volume of distilled water containing the luciferase reagent was added, so that only salts and ATP were diluted by 30%. The addition of isotonic saline containing luciferase had little effect on luminescence, demonstrating that enhancement of bioluminescence is not due to added fresh luciferase reagent (arrow marked *isotonic*). The traces shown here were recorded approximately 10 min after the addition of 100 nM ATP (*high ATP*, upper trace) or 10 nM ATP (*low ATP*, lower trace), when bioluminescence had already declined to approximately 50% of the initial value and reached a relatively steady level (time 0 on the graph). The relative light signal from the luminometer was acquired at the 5 Hz sampling rate and was interrupted for approximately 10 s during each addition (breaks on the time axis). The data are representative of 3 experiments.

B. Dose-dependent inhibition of bioluminescence observed with EDTA-containing luciferase reagent. The reagent concentration was 1 mg/ml. Luminescence was recorded approximately 10 min after the addition of 10 nM ATP, as described in A. Gd^{3+} was added to the test tube (arrow) at final concentrations of 100 μM, 200 μM or 500 μM. The addition of water served as a control. The figure shows that inhibition of bioluminescence required a relatively high concentration of Gd^{3+} ($\geq$100 μM), when an EDTA-containing luciferase reagent was used. The data are representative of 4 experiments.

C. Inhibition of bioluminescence by Gd^{3+} was time-dependent. Gd^{3+} was added at different concentrations to 10 nM Mg-ATP samples. At different time points, 50 μl aliquots were taken, and luciferase bioluminescence was measured after mixing with

50 μl of luciferase reagent. The luminescence observed in the absence of Gd^{3+} was set to 100%. Note the significant time-dependent shift of the dose-inhibition curve.

Figure 2.   Chelation of Gd^{3+} by EDTA shifts the luminescence dose-inhibition curve.

A. When a nominally EDTA-free luciferin/luciferase mixture was used in an experiment similar to that shown in Figure 1 B, 50% inhibition of bioluminescence was observed with 10 μM Gd^{3+}. This inhibition could be prevented by adding 250 μM EDTA. The data are representative of 3 experiments.

B. Comparison of bioluminescence dose-inhibition curves obtained in the absence and presence of 250 μM EDTA. The observed shift of the dose-inhibition curve is consistent with approximately 1:1 binding of Gd^{3+} to added EDTA. To avoid the time-dependence shown in Figure 1 C, the protocol used here was slightly modified. In the experiment in Figure 1 C, Gd^{3+} and ATP were first mixed together and incubated for different time periods before being added to the test tube containing the luciferase reagent. In this experiment, Gd^{3+} was pre-incubated with the luciferase reagent for 5 min, and then peak luminescence was recorded immediately upon the addition of 10 nM of ATP. Luminescence was normalized to that observed in the absence of Gd^{3+}.

Figure 3.   Chelation of Gd^{3+} by EGTA fully restores luciferase bioluminescence.

Luminescence observed with 100 nM Mg-ATP in samples of physiological solution containing Gd^{3+} at a final concentration of 0, 200 or 500 μM (*white bars*). Gd^{3+} was incubated with Mg-ATP for 15 min before peak luminescence was determined using Sigma F3641 luciferase reagent. Note the complete inhibition of luciferase bioluminescence by 500 μM Gd^{3+}. This inhibition could be reversed if the samples were mixed at a 1:1 ratio with a solution containing 50 mM EGTA and 10 mM $MgSO_4$. After additional 15 min incubation to chelate Gd^{3+}, bioluminescence was almost completely restored to the control level observed with the Gd^{3+}-free, EGTA-treated sample (*filled bars*). Note that the 2 sets of control samples, one treated with

EGTA and the other not treated, were set to 100%, although the EGTA-treated sample showed approximately 10% reduction in absolute luminescence due to the combined effect of a 2-fold dilution of ATP, the salt content in the sample and the presence of EGTA. The data are means ± S.D. of 6 independent experiments.

Figure 4.   Effect of Gd^{3+} on ATP accumulation in the extracellular media of hypotonically-swollen cells.

ATP efflux was stimulated by applying 50% hypotonic shock to NIH 3T3 fibroblasts (**A**), lung carcinoma A549 cells (**B**) and bronchial epithelial 16HBE14o⁻ cells (**C**) in the absence or presence of different $GdCl_3$ concentrations. This was achieved by diluting extracellular salts with hypotonic solution (see Methods) which contained $GdCl_3$ at final concentrations as indicated in the figure. 25 min after hypotonic shock, 25 µl aliquots of extracellular media were taken from control (no Gd^{3+}) and Gd^{3+}-treated cells, then mixed with 25 µl of solution containing EGTA + $MgSO_4$ to chelate Gd^{3+}. After 15 min incubation, 50 µl of the luciferase reagent was added to each sample, and peak luminescence was recorded. ATP accumulated in the extracellular media was expressed in % of control after subtraction of basal ATP content observed before hypotonic shock. The control values of ATP released by hypotonic shock i.e. in the absence of Gd^{3+} were 1.5 ± 0.6, 17 ± 4 and 11 ± 5 picomoles/10^5 cells for 3T3 fibroblasts, A549 and 16HBE14o⁻ cells respectively. The data are average ± S.E.M. of 6 cell monolayers from 2 to 3 independent experiments and, the data points showing statistically significant differences compared to the control (ANOVA and Fisher's PLSD, P < 0.05) are labeled with *. For 3T3 fibroblasts, the accumulated ATP was significantly enhanced by 10 µM to 200 µM Gd^{3+} (P ≤ 0.01), but it was not different from control for 500 µM Gd^{3+}. For A549 cells, the accumulated ATP was statistically not different from the control for Gd^{3+} concentrations of up to 100 µM, but showed significant inhibition (P < 0.0001) at 200 µM and 500 µM. For 16HBE14o⁻ cells, all tested concentrations of Gd^{3+} appear to inhibit ATP accumulation, although the effect was only statistically significant (P < 0.001) at concentrations of 100 µM and higher.

ACKNOWLEDGEMENTS

REFERENCES

1. Bales PJ, Zerbes M, Powis DA, and Marley PD. Effect of Gd^{3+} on bradykinin-induced catecholamine secretion from bovine adrenal chromaffin cells. *Br.J Pharmacol.* 128: 1435-1444, 1999.

2. Bentz J, Alford D, Cohen J, and Duzgunes N. La^{3+}-induced fusion of phosphatidylserine liposomes. Close approach, intermembrane intermediates, and the electrostatic surface potential. *Biophys.J.* 53: 593-607, 1988.

3. Bodas E, Aleu J, Pujol G, Martin-Satue M, Marsal J, and Solsona C. ATP crossing the cell plasma membrane generates an ionic current in *Xenopus* oocytes. *J.Biol.Chem.* 275: 20268-20273, 2000.

4. Bodin P, Bailey D, and Burnstock G. Increased flow-induced ATP release from isolated vascular endothelial cells but not smooth muscle cells. *Br.J.Pharmacol.* 103: 1203-1205, 1991.

5. Boucher RC. Human airway ion transport. Part one. *Am.J.Respir.Crit.Care.Med.* 150: 271-281, 1994.

6. Braunstein GM, Roman RM, Clancy JP, Kudlow BA, Taylor AL, Shylonsky VG, Jovov B, Peter K, Jilling T, Ismailov II, Benos DJ, Schwiebert LM, Fitz JG, and Schwiebert EM. Cystic fibrosis transmembrane conductance regulator facilitates ATP release by stimulating a separate ATP release channel for autocrine control of cell volume regulation. *J. Biol.Chem.* 276: 6621-6630, 2001.

7. Burnstock G, and Williams M. P2 purinergic receptors: modulation of cell function and therapeutic potential. *J.Pharmacol.Exp.Ther.* 295: 862-869, 2000.

8. Caldwell RA, Clemo HF, and Baumgarten CM. Using gadolinium to identify stretch-activated channels: technical considerations. *Am.J. Physiol.* 275: C619-C621, 1998.

9. Cheng Y, Liu M, Li R, Wang C, Bai C, and Wang K. Gadolinium induces domain and pore formation of human erythrocyte membrane: an atomic force microscopic study. *Biochim.Biophys.Acta* 1421: 249-260, 1999.

10. Cozens AL, Yezzi MJ, Kunzelmann K, Ohrui T, Chin L, Eng K, Finkbeiner WE, Widdicombe JH, and Gruenert DC. CFTR expression and chloride secretion in polarized immortal human bronchial epithelial cells. *Am.J.Cell Mol.Biol.* 10: 38-47, 1994.

11. Cui C, Smith DO, and Adler J. Characterization of mechanosensitive channels in *Escherichia coli* cytoplasmic membrane by whole-cell patch clamp recording. *J.Membr.Biol.* 144: 31-42, 1995.

12. Dubyak GR, and El-Moatassim C. Signal transduction via P2-purinergic receptors for extracellular ATP and other nucleotides. *Am. J. Physiol.* 265: C577-C606, 1993.

13. Ermakov YA, Averbakh AZ, Yusipovich AI, and Sukharev S. Dipole potentials indicate restructuring of the membrane interface induced by gadolinium and beryllium ions. *Biophys. J.* 80: 1851-1862, 2001.

14. Evans CH. *Biochemistry of Lanthanides*. New York, London: Plenum Press, 1990.

15. Fujimori T, and Jencks WP. Lanthanum inhibits steady-state turnover of the sarcoplasmic reticulum calcium ATPase by replacing magnesium as the catalytic ion. *J.Biol.Chem.* 265: 16262-16270, 1990.

16. Grygorczyk R, and Hanrahan JW. CFTR-independent ATP release from epithelial cells triggered by mechanical stimuli. *Am.J.Physiol.Cell Physiol.* 272: C1058-C1066, 1997.

17. Halaszovich CR, Zitt C, Jungling E, and Luckhoff A. Inhibition of TRP3 channels by lanthanides. Block from the cytosolic side of the plasma membrane. *J.Biol.Chem.* 275: 37423-37428, 2000.

18. Hamill OP, and Martinac B. Molecular basis of mechanotransduction in living cells. *Physiol Rev.* 81: 685-740, 2001.

19. Hamill OP, and McBride DW, Jr. The pharmacology of mechanogated membrane ion channels. *Pharmacol.Rev.* 48: 231-252, 1996.

20. Hazama A, Shimizu T, Ando-Akatsuka Y, Hayashi S, Tanaka S, Maeno E, and Okada Y. Swelling-induced, CFTR-independent ATP release from a human epithelial cell line: lack of correlation with volume-sensitive Cl⁻ channels. *J.Gen.Physiol* 114: 525-533, 1999.

21. Koyama T, Oike M, and Ito Y. Involvement of Rho-kinase and tyrosine kinase in hypotonic stress-induced ATP release in bovine aortic endothelial cells. *J.Physiol.* 532: 759-769, 2001.

22. Lazarowski ER, Homolya L, Boucher RC, and Harden TK. Direct demonstration of mechanically induced release of cellular UTP and its implication for uridine nucleotide receptor activation. *J.Biol.Chem.* 272: 24348-24354, 1997.

23. Maroto R, and Hamill OP. Brefeldin A block of integrin-dependent mechanosensitive ATP release from *Xenopus* oocyte reveals a novel mechanism of mechanotransduction. *J.Biol.Chem. 276:23867-23872,* 2001.

24. Martell AE, and Smith RE. *Critical Stability Constants. Inorganic Complexes.* New York: Plenum, 1974.

25. McElroy M C, and DeLuca, M. Chemistry of firefly luminescence. In Herring PJ, ed. *Bioluminescence in Action.* London, New York, San Francisco: Academic Press, 1978, 109-127.

26. Mitchell CH, Carre DA, McGlinn AM, Stone RA, and Civan MM. A release mechanism for stored ATP in ocular ciliary epithelial cells. *Proc Natl Acad Sci U S A* 95: 7174-7178, 1998.

27. Nakamura F, and Strittmatter SM. P2Y1 purinergic receptors in sensory neurons: contribution to touch- induced impulse generation. *Proc. Nat.l Acad. Sci. U. S. A.* 93: 10465-10470, 1996.

28. Roman RM, Feranchak AP, Davison AK, Schwiebert EM, and Fitz JG. Evidence for Gd^{3+} inhibition of membrane ATP permeability and purinergic signaling. *Am.J. Physiol.* 277: G1222-G1230, 1999.

29. Sauer H, Hescheler J, and Wartenberg M. Mechanical strain-induced Ca^{2+} waves are propagated via ATP release and purinergic receptor activation. *Am.J.Physiol. Cell Physiol.* 279: C295-C307, 2000.

30. Taylor AL, Kudlow BA, Marrs KL, Gruenert DC, Guggino WB, and Schwiebert EM. Bioluminescence detection of ATP release mechanisms in epithelia. *Am. J. Physiol.* 275: C1391-C1406, 1998.

31. Wang Y, Roman R, Lidofsky SD, and Fitz JG. Autocrine signaling through ATP release represents a novel mechanism for cell volume regulation. *Proc. Natl. Acad. Sci. U. S. A.* 93: 12020-12025, 1996.

32. Yang XC, and Sachs F. Block of stretch-activated ion channels in *Xenopus* oocytes by gadolinium and calcium ions. *Science* 243: 1068-1071, 1989.

33. Yang Z, Batra R, Floyd DL, Hung HC, Chang GG, and Tong L. Potent and competitive inhibition of malic enzymes by lanthanide ions. *Biochem.Biophys.Res.Commun.* 274: 440-444, 2000.

34. Zhang Y, and Hamill OP. On the discrepancy between whole-cell and membrane patch mechanosensitivity in *Xenopus* oocytes. *J.Physiol.* 523(1): 101-115, 2000

EVALUATION OF RAPID VOLUME CHANGES OF SUBSTRATE-ADHERENT CELLS BY CONVENTIONAL MICROSCOPY 3D IMAGING

Francis Boudreault and Ryszard Grygorczyk

Research Centre, (CHUM) – Hôtel-Dieu, and Department of Medicine, Université de Montréal, Montréal, Québec, Canada

ACCORD DES COAUTEURS

Identification

Francis Boudreault
Ph.D. en Génie Biomédical

Description de l'article
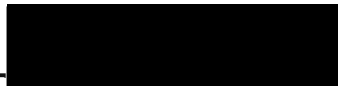
Francis Boudreault et Ryszard Grygorczyk
Conventional microscopy 3D imaging technique to evaluate rapid volume changes of
substrate-adherent cells
Journal of Microscopy, à paraître en septembre 2004

Déclaration de tous les coauteurs autres que l'étudiant

À titre de coauteur de l'article identifié ci-dessus, je suis d'accord pour que *Francis Boudreault* inclue cet article dans sa thèse de doctorat qui a pour titre: *Contribution à l'étude du mécanisme de sécrétion d'ATP par des cellules épithéliales pulmonaires et des fibroblastes soumis à un choc hypotonique.*

Ryszard Grygorczyk   13 Aug. 2004
Coauteur   Signature   Date

ABSTRACT

Precise measurement of rapid volume changes of substrate-adherent cells is essential to understand many aspects of cell physiology. Yet, techniques to evaluate volume changes with sufficient precision and high temporal resolution are limited. Here, we describe a novel imaging method that surveys the rapid morphology modifications of living, substrate-adherent cells based on phase-contrast, digital video microscopy. Cells grown on a glass substrate are mounted in a custom-designed, side-viewing chamber and subjected to hypotonic swelling. Side-view images of a rapidly-swelling cell are acquired, and at the end of the assay, an image of the same cell viewed from a perpendicular direction through the substrate. Based on these images, off-line reconstruction of 3D cell morphology is performed, which precisely measures cell volume, height and surface at different points during cell volume changes. Volume evaluations are comparable to those obtained by confocal laser scanning microscopy (ΔVolume $\leq$14%), but our method has superior temporal resolution limited only by the time of single-image acquisition, typically ~100 ms. The advantages of using standard phase-contrast microscopy without the need for cell staining or intense illumination to monitor cell volume make this system a promising new tool to investigate the fundamentals of cell volume physiology.

Keywords: cell volume, hypotonic shock, regulatory volume decrease, digital video microscopy, 3D cell imaging

ABBREVIATIONS:
1-HAF – 1-hexadecanoylaminofluorescein
CLSM – confocal laser scanning microscopy
DISUR – dual image surface reconstruction
RVD – regulatory volume decrease
SICM – scanning ion conductance microscopy

INTRODUCTION

Accurate measurements of rapid cell volume changes in response to different stimuli are essential in studies examining many aspects of cell physiology and pathology, including cell volume sensor identification Mongin and Orlov, (2001); Lang et al., (1998); Wehner et al., (2003). However, commonly-available methods of cell volume evaluation have several limitations of accuracy, temporal resolution and applicability to specifically-prepared cells. For example, the Coulter counter technique can only be used with floating, ideally almost perfectly spherical cells. Substrate-adhering cells must, therefore, be dispersed, e.g. by trypsinization, which may modify signaling pathways and, thus, cell volume responses. Moreover, this method does not distinguish between changes in cell shape and cell volume, making volume readings prone to artifacts. Relative modifications in the cell water content of substrate-adherent cells could be monitored with high temporal resolution by measuring alterations in intracellular ion concentration with ion-selective electrodes Alvarezleefmans et al., (1992), or fluorescence intensity emitted by cells loaded with an appropriate fluorescent probe Crowe et al., (1995). The latter technique, however, could suffer from dye leakage and photobleaching. In addition, the properties of some fluorophores could be affected by variation of $[Ca]_i$, pH or cytoplasm viscosity during cell volume changes. Light microscopy techniques, such as video-enhanced contrast microscopy, have been developed to assess cell shape and volume. Since such methods provide 2-dimensional (2D) cell images, cell volume could be inferred only indirectly for cells of well-defined shape.

Optical microscopy techniques usually have good temporal resolution, but spatial resolution is often limited by poor visibility of the plasma membrane. Other optical techniques for cell volume determination employ laser light-scattering or spatial filtering microscopy Mcmanus et al., (1993); Farinas et al., (1997), but do not provide detailed information on the shape of individual cells. Full 3D information on cell shape is possible with confocal laser scanning microscopy (CLSM), atomic force microscopy and scanning ion conductance microscopy (SICM) Korchev et al., (2000); Korchev et al., (1997). However, acquisition of a full set of images with CLSM usually requires about 1 min. Such temporal resolution does not permit

monitoring of rapid volume changes induced by osmotic shock, where regulatory volume decrease (RVD) or increase is often fully completed within 2-3 min. Further limitations are related to photodynamic damage of cells during longer exposure to laser light Saito et al., (1998); Kunz and Stark, (1997). This problem is avoided with scanning probe microscopy, such as SICM, which is also capable of providing high resolution images of membrane structures, such as lamellipodia, dendrites and microvilli. Like CLSM, however, its time resolution does not allow monitoring of rapid cell volume changes. Faster volume changes could be monitored with these techniques by limiting the measurements to 1D, that is, cell height. Cell height estimation may be sufficient in some situations, as in the case of cell monolayers, where expansion is restricted mainly to the vertical direction. Other techniques have been developed to assess changes in cell height as, for example, by monitoring the position of fluorescent beads deposited on the cell surface Van Driessche et al., (1993) or by measuring current through a patch electrode positioned above the cell, an arrangement similar to that deployed in SICM Kawahara et al., (1994).

We were interested in assessing, with high temporal and spatial resolution, rapid volume changes of intact, substrate-adherent single cells, and found that none of the methods described above could adequately satisfy these requirements. We, therefore, developed a novel approach based on phase-contrast, digital video microscopy. During the experiment, side-view images of rapidly-swelling cells attached to a glass substrate were acquired. An image of the same cell viewed from the perpendicular direction through the substrate was also recorded at the end of the assay. During off-line analysis, 3D topographical maps of the cell surface were reconstructed, and thus cell volume and surface area could be determined for each time point. Cell volume could be measured with accuracy similar to CLSM (ΔVolume $\leq 14\%$), but our method had significantly higher temporal resolution limited only by the time needed to acquire a single image. Because no special treatment of cells is required, they could be maintained viable under near-physiological conditions throughout the experiment.

METHODS

Side-view chamber

To evaluate the morphology of a substrate-adherent cell and to follow its changes during hypotonic challenge, we designed the flow chamber shown in Figure 1. A glass coverslip with attached cells was mounted vertically in the chamber and perfused continuously with pre-warmed saline (37°C, 1.3 ml/min). The chamber was placed on the stage of a NIKON TE300 inverted microscope (Nikon Canada Inc., Montreal, QC) and attached to a motorized xy-stage translator which allowed fine positioning of the chamber. Vertical mounting of the coverslip permitted visualization of the lateral shape of cells localized close to the lower edge of the coverslip (Figure 1A). The exact position of the cell of interest along the lower coverslip edge (x-axis) was measured with a digital caliper attached to the microscope stage. A top view – an inverted image of a cell viewed from the bottom – of the same cell was also recorded at the end of the experiment. For this purpose, the coverslip was removed from the chamber and laid flat in a solution-filled Petri dish. The selected cell was then localized from its predetermined x-position along the coverslip edge. As discussed below, for the substrate-adherent cells used in this study, it was sufficient to acquire a single top-view image, because the shape of the cell base was found to be invariant during cell volume changes.

Imaging

Phase contrast images of cell side-view profile and top-view of the cell base were recorded for 100 ms with a T57 MICROMAX CCD camera (Princeton Instruments, Trenton, NJ) and MetaFluor software (Universal Imaging, West Chester, PA). The camera chip had 512x512 resolution with individual pixels of 13 μm in size. The use of a 20X objective combined with the presence of a 4X zoom lens attached to the camera resulted in 0.16-μm/pixel resolution (13 μm/20/4). Pixel coordinates were converted into physical dimensions according to this ratio. Images were saved on hard disk and analyzed off-line. For validation experiments (see below), cells were illuminated with light emitted from a 100 W mercury lamp passed through a narrow bandwith 490 nm filter (Chroma Technology, Brattleboro, VT). Fluorescence

emission images were observed using a GFP filter block (Chroma Technology) and recorded as described above.

Cell surface reconstruction

To reconstruct the 3D topography of the cell surface, we developed a method based on cell images acquired from 2 perpendicular directions, and named it dual image surface reconstruction (DISUR). The end result of the DISUR procedure is a stack of slices similar to a stack of images extracted with a confocal microscope. The outline of the cell base observed close to the glass substrate serves as a template to generate a stack of cell slices. As we progress from the cell base to its summit, the slice outline is progressively shrunk in a proportion dictated by the cell side-view profile. Digitization of the cell profile and cell base as well as reconstruction of cell 3D topographical maps are described in more detail in the APPENDIX. Cell volume, surface and height were calculated from such a reconstructed cell model. All calculations were carried out entirely with EXCEL (Microsoft, Redmond, WA).

To visualize the reconstructed cell model in 3D perspective, data obtained with the help of the DISUR technique or with CLSM were used to generate a 2D matrix containing the approximate z-coordinates of points on the membrane surface. The 3D perspective of the model cell was then plotted with ORIGIN (Microcal Software, Northampton, MA).

Validation

Fluorescent staining and fixation. For confocal and epifluorescence imaging of the cell surface, the plasma membrane of A549 cells was stained with the fluorescent lipophilic dye 1-hexadecanoylaminofluorescein (1-HAF, Molecular Probes, Eugene, OR) applied for 5 min (~15 µM, room temperature). The cells were then fixed with 3% formaldehyde in PBS solution. Cell fixation allowed the morphology of the same cell to be evaluated by both DISUR and CLSM.

Confocal Laser Scanning Microscopy. A Zeiss AXIOVERT LSM510 microscope equipped with a confocal system laser (488 nm - argon) scanned the cell body. Each scanning plane was separated by 0.4 or 0.5 µm. Fluorescence emission was collected

at 0.14-μm/pixel resolution with an Apochromat 63X (N.A.=1.4) oil-immersion objective.

3D reconstruction of hypotonically-swelling cells

In the course of this study, we observed that A549 cells exposed to hypotonic shock stay firmly attached to the substrate throughout the challenge. As a result, the outline of their base remains nearly invariant, even during significant (~3-fold) volume expansion. Therefore, to reconstruct cell 3D morphology at different time points during hypotonic cell swelling, it was sufficient to acquire a single image of the cell viewed from the top, in addition to a series of side-view images. During the experiment, a series of side-view images were acquired at 15- to 60-s intervals, and at the end of the experiment, the coverslip was removed from the chamber, and the cell top-view image recorded.

Cells

Human adult lung carcinoma A549 cells were grown in DMEM supplemented with 10% FBS, 20 mM L-glutamine, 60 μg/mL penicillin-G and 100 μg/mL streptomycin. All constituents of the culture media were from GIBCO-BRL (Burlington, ON). Cells were grown on small 22x22-mm glass coverslips.

Solutions

Physiological saline solution contained (in mM) 140 NaCl, 5 KCl, 1 $MgCl_2$, 1 $CaCl_2$, 10 glucose and 10 HEPES, pH 7.4, adjusted with NaOH. All reagents were from Sigma (Oakville, ON). To apply hypotonic shock, the cells were perfused with media of lower tonicity prepared by reducing NaCl and KCl concentration but keeping the concentration of divalent cations constant.

RESULTS

Validation by CLSM

To evaluate the accuracy of DISUR, we analyzed and reconstructed the same set of cells with both DISUR and CLSM. Because it was unfeasible to simultaneously observe the same living cell with both techniques, the cells were fixed with 3% formaldehyde prior to imaging. Three randomly-selected cells were imaged and 3D-reconstructed with the DISUR procedure. The cells were kept overnight at 4°C and then individually scanned with CLSM to generate a stack of cell cross-section images every 0.4 or 0.5 μm along the z-axis. Cell cross-section outlines were digitally processed, and the entire cell morphology reconstructed, as explained in METHODS.

Cell geometry from phase-contrast-acquired images was similar to epifluorescent-acquired images of the same 1-HAF-stained cells (data not shown), and only an example of the fluorescent side-view and top-view images of a selected cell (cell A, see Table 1) is shown in Figure 2A (top and bottom). A picture of the cell profile was taken with the coverslip mounted in the side-view chamber, and an outline of the cell base was obtained in a standard top-view configuration after placing the same coverslip in a 35-mm Petri dish. Although the DISUR technique allows us to select any distance separating planes of reconstruction, we chose here a 0.4-μm z-distance increment to standardize the data with CLSM. The results of such reconstructions are the cell surface cross-section curves shown in Figure 2B, which are projected on a single plane and thus resemble a topographic map of the cell with level curves. To visualize the cell in 3D perspective, point coordinates were converted to fit in an appropriately-sized matrix containing z-position information in relation to xy-coordinates. After numerical smoothing to decrease surface roughness introduced during the process of matrix calculation, a color-coded plot indicating height was generated (Figure 2C).

The same cell was then analyzed with CLSM. Scanning the entire cell along the z-axis with confocal microscopy required the acquisition of 16 planes which are shown in Figure 2D. A 3D view had been also generated from a matrix calculated

according to the procedures described above (Figure 2E). The similarity of cell shape, reconstructed with both methods, is demonstrated in Figures 2C and 2E. As seen in Table 1, the differences in cell height, surface and volume determined by both DISUR and CLSM from 3 different cells did not exceed 17%, 14% and 14% respectively, proving the validity of our system.

Kinetics of hypotonic cell swelling evaluated by DISUR

Volume changes of single A549 cells were triggered by acute 50% reduction of tonicity of the perfused solution. Figure 3 shows that an A549 cell (cell D, see Table 2), when exposed to hypotonic medium, went through a complete swelling-shrinking cycle, which lasted approximately 10 min. The cell reached maximum volume during the first 90 s, and after a short plateau, shrank back to the original volume in the next 5 min. The reconstructed 3D shape of the cell before and after 1.4- and 1.9-fold change of its initial volume is also illustrated in Figure 3. It reveals that, during swelling, the cell upper membrane rose mainly in a vertical direction in a symmetric manner with respect to the cell apex, while the cell base did not expand in the *xy*-plane. We rarely observed a noticeable cell base expansion, even at 2- to 3-fold volume increase.

Changes of cell height and surface

Figure 4 shows that cell volume, height and surface increased simultaneously during the swelling phase and remained constant during the volume plateau. However, this synchronicity was lost during RVD; cell height declined at a slower pace than volume, and at 10 to 15 min, it remained slightly elevated although volume had returned to its original level. At the end of RVD, the cell appeared to reorganize its shape without any further changes in volume. This emphasizes the DISUR advantage which detects changes in cell shape, as opposed to techniques which rely solely on cell height to infer volume. In such a situation, other methods may miscalculate the real dynamics of volume restoration.

Our experiments have revealed that the maximal cell volume increase in response to 50% hypotonic shock was always close to 90%, while changes in height

and surface were much smaller (Table 2). This is likely the result of an elementary geometric relationship; for example, for a 2-fold volume increase, very flat cells require much less change of surface area compared to rounded cells. Thus, initial cell geometry dictates the magnitude of changes in height and surface that a given cell will experience. To the best of our knowledge, this is the first time such a fundamental result has been demonstrated.

The relative changes in surface reported here are based on calculations of the whole cell surface, including the membrane area of the cell base gripping the coverslip. Conceptually, swelling of adherent cells likely involves only the upper portion of the cell membrane, which is free to expand. Therefore, relative changes in cell surface area will be higher with respect to the freely-expandable portion of the cell membrane.

DISCUSSION

The imaging method described here allowed us to view the side profile of substrate-attached A549 cells and to observe their changes in response to hypotonic shock with high temporal resolution. Enough information could be extracted from the combination of side-view and top-view time-lapse images to reconstruct the entire 3D shape of the cell at specific time-points with the DISUR method. Validation experiments showed that estimates of cell volume, surface and height calculated from the DISUR 3D cell model were very close to those obtained with confocal microscopy, making this method an attractive tool to evaluate the fast morphology changes of adherent cells. Its advantages also include the use of standard phase-contrast microscopy without the need for cell staining or intense illumination to monitor cell volume. We utilized a motorized xy-stage translator for convenient high precision positioning of the chamber, but this is not an absolute requirement. Our initial experiments were performed successfully with a manual mechanical microscope stage. Because substrate-adherent cells are studied with this method, it allows the monitoring of cell responses submitted to experimental manipulations similar to those usually performed with cells plated on a Petri dish. Drugs could be applied and washed away, and perfusate temperature could be changed as needed.

The DISUR method permits us to directly view how cell volume responds to a given stimulus. For example, the reconstructed 3D cell models assembled in a time-lapse movie permitted us to visualize 3D changes of cell shape during hypotonic shock, a feature that could help to improve our understanding of cell swelling and RVD processes.

It is also important to note certain limitations of the method. Many cell types are prickled with microvilli and deep membrane invaginations. These structures are too small to be resolved with phase contrast microscopy, although the same applies to several other methods, including confocal laser microscopy. As a result, the reconstructed surface of a model cell is stripped of such microstructures. This may underestimate the true surface area of the plasma membrane. Nevertheless, our technique permits estimation of the minimal amount of membrane necessary to adapt to increasing cell volume, an important parameter to quantify the magnitude of membrane stretch a cell may experience.

In our initial experiments, to enhance cell membrane visibility and to better visualize the profile of swelling cells, we used the lipophilic fluorophore 1-HAF. Although membrane visibility was improved, we noticed that the RVD was abolished in these cells. Intense illumination with 490 nm wavelength light via a wide band filter was the likely cause of this effect, since RVD was not hindered in cells outside the illumination field. Whether the dye itself or the production of reactive oxygen species by light exposure Saito et al., (1998) was accountable for the inhibition of RVD remains to be investigated. In later experiments, to avoid interference with cellular physiology, we decided not to apply fluorophores or intense light. We were able to image cells with standard phase contrast microscopy to satisfactorily distinguish cell profile from background, and evaluate cell silhouette with accuracy sufficient for volume measurements.

In our studies, the base of A549 cells, seen from the standard top-view, remained unperturbed during the entire swelling/shrinking process. This observation, however, should be verified for each new cell type to be tested in the future. An elegant, but somehow complex solution will require both views of the cell to be followed in real-time: side and top. This amelioration could be achieved with a prism,

mirror or other optical devices. Although such modifications may increase the complexity of the technique, if successful, it may greatly expand DISUR capabilities. We are also looking forward to simplifying the mathematics of cell volume and surface calculation. For instance, a thorough investigation of cell topology may identify parameters that govern cell shape, or calculus-based equations instead of linear algebra may help to avoid repetitive calculations.

In a preliminary analysis of a small number of A549 cells, we repeatedly observed a general pattern of responses to hypotonic shock consisting of swelling-plateau-RVD. In all analyzed cells, the time required to reach maximal expansion was remarkably constant, but the duration of the plateau and the time required for volume restoration showed variability. Complete analysis of a large population of cells is warranted for a thorough understanding of such heterogeneity of cell volume restoration. Our technique, in its present form, allows us to monitor a sharply-focused side-view image of only 1 cell at a time. Therefore, it is not possible to simultaneously monitor volume changes of several cells. Although reconstructing a large number of cells might be a time-consuming process, it will be rewarded by gaining detailed information about individual cell responses. Such information is lost when using high-throughput techniques, such as the Coulter counter, which averages responses from a large number of cells.

In summary, we consider DISUR to be a promising new tool to study cell volume responses to various stimuli. Importantly, by using standard light microscopy, the adverse effects of UV light are avoided, and cells retain their functionality throughout the experiment. The method allows direct viewing of a time-lapse movie of a single adherent cell swelling rapidly and then shrinking back to its original proportions after hypotonic shock. This unique feature combined with the capability of measuring absolute changes in cell volume and surface should greatly improve our understanding of cell volume regulation under physiological and pathological conditions.
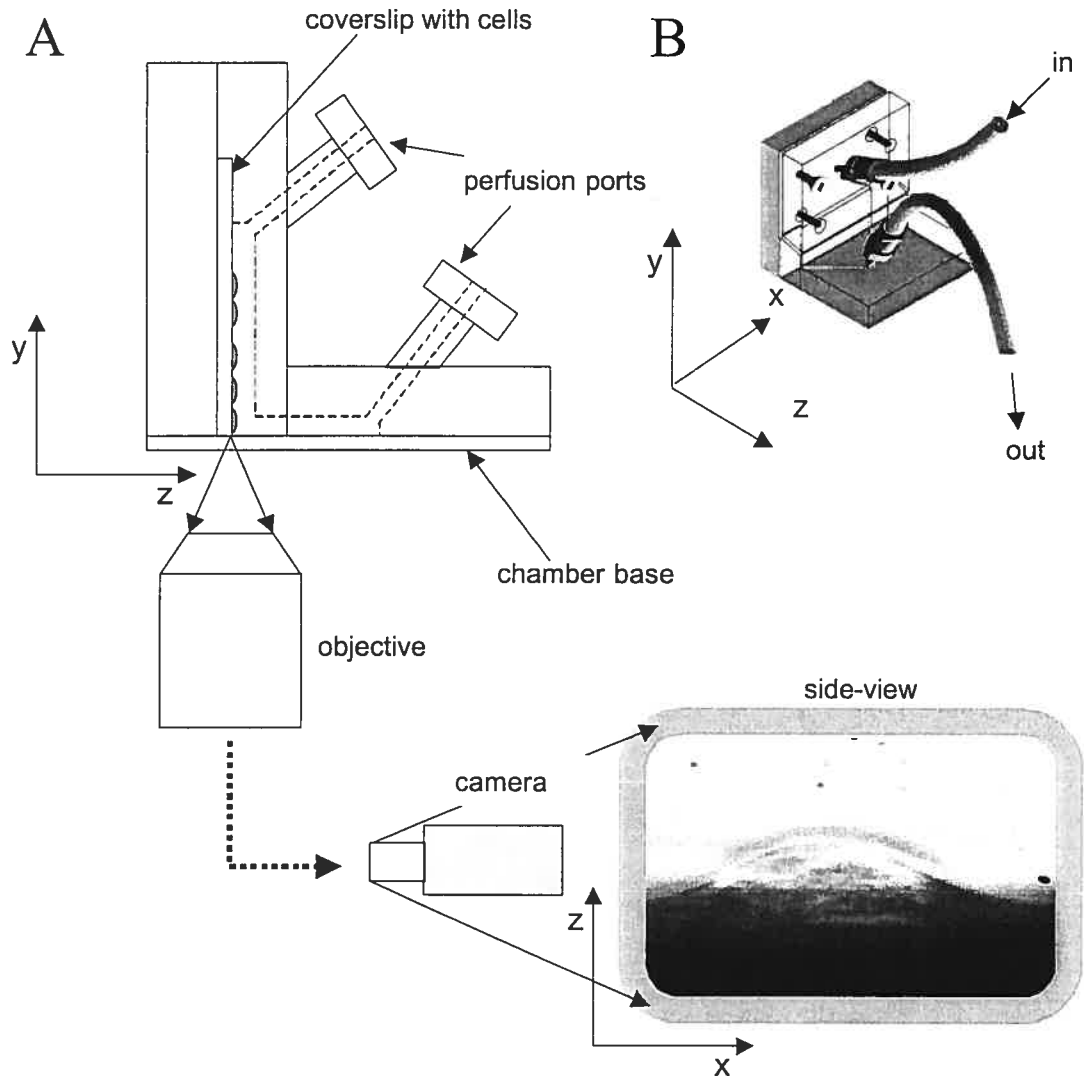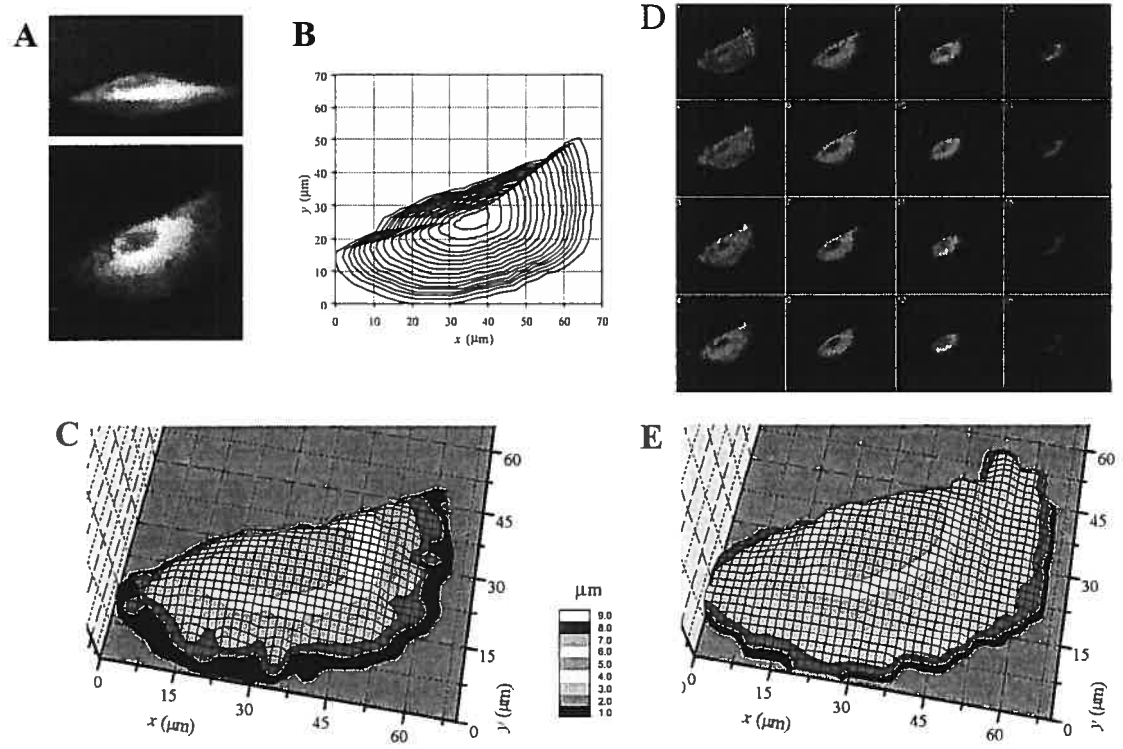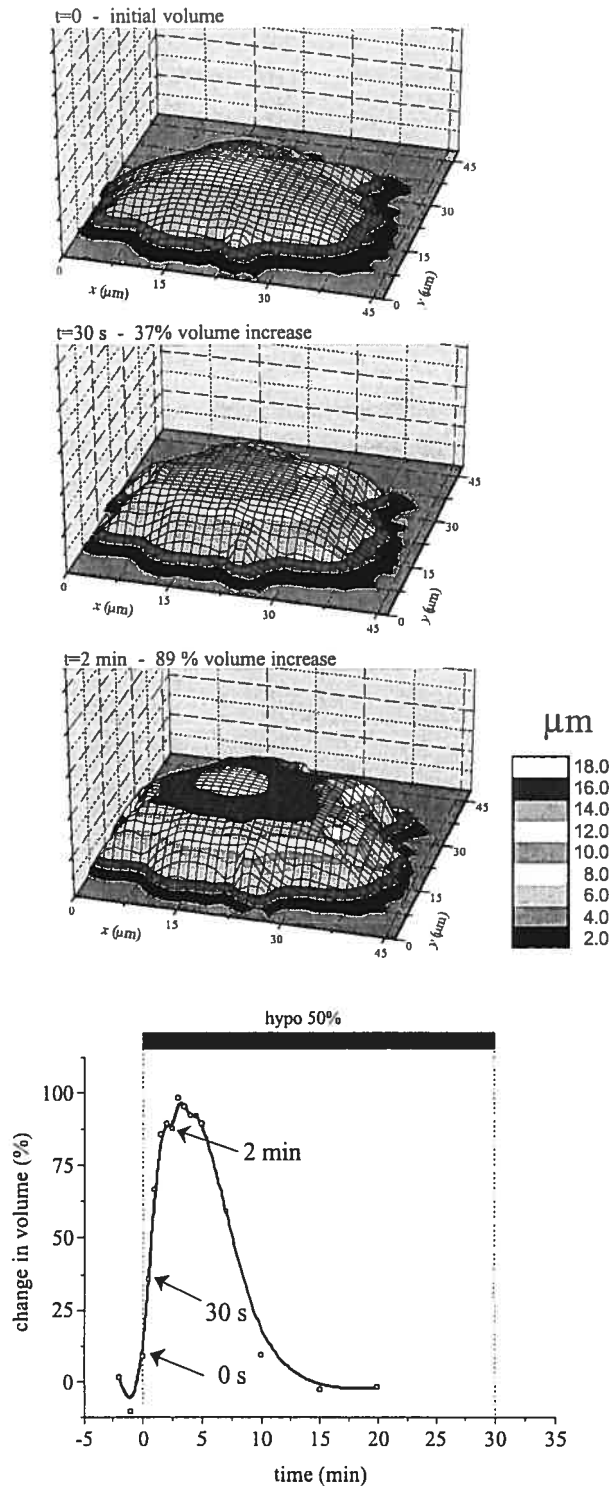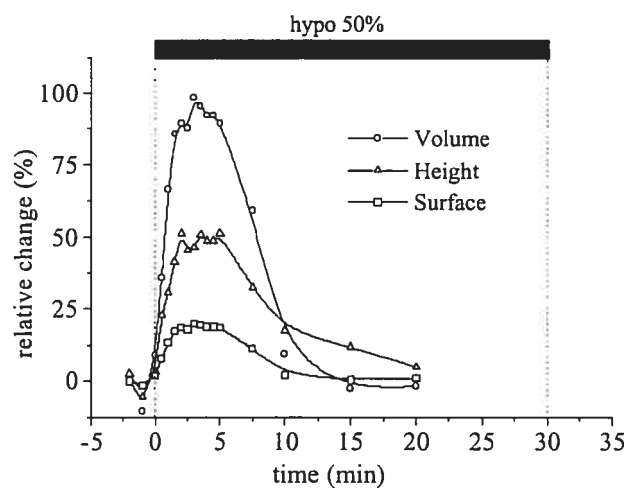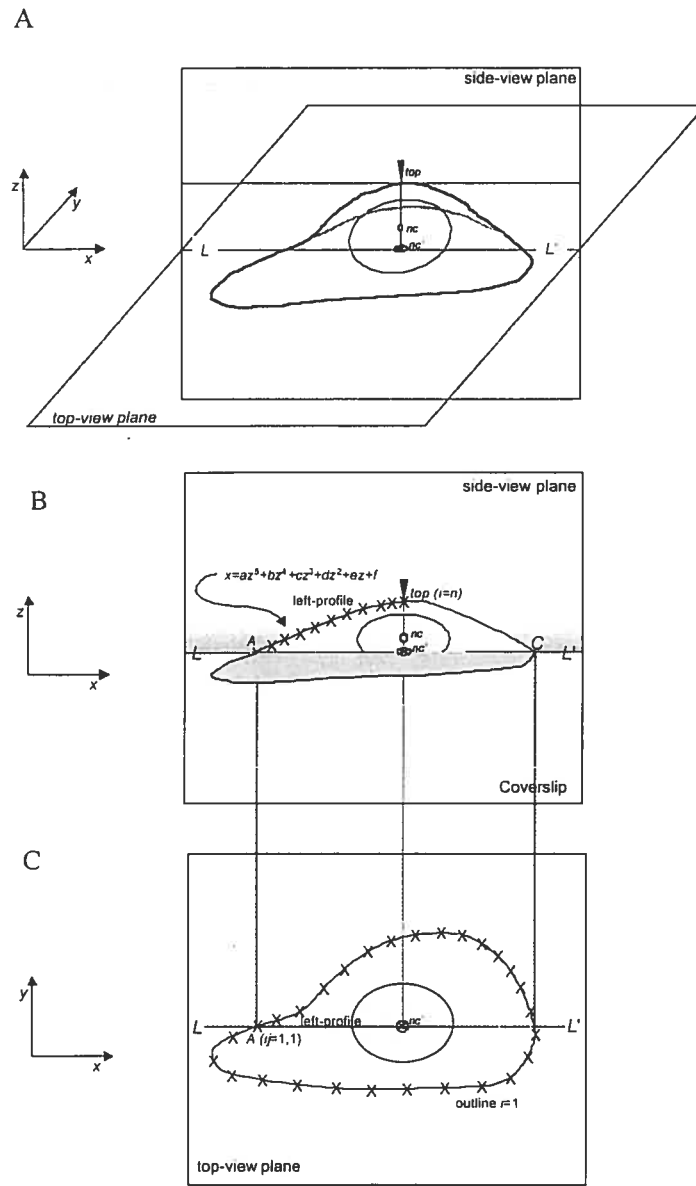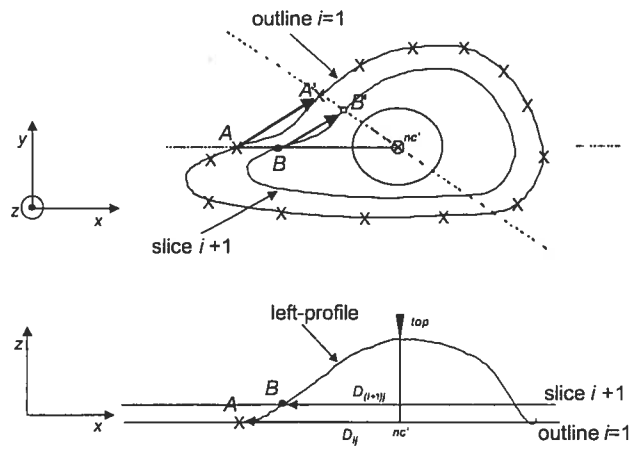
Figure 1

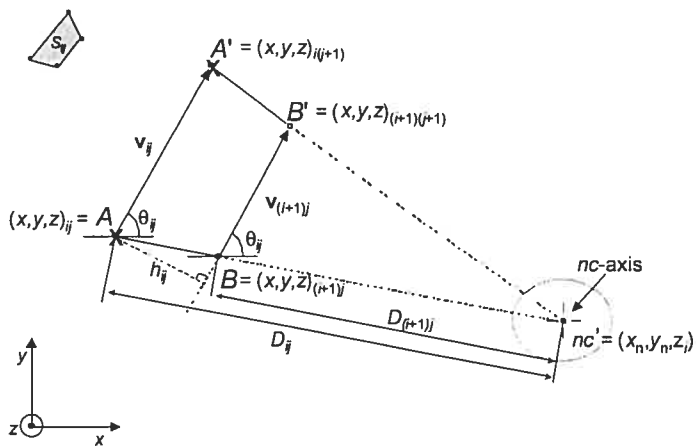Figure 2

Figure 3

Figure 4

A
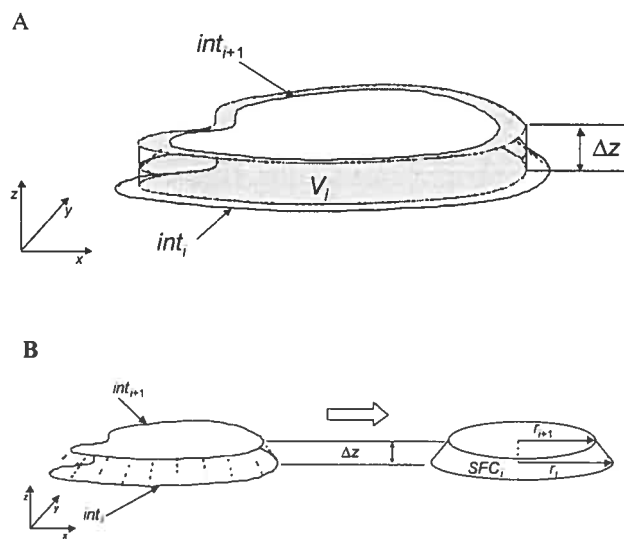

B

C

Figure 5

Figure 6

Figure 7

FIGURE LEGENDS

Figure 1. Side-view flow chamber

A: Functional diagram of the side-view chamber. The acrylic side-view chamber is glued at its base to a ~170-μm thick glass coverslip. A standard 22x22-mm coverslip, serving as a substrate for cells, is positioned vertically along the inner chamber wall with the cover of the chamber tightly screwed above. In this orientation, the lower coverslip edge is facing the microscope objective, and its surface covered with cells is oriented in the $+z$-direction. The nominal depth of the cavity inside the chamber is approximately 0.5 mm, and the total inner volume approximates 200 μL. A video-recorded phase-contrast image of an adherent cell profile close to the lower edge is shown at the bottom right.

B: Isometric perspective of the side-view chamber. The tubes circulate a warm fluid (T=37°C) inside the chamber cavity. The orientation of the Cartesian coordinate system shown here is used throughout this study.

Figure 2. Comparison of 3D cell reconstructions with the DISUR and CLSM techniques

A: Side-view (top) and top-view (bottom) fluorescent images of a single, fixed cell. The cell, marked A in Table 1, was fixed with 3% formaldehyde prior to imaging.

B: Plasma membrane mapping of cell A. All slices generated from cell A are plotted in the xy-plane, producing a graph similar to a topographical map. Each closed curve lies in an horizontal plane separated by 0.4 μm along the z-axis. The "altitude" is increasing from the cell outskirts to the centre.

C: 3D visualization of cell A from DISUR-generated data. As detailed in METHODS, the entire set of data coordinates generated by the DISUR technique was transformed to visualize cell A in a 3D perspective. Each color-coded region of the image corresponds to a region 1.0-μm thick.

D: Stack of confocal images acquired from cell A. Sequential images are shown (from top to bottom and left to right) separated by 0.4 μm along the z-axis. The images were acquired with a confocal microscope from the same formaldehyde-fixed and 1-HAF-stained cell (see METHODS) as in A. Note the striking similarity between the silhouette of the cell plasma membrane for each confocal plane and the "topographic map" of the same cell shown in B, generated with the DISUR technique.

E: 3D visualization of cell A from a stack of confocal images. The cell outlines in the 16 confocal planes shown in D were digitized and processed as described in METHODS to obtain a 3D view of the cell. Note the similarity of cell 3D shape reconstructed by both CLSM and the DISUR methods (see C).

Figure 3. Kinetics of volume changes in a single swelling A549 cell

Cells were mounted in the side-view chamber, and at time 0, the perfusion solution was switched from isotonic to 50% hypotonic. Cell side-view pictures were recorded every 15 s. The DISUR technique was subsequently used to reconstruct cell 3D shape at each time point. In the example shown here, cell volume (cell D, see Table 2) was calculated from the reconstructed model. In response to hypotonic shock, cell volume expanded by an average of 92% in approximately 1 min 30 s. After a 3-min plateau, the cell returned to its original volume in the next 5 min. Isometric 3D cell models are shown at the onset of shock (initial volume), and when cell volume increased 1.4- and 1.9-fold. Note that the cell apex is progressively rising during cell volume expansion, but no lateral expansion of the cell base is observed. Cell height is shown in color-coded scale.

Figure 4. Comparison of cell height, surface and volume changes during swelling and RVD

After 50% hypotonic challenge, cell volume changes were paralleled by a progressive increase in cell height and surface. A representative example is shown here (cell D). Maximal expansion of cell volume, surface and height (cell D) occurred during a similar time period of approximately 1 min 30 s. Note, however, that during RVD, cell height remained slightly elevated for an additional 10 min after the cell had already returned to its original volume.

Figure 5. Schematic description of cell image digitization

A: 3D view of a typical single adherent cell. Side-view and top-view images acquired during the experiment correspond to 2 mutually-perpendicular planes: a top-view plane, coincident with the glass coverslip surface (parallel to the xy-plane), shown in C; and a side-view plane (parallel to the xz-plane), which contains the cell profile and its summit, illustrated in B.

B: The cell left-profile is digitized from the side-view image. The base of the cell, at the level of the substrate surface is not readily apparent owing to out-of-focus details blurring the image. In this image, the cell base is defined as an horizontal line LL', and is localized as described in the APPENDIX. Xs depict points selected to digitize the cell profile, starting at the base of the cell ($i=1$) and ending at the summit (*top, i*=n). A 5th degree polynomial spline is fitted afterwards to smooth the digitized profile and to enable the building of a set of equally Δz-spaced points along the profile.

C: The outline of the cell base is digitized from the top-view image. This top-view plane contains the outline of the cell base, the nucleus silhouette, and the projection of its geometric centre nc'. Xs represent pixels which were selected clockwise to digitize the cell outline. Digitization starts at the base of the profile (identified as point A) having indices $i\,j=1,1$.

Figure 6. Slice generation

A: A pair of vectors $A\overrightarrow{}A'$, and $B\overrightarrow{}B'$ is used for slice reconstruction. The vector $B\overrightarrow{}B'$ shown here (top) has 2 fundamental characteristics: it is parallel to vector $A\overrightarrow{}A'$, defined by the first 2 adjacent points from the outline curve, and it is located above the outline level (see A bottom) in a plane to be generated. D_{ij} and $D_{(i+1)j}$ (bottom) define the distance between the tail of the vectors and a vertical axis that spans from the cell base through the top of the cell (nc-axis)

B: Details of the geometrical relationship that serves for extrapolation. The vectors $A\overrightarrow{}A'$ and $B\overrightarrow{}B'$ (identified as $\mathbf{v}_{ij}$ and $\mathbf{v}_{(i+1)j}$ each with a θ_{ij} orientation) and distances D_{ij} and $D_{(i+1)j}$ correspond to the sides of 2 mutually-inscribed, oblique-angled triangles having nc' as the common vertex. Vectors $\mathbf{v}_{ij}$ and $\mathbf{v}_{(i+1)j}$ are also the base and the upper side of a trapezoid with surface S_{ij} (top left). Note that the trapezoid shown in this representation is slightly tilted (because the 2 vectors are lying in different planes along the z-axis, see A bottom); thus h_{ij}, trapezoid height, is also seen as a projection in this drawing.

Figure 7. Volume evaluation and CLSM-acquired image surface approximation

A: The entire cell volume is evaluated by summing n-1 elemental volumes (V_i). An element of volume V_i is the product of multiplication of the mean of 2 adjacent cross-section areas (int_i and int_{i+1}) times the Δz-distance separating these 2 planes.

B: CLSM-acquired images require a different approach to evaluate the cell surface. A technique involving topological transformation, symbolized by the arrow in the figure, is used to evaluate the surface of CLSM-acquired cell geometry. The cross-section areas (int_i and int_{i+1}) measured from the CLSM-scanned outlines are changed into 2 circles having int_i and int_{i+1} of surface and r_i and r_{i+1} of radius, respectively. The lateral surface (SFC_i) of the frustrum of the cone, which results from such transformation, corresponds approximately to the lateral surface.

TABLES

Table 1. Comparison of A549 cell height, surface and volume evaluated from
confocal images or from a 3D model generated with the DISUR technique

	Height (μm)			Surface (μm^2)			Volume (pL-10^3 μm^3)		
Cell	A	B	C	A	B	C	A	B	C
Confocal	6.0	7.2	6.5	4,461	3,670	2,984	6.1	5.7	4.2
3D reconstruction	7.0	7.4	6.9	4,088	3,159	3,159	5.9	6.5	4.8
Difference (%)	17	3	6	-8	-14	6	-3	14	14

Table 2. Maximal changes of a single A549 cell's height, surface and volume
resulting from 50% hypotonic shock and evaluated by the DISUR method

	Height (μm)			Surface (μm^2)			Volume (pL-10^3 μm^3)		
Cell	D	E	F	D	E	F	D	E	F
Initial	11.1	8.3	13.1	3,691	2,590	2,569	8.7	4.5	7.0
Maximum	16.5	14.7	22.1	4,383	2,978	3,224	16.8	8.5	13.0
Change (%)	49	77	69	19	15	25	93	89	86

ACKNOWLEDGEMENTS

REFERENCES

1. Alvarezleefmans,F.J., S.M.Gamino, and L.Reuss. 1992. Cell-Volume Changes Upon Sodium-Pump Inhibition in Helix-Aspersa Neurons. *Journal of Physiology-London* 458:603-619.

2. Crowe,W.E., J.Altamirano, L.Huerto, and F.J.Alvarezleefmans. 1995. Volume Changes in Single N1E-115 Neuroblastoma-Cells Measured with A Fluorescent-Probe. *Neuroscience* 69:283-296.

3. Farinas,J., M.Kneen, M.Moore, and A.S.Verkman. 1997. Plasma membrane water permeability of cultured cells and epithelia measured by light microscopy with spatial filtering. *Journal of General Physiology* 110:283-296.

4. Kawahara,K., M.Onodera, and Y.Fukuda. 1994. A Simple Method for Continuous Measurement of Cell Height During A Volume Change in A Single A6 Cell. *Japanese Journal of Physiology* 44:411-419.

5. Korchev,Y.E., C.L.Bashford, M.Milovanovic, I.Vodyanoy, and M.J.Lab. 1997. Scanning ion conductance microscopy of living cells. *Biophysical Journal* 73:653-658.

6. Korchev,Y.E., J.Gorelik, M.J.Lab, E.V.Sviderskaya, C.L.Johnston, C.R.Coombes, I.Vodyanoy, and C.R.Edwards. 2000. Cell volume measurement using scanning ion conductance microscopy. *Biophys. J.* 78:451-457.

7. Kunz,L. and G.Stark. 1997. Photodynamic membrane damage at the level of single ion channels. *Biochimica et Biophysica Acta-Biomembranes* 1327:1-4.

8. Lang,F., G.L.Busch, M.Ritter, H.Volkl, S.Waldegger, E.Gulbins, and D.Haussinger. 1998. Functional significance of cell volume regulatory mechanisms. *Physiol Rev.* 78:247-306.

9. Mcmanus,M., J.Fischbarg, A.Sun, S.Hebert, and K.Strange. 1993. Laser Light-Scattering System for Studying Cell-Volume Regulation and Membrane-Transport Processes. *American Journal of Physiology* 265:C562-C570.

10. Mongin,A.A. and S.N.Orlov. 2001. Mechanism of cell volume regulation and possible nature of the cell volume sensor. *Pathophysiology* 8:77-88.

11. Saito,T., N.A.Hartell, H.Muguruma, S.Hotta, S.Sasaki, M.Ito, and I.Karube. 1998. Light dose and time dependency of photodynamic cell membrane damage. *Photochemistry and Photobiology* 68:745-748.

12. Van Driessche,W., P.De Smet, and G.Raskin. 1993. An automatic monitoring system for epithelial cell height. *Pflugers Arch.* 425:164-171.

13. Wehner,F., H.Olsen, H.Tinel, E.Kinne-Saffran, and R.K.Kinne. 2003. Cell volume regulation: osmolytes, osmolyte transport, and signal transduction. *Rev. Physiol Biochem. Pharmacol.* 148:1-80.

APPENDIX – CELL RECONSTRUCTION AND PARAMETER EVALUATION

Image analysis

We hypothesized (assumption 1) that because of the voluminous size of the nucleus in a typical substrate-adherent cell, its summit (*top*) will be centered above the geometrical centre of its nucleus (*nc*) as depicted in Figure 5A, a shape similar, to some extent, to a fried egg "sunny side up". As verified by confocal microscopy, the entire 3D shape of such a cell could be reconstructed, to sufficient accuracy, with the help of only 2 images, one showing the cell side-view profile sharply focused on the cell summit (Figure 2A, top), and the other presenting the outline of the cell base, focused near the coverslip surface (Figure 2A, bottom). Since substrate-attached cells rarely show radial symmetry, the profile recorded in one direction will be different from the others. To overcome the need to take pictures at different angles, we hypothesize (see below) that the shape of this profile is proportional to the length of its base (D). In other words, there is an hypothetical law of proportion which regulates the profile's shape: the greater the distance D compared to the originally recorded profile, the more stretched the profile became in a different direction, and vice-versa. Thus no more than two images are necessary to reconstruct an entire cell in 3D. The planes that correspond to such images are mutually perpendicular and intersect each other along line *LL'* (Figure 5A). We hypothesized (assumption 2) that line *LL'* runs through point *nc'* (projection of the nucleus centre *nc)* and intersects the base of the cell profile at points *A* and *C*.

When selecting cells for analysis and reconstruction, we avoided cells that were too close to the coverslip edge, since, on many occasions, they were damaged during mounting the coverslip in the chamber. This might be the result of intense capillary forces at the coverslip edge. However, when focusing on cells away from the edge, we could not clearly distinguish the substrate surface (which corresponds to *LL'*) due to out-of-focus details blurring the image. Nevertheless, its exact location could be determined with the help of the top-view image. In this image, the position of line *LL'* is easily found, because it had to be horizontal and to cross point *nc'* (Figure 5C). Line *LL'* also intersects the cell outline at points *A* and *C*. The *x*-position

of any of these points is sufficient to localize *LL'* in the side-view plane. Here, we chose the one at the left of *nc'* (identified as *A*).

Digitization of the cell profile

The vertical axis passing through the nucleus centre (*nc*-axis, Figure 5B) divides the cell profile into 2 halves. We routinely observed that each half-profile could be transformed into another, with fair accuracy, by symmetry transformation that involves 180° rotation and scaling proportional to the distance of the cell edge from this axis (data not shown). Thus, to avoid redundant information, we digitized only the cell left-profile. Pixels outlining the half-profile of the cell side-view image (between line *LL'* and the cell summit) were manually selected with MetaView software (Universal Imaging, West Chester, PA) as described in Figure 5B, and their coordinates logged to an EXCEL data sheet. The digitized half-profile was smoothed afterwards with a 5th degree polynomial fit (least-square method). This equation was then used to generate a set of n equally-spaced points along the z-axis, typically 20 to 25, depending on the resolution needed. These points later generate a set of cell slices.

Digitization of the cell outline

The outline of the cell base was similarly digitized (a total of m points), using a top-view image as described schematically in Figure 5C. This procedure generally requires 50 to 75 points to sufficiently map the cell outline without an excessive amount of data. It was unnecessary to smooth the outline.

Slice generation

Having digitized the cell profile and the outline of the cell base, the entire set of n-1 slices was generated with the outline of the cell base as a template. The goal was to generate slices which correspond to planar cross-sections of the cell plasma membrane along the z-axis. The initial coordinates of each slice were defined by a point in the set already generated from the half-profile (see Digitization of the cell profile); m-1 points were then successively extrapolated from this initial point to

complete 1 slice. To exemplify the whole procedure, we depict, in Figure 6, the calculation of the first extrapolated point B' in a slice (i+1). Its position is determined according to a method based on a pair of parallel vectors. Figure 6A (top) shows vector $A^{\rightarrow}A'$, defined by 2 adjacent points on the outline, which serve as a reference to vector $B^{\rightarrow}B'$ lying in a plane above (Figure 6A bottom). The origin of vector $B^{\rightarrow}B'$ is known; the coordinates of point B are calculated from the cell left-profile, but its magnitude and orientation are unknown and require 2 additional assumptions to solve them. We postulate (assumption 3) that, from a macroscopic point of view, the cell surface is continuous, smooth or, stated otherwise, it contains no twist. In such a case, the vectors $A^{\rightarrow}A'$ and $B^{\rightarrow}B'$ are parallel to each other. It is also hypothesized (assumption 4) that vector $B^{\rightarrow}B'$ ($\mathbf{v}_{(i+1)j}$) is proportional in magnitude to vector $A^{\rightarrow}A'$ ($\mathbf{v}_{ij}$) according to its distance from the nc-axis (Figure 6B). This distance D is measured between the tail of the vectors (points A or B) and the nc-axis (see also Figure 6A bottom). Each of the vectors now corresponds to the side of an oblique-angled triangle. One triangle has points B, B' and nc' as vertices and is inscribed in the other triangle defined by A, A' and nc'. In this situation, the amplitude ratio of vector $\mathbf{v}_{ij}$ over $\mathbf{v}_{(i+1)j}$ is proportional to the ratio of triangular side length D_{ij} over $D_{(i+1)j}$, as described by equation 1.

$$\left|\mathbf{v}_{ij}\right|/\left|\mathbf{v}_{(i+1)j}\right| = D_{ij}/D_{(i+1)j} \qquad (1)$$

Once the magnitude of $\mathbf{v}_{(i+1)j}$ or $B^{\rightarrow}B'$ is solved, the position of B' is easily determined. The process described here is repeated incrementally until a new slice consisting of m data points is completed.

Evaluation of cell parameters from the 3D model and CLSM-acquired geometry

3D Model

Height. Cell height corresponds to the z-coordinate of the cell summit (*top*) evaluated from side-view pictures.

Volume. Cell volume is approximated by the sum of n-1 elemental volumes V_i, as described in Figure 7A. Each elemental volume V_i is an approximation of the space contained between 2 adjacent planes and bounded by the cell surface. It is generated

by extruding a cylinder of Δz height from a surface averaging the 2 cross-section areas: int_i and int_{i+1}. Equation 2 serves to evaluate cell cross-section area int_i. The entire cell volume calculated with equation 4 corresponds to the summation of all individual V_i elements, as defined by equation 3.

$$int_i = \sum_{j=1}^{m}\left(x_{i(j+1)} - x_{ij}\right)\left(y_{ij} + y_{i(j+1)}\right)/2 \qquad (2)$$

$$V_i = \Delta z \left(int_i + int_{i+1}\right)/2 \qquad (3) \qquad\qquad V = \sum_{i=1}^{n-1} V_i \qquad (4)$$

Surface. To evaluate the cell surface, we took advantage of the fact that vectors $\mathbf{v}_{ij}$ and $\mathbf{v}_{(i+1)j}$ are respectively the basis and upper side of a trapezoid in the configuration shown in Figure 6B. The individual trapezoid surface S_{ij} is the product of height (h_{ij}) multiplied by the mean of the base ($\mathbf{v}_{ij}$) and upper side ($\mathbf{v}_{(i+1)j}$), as described by equation 5. Thus, the entire cell surface above the coverslip corresponds to a mesh of trapezoids such as the one depicted in Figure 6B (top left). Summation of all these surface elements S_{ij}, plus the area of the cell base attached to the coverslip, corresponds to the total cell surface (see equation 6).

$$S_{ij} = h_{ij}\left(\left|\mathbf{v}_{ij}\right| + \left|\mathbf{v}_{(i+1)j}\right|\right)/2 \qquad (5) \qquad\qquad S_{exact} = int_1 + \sum_{i=1}^{n-1}\sum_{j=1}^{m} S_{ij} \qquad (6)$$

CLSM-acquired geometry

Cell outline from each confocal plane was digitized and processed by the same technique, as described above, for the contour of the cell base in top-view image.

Height. The total number of planes necessary to scan the whole cell, minus the basement, times z-resolution corresponds to cell height.

Volume. Cell volume is approximated with equations developed for a DISUR-reconstructed cell, as described above.

Surface. The trapezoid-based technique was no longer suitable to evaluate the entire cell surface from CLSM-acquired images owing to the absence of order in manually-digitized data. A slightly less accurate, but still reliable technique when limited to cells with sufficient axial symmetry, was used instead. In Figure 7B, the asymmetrical cross-section areas (int_i and int_{i+1}) are transformed into 2 circles of

equivalent surface having r_i and r_{i+1} of radius, respectively, as calculated with equation 7. The symmetrical shape resulting from such transformation is the frustrum of a cone. The lateral surface (SFC_i) of this particular geometry (equation 8) is hypothesized to amount to a value close to the lateral surface of the irregular cell slice. The sum of n-1 lateral surface SFC_i having Δz of height plus the surface of the membrane attached to the coverslip int_1 corresponds to the cell surface, as defined by equation 9. This technique was also used to evaluate the cell surface from DISUR-reconstructed cells in validation experiments only.

$$r_i = \left(int_i / \pi\right)^{1/2} \qquad (7) \qquad\qquad SFC_i = \pi\left(r_i + r_{i+1}\right)\left(\left(r_i - r_{i+1}\right)^2 + \Delta z^2\right)^{1/2} \qquad (8)$$

$$S_{approx} = int_1 + \sum_{i=1}^{n-1} SFC_i \qquad (9)$$

Cell swelling-induced ATP release is synchronized with intracellular calcium elevations

Francis Boudreault and Ryszard Grygorczyk

Research Centre, Centre hospitalier de l'Université de Montréal – Hôtel-Dieu, and Department of Medicine, Université de Montréal, Montréal, Québec, Canada

ACCORD DES COAUTEURS

Identification

Francis Boudreault
Ph.D. en Génie Biomédical

Description de l'article

Francis Boudreault et Ryszard Grygorczyk
Cell swelling-induced ATP release is synchronized with intracellular calcium elevations
Journal of Physiology, soumis le 20 juillet 2004

Déclaration de tous les coauteurs autres que l'étudiant

À titre de coauteur de l'article identifié ci-dessus, je suis d'accord pour que *Francis Boudreault* inclue cet article dans sa thèse de doctorat qui a pour titre: *Contribution à l'étude du mécanisme de sécrétion d'ATP par des cellules épithéliales pulmonaires et des fibroblastes soumis à un choc hypotonique.*

| Ryszard Grygorczyk | ██████████ | 13 Aug 2004 |
| Coauteur | Signature | Date |

SUMMARY

Mechanical stresses release ATP from a variety of cells by a poorly-defined mechanism(s). Using custom-designed flow-through chambers, we investigated the kinetics of cell swelling-induced ATP secretion, cell volume and intracellular calcium changes in epithelial A549 (alveolar type II) and 16HBE14o⁻ cells, and NIH/3T3 fibroblasts. Fifty percent hypotonic shock triggered transient ATP release from cell confluent monolayers, which consistently peaked at around 1 min 45 s for A549 and NIH/3T3 and at 3 min for 16HBE14o⁻, then declined to baseline within the next 15 min. Whereas the release time-course had a similar pattern for the 3 cell types, the peak rates differed significantly (294 ± 67, 70 ± 22 and 17 ± 2.8 pmoles/min/10^6 cells, for A549, 16HBE14o⁻ and NIH/3T3 respectively). The concomitant volume changes of substrate-attached cells were analyzed by a 3-dimensional cell shape reconstruction method based on images acquired from 2 perpendicular directions. The 3 cell types swelled at a similar rate, reaching maximal expansion in 1 min 45 s, but differed in the duration of the volume plateau and regulatory volume decrease (RVD). These experiments revealed that ATP release correlates neither with cell volume expansion and the expected activation of stretch-sensitive channels, nor with the activation of volume-sensitive, 5-nitro-2-(3-phenylpropylamino) benzoic acid-inhibitable anion channels during RVD. By contrast, ATP release was tightly synchronized, in all 3 cell types, with cytosolic calcium elevations. Furthermore, loading A549 cells with the calcium chelator BAPTA significantly diminished ATP release (71% inhibition of the peak rate), while the calcium ionophore ionomycin triggered ATP release in the absence of cell swelling. Lowering the temperature to 10°C almost completely abolished A549 cell swelling-induced ATP release (95% inhibition of the peak rate). These results strongly suggest that calcium-dependent exocytosis plays a major role in hypotonically-induced ATP release.

INTRODUCTION

Adenosine 5'-triphosphate (ATP) regulates diverse biological functions by providing chemical energy for all living cells. As an extracellular mediator, ATP was recognized as the main neurotransmitter in non-adrenergic and non-cholinergic (NANC) post-ganglionic synapses from efferent autonomic innervation of the gut and bladder (Burnstock et al., 1970;Burnstock et al., 1972). Sensing pain through peripheral afferent innervation, at inflammation sites or from an overloaded bladder, is also thought to be mediated by ATP acting as a neurotransmitter (Birder et al., 2003). ATP was found to be co-stored with acetylcholine in pre-synaptic vesicles of the neuro-motor plate junction (Unsworth & Johnson, 1990) as well as with catecholamines in neuro-endocrine chromaffin granules (Bankston & Guidotti, 1996), supporting its role as a co-transmitter.

Signaling by extracellular ATP is not unique to neurons. Indeed, endothelial as well as epithelial cells release ATP by a regulated non-lytic mechanism (Bodin & Burnstock, 1998;Grygorczyk & Hanrahan, 1997), and express multiple isoforms of ionotropic P2X and metabotropic P2Y receptors (Communi et al., 1999;Glass et al., 2002). In these cells, ATP release is triggered by mechanical stimuli as diverse as shear stress (Grierson & Meldolesi, 1995), compression (Sauer et al., 2000), single cell micro-pipette stimulation (Stout et al., 2002), hypotonic shock (Hazama et al., 1999;Niggel et al., 2000) and stretch (Grygorczyk & Hanrahan, 1997). Such observations led to the suggestion that cells respond to mechanical stress by releasing ATP which, in turn, activates the purinergic signaling pathway. It is believed, that such diverse physiological processes as regulation of vascular tone (Burnstock, 1987), airway mucociliary clearance (Stutts et al., 1992;Morse et al., 2001;Chen et al., 2001) and lactate secretion from mammary glands (Blaug et al., 2003) could involve an autocrine/paracrine loop with ATP serving as ecto-messenger.

Although vesicular exocytosis is a generally-accepted mechanism of ATP release at NANC synapses or from activated blood platelets and chromaffin cells, early studies with other cell types pointed to a channel-mediated process. In epithelial cells, 2 ATP-binding cassette proteins, the cystic fibrosis transmembrane conductance

regulator (Prat *et al.*, 1996) and multidrug-resistance proteins (Abraham *et al.*, 1993), were implicated in conducting ATP across the cell plasma membrane. Those assertions, however, were contradicted by later studies (Reddy *et al.*, 1996;Li *et al.*, 1996). Meanwhile, alternative candidates were proposed, such as the hemi-channel connexin (Cotrina *et al.*, 1998), the ecto-apyrase CD39 (Bodas *et al.*, 2000) and some unidentified stretch-sensitive anionic channels (Sauer *et al.*, 2000;Hazama *et al.*, 1999;Mitchell *et al.*, 1998). The identities of the latter may have been unmasked as a voltage-dependent anion channel (VDAC) or VDAC-like channels (Sabirov *et al.*, 2001) or volume-sensitive chloride channels (VSCC) (Hisadome *et al.*, 2002).

On the other hand, brefeldin A block of mechano-sensitive ATP release from amphibian *Xenopus laevis* oocytes (Maroto & Hamill, 2001) as well as the suppression of fluid shear-triggered ATP efflux from endothelial cells by monensin and N-ethylmaleimide (Bodin & Burnstock, 2001), all compounds known to interfere with vesicular trafficking machinery, indicated exocytotic ATP release. Indirect evidence of such a release mechanism was also demonstrated by the ambiguous pharmacological effects of the trivalent lanthanide gadolinium, which appeared consistent with an action on lipid membrane and membrane-dependent processes, such as exocytosis, rather than on stretch-sensitive channels (Boudreault & Grygorczyk, 2002).

To further investigate the nature of the ATP release pathway, we studied the relationship between the kinetics of hypotonically-triggered ATP release, cell swelling and intracellular calcium changes. To cover a wider spectrum of responses, 2 epithelial cell lines and fibroblasts were tested. ATP release and intracellular calcium changes during hypotonic challenge were evaluated from cell monolayers in a custom-designed flow-through chamber. Hypotonic swelling-induced alterations in the morphology (height, surface and volume) of a single substrate-adherent cell were examined by analyzing images recorded in a previously-described side-view chamber (Boudreault & Grygorczyk, 2004).

Our results show that in response to hypotonic shock, all cells released ATP in a similar transient manner, despite different kinetics of volume restoration. While the

kinetics of ATP release did not correlate directly with cell volume changes, it was strikingly synchronized for all 3 cell lines with intracellular calcium elevations. Calcium dependence was further demonstrated by the effects of the calcium ionophore ionomycin, which triggered transient ATP release in the absence of cell swelling. In addition, hypotonicity-induced ATP secretion was suppressed by loading cells with the calcium chelator BAPTA, or by lowering the temperatures. Our findings are consistent with the concept that calcium-dependent exocytosis is a major mechanism of cell swelling-induced ATP release.

METHODS

Cells

Human lung carcinoma A549 cells and murine NIH/3T3 fibroblasts were grown in Dulbecco's Modified Eagle Medium supplemented with 10% FBS, 20 mM L-glutamine, 60 µg/mL penicillin-G and 100 µg/mL streptomycin. Human bronchial epithelial 16HBE14o⁻ cells, a generous gift from Dr. D. Gruenert, were cultured as described (Cozens *et al.*, 1994). All constituents of the culture media were from GIBCO-BRL (Burlington, ON). ATP efflux and calcium changes were measured in cell monolayers grown to confluency on 24x60-mm glass coverslips. Cellular morphology was analyzed in cells plated at low density on 22x22-mm glass coverslips.

ATP efflux assay

To measure ATP efflux during hypotonic challenge with high temporal resolution, we used a custom-designed, low-volume (325 µL) flow-through chamber, Figure 1A. Warm solution (37°C/in-line heater Warner Instrument Co., Hamden, CT), perfused at a rate of 1.3 mL/min, was continuously collected for 15-s intervals during the initial burst of ATP secretion (0-10 min), and during 1 or 5 min elsewhere. ATP content in the samples was measured by luciferase/luciferin based assay (Boudreault & Grygorczyk, 2002). Because of the finite internal volume of the chamber, washing of

ATP released from the cells is a time-dependent process, which distorts the real time-course of ATP secretion. To correct for this effect, in a cell-free experiment, we determined the time needed for 2-fold dilution of known ATP concentration inside the chamber, Figure 1B. The chamber was filled with a solution containing 100 nM ATP and then washed. Under these conditions, half-dilution of ATP in the solution is achieved in 15 s. Thus, with 15-s sampling period, the first sample (t=15 s) at the outlet of the chamber contained only half of the actual amount of ATP released by the cells ($X_0/2$), while the subsequent sample contained ($X_0/2+X_1)/2$, etc. With this iterative formula, all ATP efflux data were corrected to eliminate the effect of chamber-buffering capacity and to measure the exact kinetics of ATP that is released from cells. Degradation of extracellular ATP by endogenous ectoATPase is also likely to occur in presence of cells. However, since we did not expect this factor to influence the kinetics of the release, only to slightly lower the amplitude of the release rate, we did not correct for this effect.

For ATP efflux experiments at low temperatures, a custom-made in-line cooler consisting of a small container filled with ice-saturated water allowed reduction of the temperatures to 10°C at the inlet of the flow chamber.

Cell volume evaluation

To evaluate cell volume changes of substrate-attached cells, a 3D imaging technique was used (Boudreault & Grygorczyk, 2004). The following is a brief description of the method.

Top- and side-view images. The method involves 3D reconstruction of cell shape based on phase-contrast cell images acquired from 2 perpendicular directions. Cells grown on small coverslip were mounted in a custom-designed side-view chamber placed on the stage of a NIKON TE300 inverted microscope (Nikon Canada Inc., Montreal, QC) and perfused continuously with pre-warmed saline (37°C, 1.3 mL/min). Vertical mounting of the coverslip permitted visualization of the lateral shape of the cell of interest close to the lower edge. After hypotonic challenge, side-view images of rapidly-swelling cell were acquired. In addition, at the beginning and at

the end of an experiment, a top-view image of the same cell was recorded while the coverslip was instead placed in a petri dish.

Imaging. Phase contrast images of the cell side-view profile and the top-view of the cell base were recorded for 100 ms with a T57 Micromax CCD camera (Princeton Instruments, Trenton, NJ) and MetaFluor software (Universal Imaging, West Chester, PA) at 0.16-μm/pixel resolution. Images were saved on hard disk and analyzed off-line.

Cell surface reconstruction and visualization. The 3D topography of the cell surface was reconstructed by a dual image surface reconstruction (DISUR) technique, which generates a set of topographical curves of the cell surface from its digitized profile and base outline. Cell volume, surface and height were calculated from such a reconstructed cell topographical model. All calculations were carried out entirely with EXCEL (Microsoft, Redmond, WA). To visualize the reconstructed cell model in 3D perspective, data obtained with the help of the DISUR technique were used to generate a 2D matrix containing approximate z-coordinates of points on the membrane surface. The 3D perspective of the model cell was then plotted with ORIGIN (Microcal Software, Northampton, MA).

In the course of this study, we observed that a majority of quiescent A549 cells exposed to 50% hypotonic shock remained firmly attached to the substrate throughout the challenge. As a result, the outline of their base remained nearly invariant. Therefore, to reconstruct cell 3D morphology at different time points during hypotonic cell swelling, it was sufficient to acquire only a single image of the cell viewed from the top, in addition to a series of side-view images acquired at 15- to 60-s intervals during the experiment. In contrast, 16HBE14o⁻ and NIH/3T3 cells often demonstrated significant changes in cell base or initiation of migration in response to hypotonic shock. Therefore, only a subset of cells whose base shape remained invariant was selected for 3D reconstruction.

Electrophysiology

For patch-clamp whole-cell experiments, freshly-trypsinized A549 cells in suspension were used. Patch pipettes, made from borosilicate glass (World Precision Instruments, Inc., Sarasota, FL), were filled with (in mM): 100 CsCl, 90 sorbitol, 2 $MgCl_2$, 1 EGTA, 1 MgATP and 10 TES,1 pH=7.4 (TRIS). The bath solution contained physiological saline (see SOLUTIONS AND CHEMICALS). Whole-cell currents were measured at room temperatures with an Axopatch 1-C amplifier (Axon instruments, Foster City, CA). Current responses from the computer-generated stimulus waveform were filtered at 2 kHz, digitized (Digidata 1200) at 1 kHz, and recorded on computer by Clampex 8 software. The data were analyzed off-line by pCLAMP 8 software. Acute 50% hypotonic shock was achieved by adding appropriate amounts of distilled water to the bath.

Fura-2 calcium measurements

To load Fura-2, cells were incubated (1 h, 37°C, 5% CO_2) in physiological solution containing 25 µM Fura-2-AM (A549 and 16HBE14o⁻) or 50 µM Fura-2-AM + 0.125% pluronic acid (NIH/3T3). For calcium imaging, cells were mounted in the same flow chamber used for ATP efflux measurements, Figure 1B. To allow microscopy viewing of the cells, the polycarbonate lower plate was replaced by a 0.8-mm thick stainless steel plate having a 13-mm diameter opening in the middle which was firmly pressed against the 24x60-mm glass coverslip. This permitted through-the-objective illumination of cells for Fura-2 calcium measurements. Changes in calcium were assessed with the microscopy system described above (see CELL VOLUME EVALUATION) which is also equipped for epifluorescent UV illumination. Fura-2-loaded cells were exposed to alternate illumination at 340 and 380 nm with a high-pressure mercury lamp (100 W) via interference filters (Chroma Technology, Brattleboro, VT, USA) mounted on a filter wheel (Sutter Lambda 10-C, Sutter Instrument Co., Novato, CA, USA) and a dichroic mirror (510/540 nm, Chroma Technology). Fluorescence images were recorded during 200-ms exposure at 15- to 60-s intervals with the digital camera and stored for later analysis.

Solutions and chemicals

Physiological saline solution contained (in mM): 140 NaCl, 5 KCl, 1 $MgCl_2$, 1 $CaCl_2$, 10 glucose and 10 HEPES, pH 7.4, adjusted with NaOH. 50% hypotonic medium was prepared by reducing salt concentration while keeping divalent cation concentration constant. Stocks of 5-nitro-2-(3-phenylpropylamino) benzoic acid (NPPB), ionomycin and BAPTA-AM were prepared in DMSO at concentrations of 100, 1 and 5 mM, respectively. All reagents were from Sigma (Oakville, ON) except for Fura-2-AM (Molecular Probes, Eugene, OR).

RESULTS

Kinetics of ATP release

When confluent monolayers of adherent A549, 16HBE14o⁻ and NIH/3T3 cells were subjected to hypotonic swelling, transient ATP release was observed, Figure 2. The shape of this burst of secretion was very similar for the 3 cell lines although the amounts of ATP released were quite different. This transient ATP secretion vanished beyond 15 min despite continuous perfusion with hypotonic solution. The data illustrated in Figure 2 were normalized to 10^6 cells in a confluent monolayer for 2 reasons. First, during the course of this study, we observed that the rate of ATP secretion always culminated at 1 min 45 s for A549 and NIH/3T3 cells regardless of cell monolayer density. However, 16HBE14o⁻ behaved differently; the timing of peak ATP release shifted from 1 min 45 s to 4 min 45 s when a slightly underconfluent cell monolayer was grown to overconfluency. Furthermore, the peak and total amount of ATP released decreased despite an increasing number of cells in the overconfluent cell monolayer (data not shown). For consistency with the other 2 cell lines, in this report, we only present 16HBE14o⁻ ATP release on the day when they just reached confluency and demonstrated a peak of ATP release at 3.0 min. The other 2 cell lines, A549 and NIH/3T3, did not show a decrease of ATP secretion, but a plateau when they reached or exceeded confluency, despite increasing cell density. This suggests,

that the amount of ATP released from these cells is mainly proportional to the area covered by cell monolayer and not the number of cells *per se*. The normalized data in Table 1 reveal major differences in terms of total amount of ATP released by different cell types. A549 cells secreted 3 times more ATP than 16HBE14o⁻ and 12 times more than NIH/3T3. Very similar differences were seen for the peak rate of ATP secretion. It is noteworthy that during the experiment, ATP concentration inside the flow chamber rarely reached 100 nM. At the peak of ATP secretion, its concentration averaged 68±15 nM, 16±5 nM and 3±0.7 nM for A549, 16HBE14o⁻ and NIH/3T3, respectively.

Kinetics of cell volume changes

Figure 3A depicts typical volume changes of substrate-attached cells in response to 50% hypotonic shock. The cells started to swell at a similar rate, which never exceeded 1%/s. They reached maximal expansion in 1 min 30 s (NIH/3T3) or 1 min 45 s (A549 and 16HBE14o⁻) after onset of the shock. After a plateau which lasted 3 min 30 s for A549 and 5 min for 16HBE14o-, the cells underwent a regulatory volume decrease (RVD) while NIH/3T3 remained swollen for 15 min after the shock. We frequently observed for A549 and 16HBE14o⁻ a period of invariant volume (plateau), which precedes RVD. This plateau can only be noted in single-cell volume measurements. It could be overlooked by most other methods, which sum up volume changes from a large cell population. Accordingly, we dissected hypotonic stress-induced volume changes into 3 different phases: swelling, plateau and RVD. Figure 3A shows that the plateau phase had not been completed by NIH/3T3 cells at 15 min past the shock. Although the duration of volume plateau and RVD varied slightly between individual A549, and especially 16HBE14o⁻ cells (data not shown), maximal swelling occurred during a similar time period for the 3 cell lines tested.

Since volume changes were evaluated for isolated cells, an important question was whether the same kinetics of volume changes apply to cells that are in close contact with their neighbours in a confluent monolayer. To verify this, we used a lower magnification objective, which allowed us to simultaneously observe, in the

side-view chamber, more than a dozen cells in a confluent monolayer. We found that time-course of 50% hypotonic shock-induced height increase of all cells in the field of view was very similar to that measured for an isolated cell (data not shown). Thus, volume expansion reported in Figure 3 for a single cell likely represents typical behaviour of a majority of cells in a confluent monolayer.

Table 2 presents the morphological parameters: height (H), surface (S) and volume (V) and their changes induced by 50% hypotonic swelling for the 3 cell types analyzed in Figure 3A. Also, 3D pictures of these cells before and after maximal swelling are shown. It is interesting, that volume changes always exceeded 50%, while the cell surface did not grow beyond 20%. Also, it could be seen that the volume increases were not directly correlated with gains in cell height. For further discussion on swelling-induced cell morphology changes see Boudreault & Grygorczyk (2004).

Relationship between ATP release and cell volume changes

Assuming that the majority of cells in a confluent monolayer alter their volume in response to hypotonic challenge in a similar way as a single cell reported in Figure 3A, one could measure the percentage of ATP secreted during each phase of volume change: swelling, plateau and RVD, Figure 3B. As illustrated in Figure 3C, very little ATP (8% to 25% for 16HBE14o⁻ and A549 cells, respectively) was released during the swelling phase, when transient rise in membrane tension could be expected. Most animal cells have an excess membrane area beyond that estimated by light microscopy. It buffers membrane tension and allows cells to undergo significant volume and shape changes without rupturing the lipid bilayer. For example, due to large membrane reserves, osmotic swelling or direct inflation of *Xenopus* oocytes did not increase lipid bilayer tension and did not activate stretch-sensitive channels (Zhang & Hamill, 2000). Similar membrane reserves might be expected for A549 cells. Thus, at maximal volume increase induced by 50% hypotonic shock, the cells are probably far from depleting their membrane reserves. One may expect that in such cells, due to the combined effects of excess membrane and its viscoelastic properties, bilayer tension could only rise transiently during dynamic volume increase and should vanish

during quasi-static conditions at volume plateau. We found in this study that most ATP is secreted during volume plateau and only a small fraction during the swelling phase. This demonstrates that most ATP is released via mechanisms other than stretch-activated channels (Taylor *et al.*, 1998) or exocytosis of vesicles whose trafficking or fusion is facilitated by heightened membrane tension.

Role of VSCC in ATP release

From Figure 3C it is apparent that only a small fraction of ATP was released during volume restoration. Since this is a period where one may expect maximal activity of VSCC, it indicates that such channels are unlikely to play a major role in ATP secretion. Many previous studies, however, reported inhibition of ATP release by NPPB, which is a potent blocker of various chloride channels, including VSCC. These findings suggested a potential role of NPPB-inhibitable channels in ATP release. We investigated this in A549 cells, which could secrete as much as 22% of ATP during volume restoration, Figure 3C.

Whole-cell patch-clamp experiments demonstrated the presence of VSCC in A549 cells, Figure 4. Cell swelling-induced whole-cell currents showed characteristic outward rectification and inactivation at large depolarizing membrane potentials. They were almost completely blocked by 125 µM NPPB (95% inhibition).

Figure 5 illustrates the effect of NPPB on hypotonicity-induced cell volume changes and ATP release. In the presence of 125 µM NPPB in the bath, cells swelled at the rate similar to that under control conditions, Figure 3A. However, RVD which normally starts 5 min after hypotonic shock, Figure 3A, was completely abolished, and cells remained maximally swollen for the next 20 min. At 20 min, the NPPB block was removed by washing away the drug. This resulted in immediate cell volume restoration. Interestingly, despite relieving the VSCC block, no parallel increase of ATP release was observed, demonstrating that ATP does not permeate via VSCC. Nevertheless, significant inhibition of ATP release (81% peak and 73% cumulative) was observed in the presence of NPPB, compare Figures 5 and 2. In a separate experiment in a test tube, we noticed that NPPB diminished light output from the

chemiluminescent luciferase-luciferin reaction with $IC_{50}=525$ μM, Figure 6. It should not, however, interfere with our ATP efflux measurements, since the concentration used in this study did not exceed the threshold of inhibition: ~250 μM, Figure 6. The ability of NPPB to strongly block a bioluminescent reaction raises concern about the specificity of this chloride channel blocker, as already reported (Brown & Dudley, 1996;Kato *et al.*, 1999).

Kinetics of intracellular calcium changes

Ratiometric Fura-2 fluorescence experiments revealed that hypotonic challenge of the A549 cell monolayer raised $[Ca^{2+}]_i$ in a majority of cells. Individual cells, however, responded in many different ways, some experiencing a single or multiple spikes, others monotonical increases of $[Ca^{2+}]_i$, Figure 7. When the responses from a large number of cells were averaged (approximately 600 cells), a transient $[Ca^{2+}]_i$ increment was observed that reached a peak 1 min 45 s after the shock and was followed by a decline to a slightly elevated level, Figure 7, bold trace. Interestingly, this averaged signal demonstrated strong similarity to the ATP release curves in Figure 2. To better highlight the synchronicity seen between changes in $[Ca^{2+}]_i$ and ATP release for A549 cells, both traces were plotted in Figure 8, left panel. A simultaneous rise of both signals, $[Ca^{2+}]_i$ and ATP release, was also discerned for 16HBE14o⁻ and NIH/3T3 cells, Figure 8, middle and right panels. Such synchronicity is not only a demonstration of the calcium dependence of swelling-induced ATP release but also that the mechanism of ATP release might be archetypal, since all three cell lines presented a very similar profile of ATP release and $[Ca^{2+}]_i$ changes. In addition, when 16HBE14o⁻ cell monolayers were grown below confluency, hypotonicity-induced peak of $[Ca^{2+}]_i$ occured approximately 1 min sooner. Interestingly, this was also accompanied by a similar 1 min earlier appearance of the peak rate of ATP release (data not shown). These results strongly suggest a close association between the rate of ATP release and $[Ca^{2+}]_i$ elevations. Both $[Ca^{2+}]_i$ and ATP signals in Figure 8 are averaged from a large number of cells. If this tight relationship holds true for each individual cell, it may indicate, that ATP could be released in a slightly different

fashion from each cell, reflecting variable $[Ca^{2+}]_i$ responses of individual cells within a monolayer, see Figure 7.

To further investigate the role of $[Ca^{2+}]_i$ in ATP release, we tested the ionophore ionomycin, which has been widely used as a non specific secretagogue for many cell lines (Unsworth & Johnson, 1990). Three minutes exposure to 5 µM ionomycin transiently induced ATP release from A549 cells near 18% of the peak rate, and 12% the amount of ATP released in response to 50% hypotonic challenge, Figure 9A, bottom trace. The peak of this transient release was reached in less than 1 min 30 s, similar to the time required for a maximal increase in $[Ca^{2+}]_i$, Figure 9A, upper trace. In addition, significant inhibition of swelling-induced ATP release (71% peak and 63% cumulative release) was observed for A549 cells loaded with the Ca^{2+} chelator BAPTA, Figure 9B. These experiments strengthen the notion that hypotonic stress-induced ATP release requires elevation of $[Ca^{2+}]_i$.

ATP release is abolished at low temperatures

Strong calcium-dependence of ATP release suggests the involvement of vesicular exocytosis, a mechanism that could be significantly inhibited by lowering the temperatures. Consistent with this notion, when A549 cells were cooled to 10°C, swelling-induced ATP release was almost completely suppressed, with 95% inhibition of the peak rate and 85% diminution of ATP accumulation, Figure 10.

DISCUSSION

In the present study we measured the kinetics of cell swelling-induced ATP release, cell volume and intracellular Ca^{2+} changes of substrate-adherent cells with sufficiently high temporal resolution to analyze the relationship between the three processes. This allowed us to evaluate the potential contribution of specific ATP release mechanisms. Among many putative ATP release mechanisms, two may be triggered solely during cell expansion, when membrane tension is expected to rise significantly. One may involve ATP-conducting channels directly activated by stretching of the membrane or

cytoskeleton. The second may occur via exocytosis of ATP-filled vesicles, whose fusion with the plasma membrane is favoured by increased membrane tension during cell swelling. Another mechanism assumes that ATP conduction through a broad family of VSCC may contribute to ATP secretion, mainly during cell volume restoration. Finally, conductive ATP release may proceed through VDAC-like channels or connexin hemichannels, but no specific time frame could be assigned, since the mechanism of their activation is not well-characterized. For the purpose of this discussion, we assume that these channels may be active at any time after hypotonicity-induced cell swelling.

The first two mechanisms fail to properly describe the ATP release kinetics observed in the present study, since only a small fraction of ATP (8%-25%) is released during the swelling phase. Furthermore, our previous experiments with Gd^{3+}, a blocker of mechano-sensitive channels, also did not support the view that such channels are involved in ATP release (Boudreault & Grygorczyk, 2002). These two mechanisms, therefore, could be excluded as major players in cell swelling-induced ATP secretion seen in our study. It is also unlikely that VSCC mediate ATP release, although some ATP is released (especially by A549 cells, up to ~22%) during VSCC-mediated RVD. Indeed, when A549 cells were swollen in the presence of NPPB, wash of the drug to relieve block of VSCC did not result in ATP secretion despite the fact that the channels were functional, as demonstrated by a rapid cell volume decrease, Figure 5. Failure of VSCC to conduct ATP is consistent with earlier report by Hazama *et al.*, (1999). Although ATP release was diminished by NPPB, it could not be interpreted as an indication of VSCC involvement because of wide non-specific effects of the compound. The exact cause of this inhibition remains to be investigated. The last category, maxi-anion or VDAC-like channels, remains a possible pathway for conductive ATP release, although it is difficult to accept that during ATP secretion from swollen cells, such large anion conductance did not induce a concomitant cell volume decrease. If ATP liberation proceeds via activated high-conductance anion channels, smaller osmolytes, such as Cl^-, should also escape the cell and contribute to RVD. Figure 3C contradicts such expectations and demonstrates that all three cell

lines tested in our study secreted ATP mainly during volume plateau (53-84% of total released ATP), i.e. in the absence of noticeable cell volume changes. Thus, in our view, none of the above mechanisms could satisfactorily explain the nature and kinetics of cell swelling-induced ATP release.

Our experiments provide strong evidence for the involvement of intracellular Ca^{2+} in ATP release. This includes the following: (i) the time-course of ATP release is strikingly coordinated with intracellular Ca^{2+} elevations; (ii) ATP secretion could be evoked solely by a rise in intracellular Ca^{2+}, i.e. in the absence of hypotonic cell swelling; (iii) ATP release is significantly inhibited by chelating intracellular Ca^{2+}. Such tight Ca^{2+} dependence is expected from an exocytotic release mechanism, and this notion is further supported by a strong inhibitory effect (95% peak inhibition) of low temperatures. The extent of such inhibition by low temperatures or Ca^{2+} chelation suggests that Ca^{2+}-dependent vesicular exocytosis is the main mechanism of cell swelling-induced ATP release and contribution of other mechanisms is negligible. While it has been suggested recently that fusion of vesicles could deliver ATP-conductive channels to the plasma membrane (Gatof *et al.*, 2004), we favour non-conductive direct secretion of ATP stored in vesicles. We base our reasoning on two factors. First, as discussed above, cell volume remains invariant during a period when a large amount of ATP is released, indicating a non-conductive mechanism. Second, ATP had been found to be stored in secretory vesicles from a large number of cell types. Although the identity of vesicles responsible for storage and cell swelling-induced ATP secretion from epithelial cells remains to be identified, it could belong to the same family of ATP-laden vesicles that had been previously reported in non-neuronal cell, such as adrenal or pancreatic cells (Hazama *et al.*, 1998;Bankston & Guidotti, 1996).

An exocytotic mechanism of ATP release could also explain the previously-reported release of other nucleotides, such as uridine triphosphate (UTP), which is released in a similar fashion as ATP by fluid flow-induced mechanical stress (Lazarowski *et al.*, 1997). It is reasonable to postulate that they originate from the same pool of vesicles since ATP and UTP are both substrates of the chromaffin

granule nucleotide transporter (Bankston & Guidotti, 1996), a transmembrane transport protein likely to be also found on ATP-filled organelles. There were significant differences in amount of ATP released between the epithelial cells and the fibroblasts. Although this could result from a different pool size of ATP-filled vesicles, it could also demonstrate cell's specifity to react at a given stimulus. Indeed, epithelial cells are constantly exposed to an anisosmotic milieu but not fibroblasts. For such cells, embedded inside connective tissue, such as ligaments or tendons, continuously exposed to mechanical forces, mechanical stretch might turn out to be a more relevant mechanism to trigger ATP release than hypotonic shock. Another interesting remark pertains to the cell swelling-induced release of other organic anions or osmolytes, such as taurine. Currently VSCC are supposed to mediate this release but it would be of great interest to evaluate if vesicular exocytosis also contributes to this efflux.

Additional interesting observations that emanate from the analysis of our data are related to cell volume. Previous studies reported volume changes in response to 50% hypotonic shock, ranging from 10 to 39%, when measured by various methods with different substrate-attached cell types (Bibby & McCulloch, 1994;Raat et al., 1996). However, Coulter-counter analysis of the same cells revealed much higher volume increases, up to 70-74% (Bibby & McCulloch, 1994;Raat et al., 1996), similar to that observed with red blood cells (Light et al., 1999) and close to those in the present study with substrate-adherent cells (50-90%). It could be speculated that other methods which indirectly evaluate the cell volume of substrate-adherent cells, e.g. by measuring only cell height or fluorescence intensity of fluorophore-loaded cells, may underestimate the actual volume changes.

Another important finding of our study relates to the role of ATP in volume restoration. In contrast to some previous reports, we found no evidence that purinergic receptor activation is needed to initiate or maintain the volume restoration process as suggested by others (Roman et al., 1999;Light et al., 1999;Darby et al., 2003). Because of continuous perfusion during ATP efflux assay, ATP concentration in the flow chamber (Figure 1A) rarely exceeded 100 nM, and was many-times lower during cell volume measurements in the side-view chamber (Boudreault &

Grygorczyk, 2004) due to the smaller number of cells under investigation. Such low ATP concentrations should not activate purinergic receptors, since their EC_{50}, as measured by a rise in $[Ca^{2+}]_i$, IP_3 synthesis or modulation of short-circuit current, is in the µM range (Homolya et al., 1999;Warburton et al., 1989;Peterson et al., 1997). In spite of this, we routinely observed complete volume restoration of 16HBE14o⁻ and A549 cells, a finding that is in agreement with the results of Van der Wijk et al. (1999).

Finally, it is noteworthy that the Ca^{2+}-dependent mechanism for vesicular ATP release hints of a somewhat different mode of signaling by extracellular ATP, which resembles signal transmission in the synaptic cleft more than the longer-range autocrine/paracrine communication. Indeed, essential features of neuronal acetylcholine- or ATP-mediated synaptic transmission (Evans et al., 1992) are now evident in epithelial cells: an apparent low-affinity binding receptors (see above), ecto-ATPases to rapidly terminate the signal (Communi et al., 1999;Lazarowski et al., 2000), and foremost, a Ca^{2+}-sensitive pool of ATP-filled vesicles. All this indicates that many non-neuronal cells are equipped to send and receive ATP-mediated signals within a confined compartments, such as regions of close physical contact between neighbouring cells. Reports that an RGD domain, found in the first putative extracellular loop of P2Y$_2$ receptor, binds to integrins $\alpha_v\beta_3$ (Erb et al., 2001) and that endogenous P2X receptors are restricted to areas of cell contact and co-localize with VE-cadherin in human endothelial cells (Glass et al., 2002) may support this hypothesis. Clearly, much remains to be studied to reassess the exact role of such ATP signaling.

In summary, based on the data presented, we propose that Ca^{2+}-dependent vesicular exocytosis is a major mechanism of cell swelling-induced ATP release. Further investigations are needed to better understand mechano-sensitive ATP release at the molecular level.
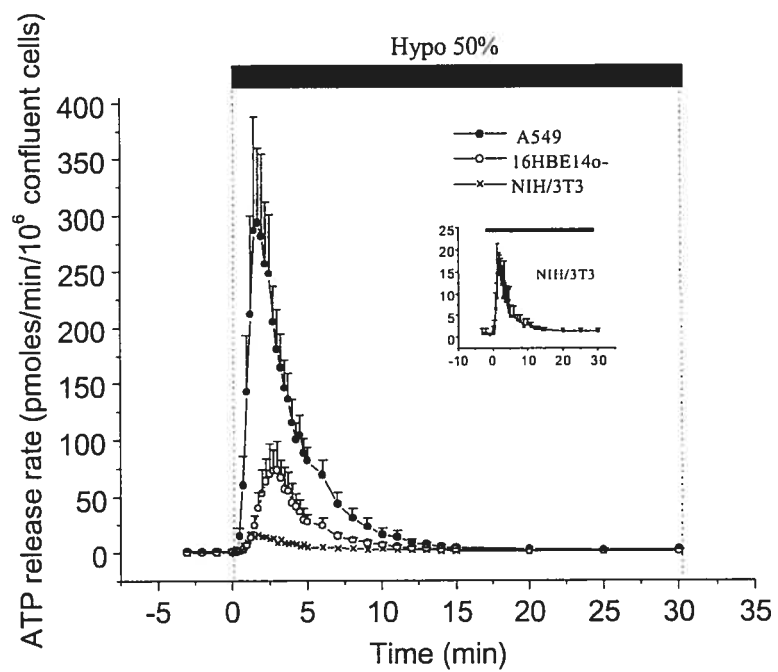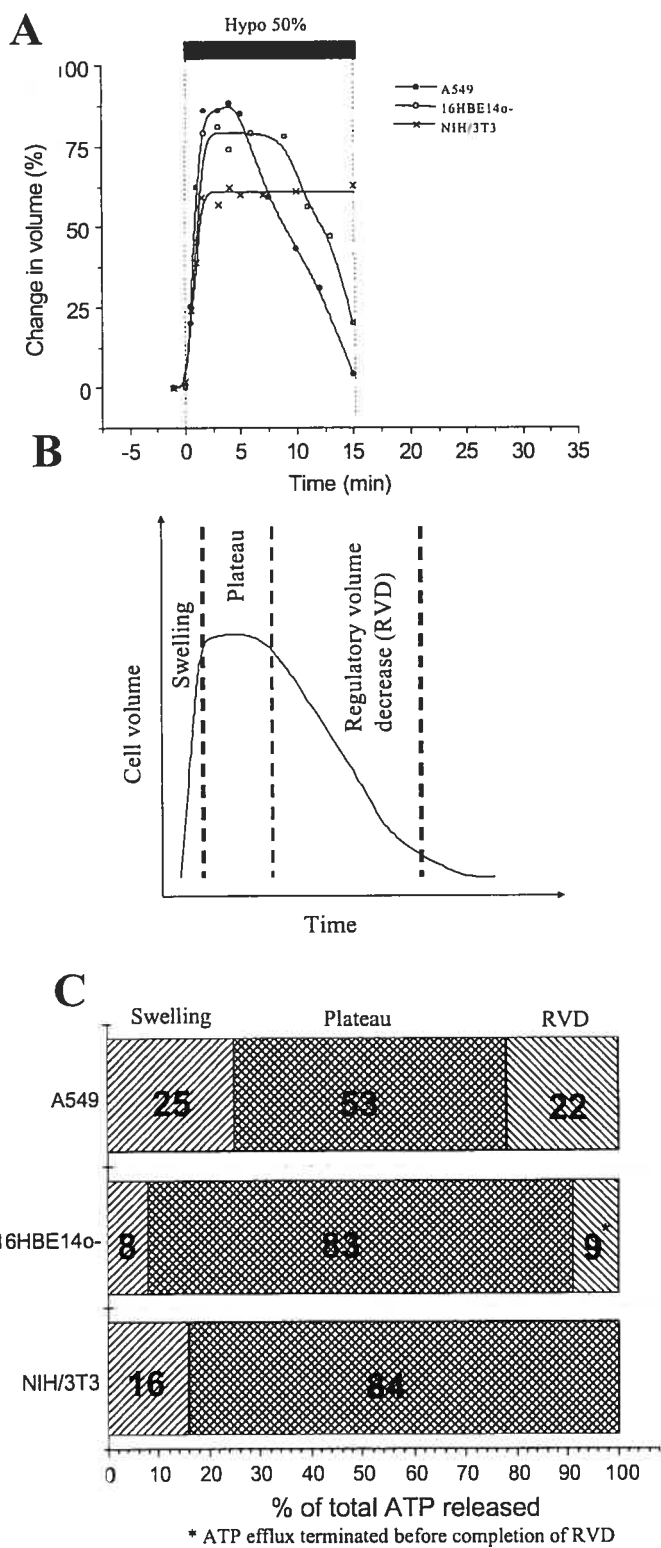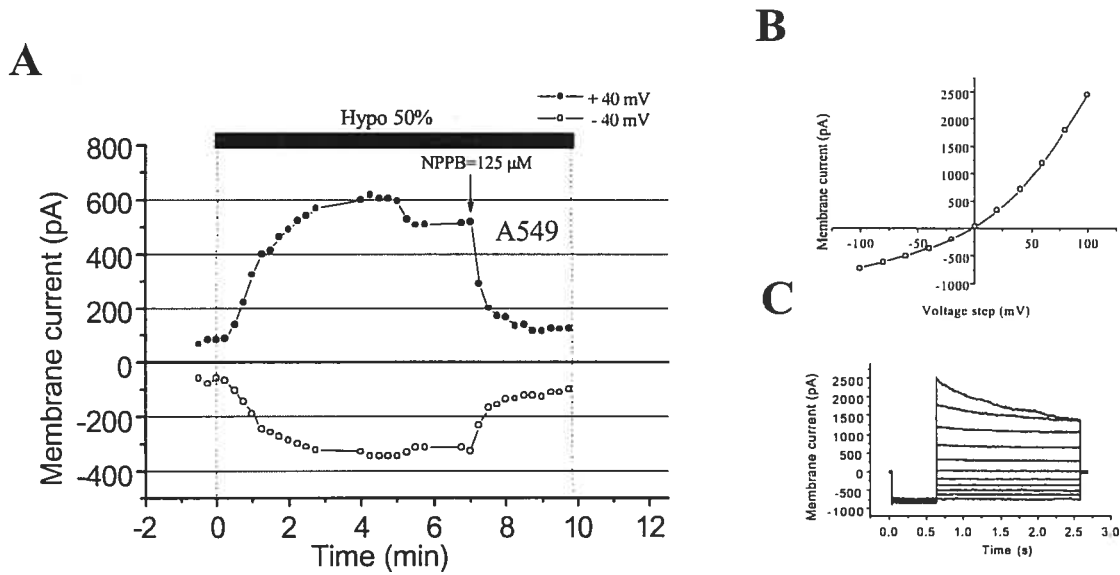
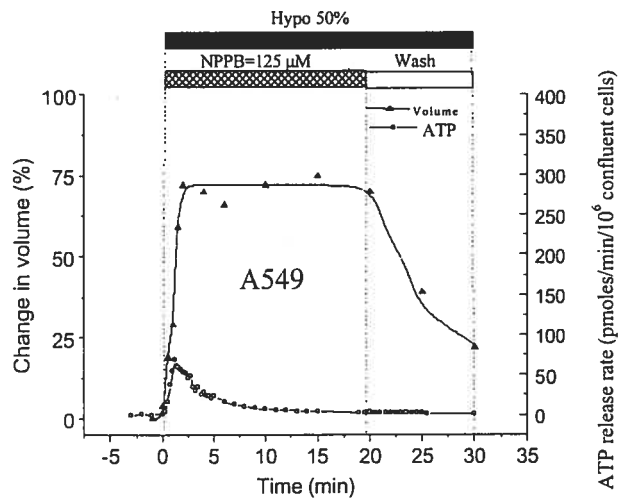**A**
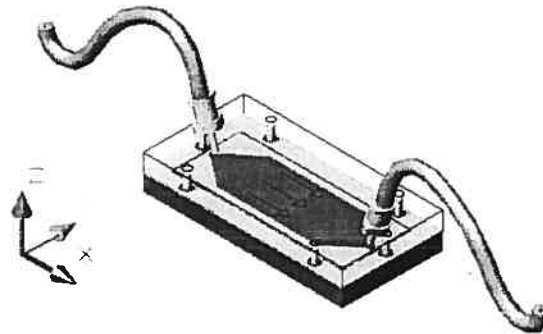
B
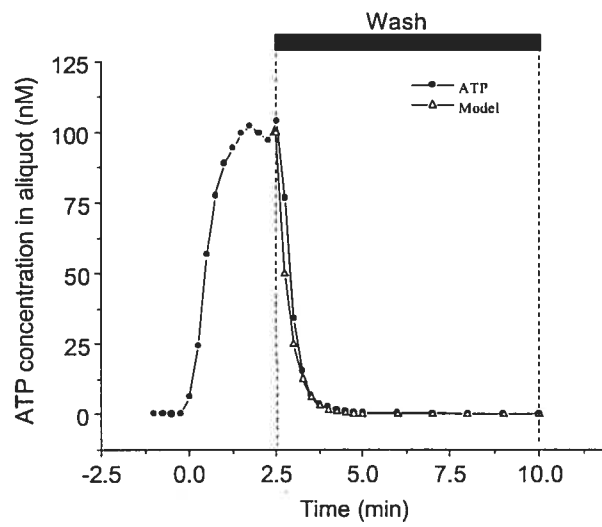
FIGURE 1

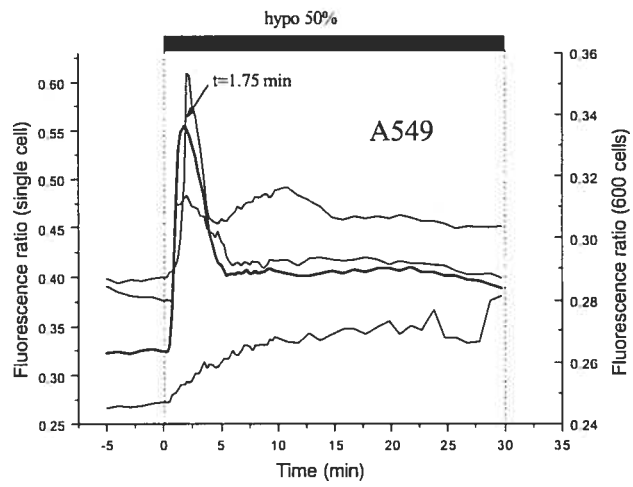**FIGURE 2**

FIGURE 3

FIGURE 4
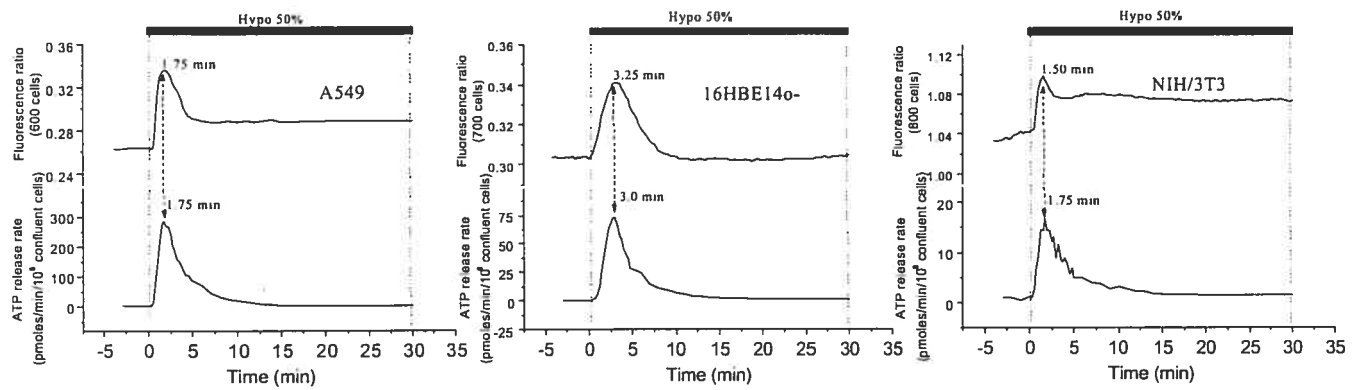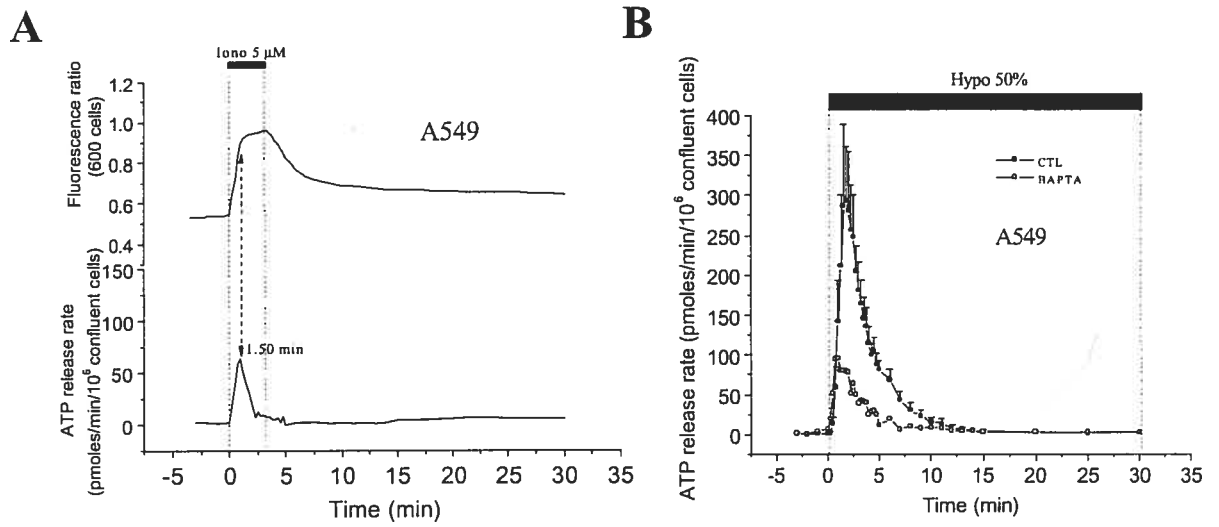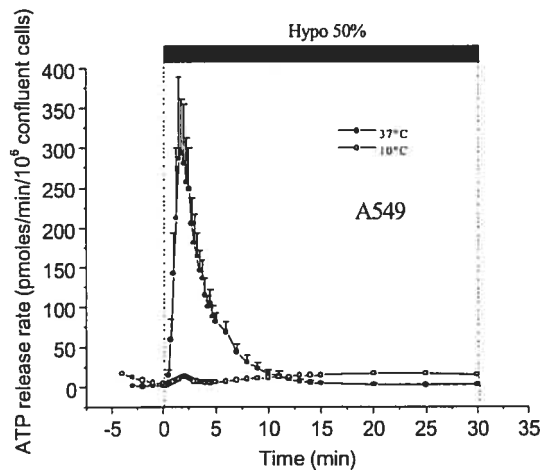

FIGURE 5
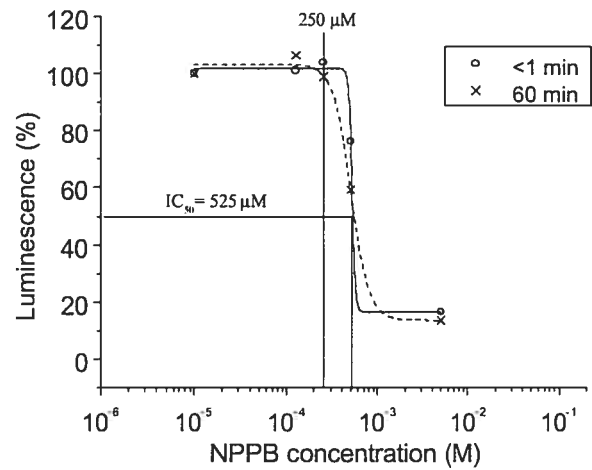
FIGURE 6

FIGURE 7

FIGURE 8

FIGURE 9

FIGURE 10

LEGENDS

Figure 1. Flow chamber for ATP efflux measurements

A: Low-volume flow-through chamber was made of 1 piece of silicone rubber cut-out from a 0.5-mm thick medical grade sheet tightly pressed between two 6-mm thick polycarbonate plates. The 24x60-mm glass coverslip with attached cells was inserted between the silicone gasket and the lower plate. The shape of the flow chamber was designed so that laminar flow is achieved throughout 87% of its surface. The surface covered by cells in this laminar section is ~600 mm². At the perfusion rate of 1.3 mL/min, the maximal theoretical fluid-shear generated in the laminar section was 0.16 Pa (1.6 dyne/cm²).

B: Chamber volume buffering-capacity was determined in a cell-free experiment. 100 nM ATP was perfused at the rate of 1.3 mL/min through the chamber for 2.5 min then washed away. ATP was evaluated in perfusate samples collected during 15-s intervals. It took 1 min 25 s to wash 95% of chamber ATP content (99% was removed after 2 min). With the configuration used in this study, the time required to dilute chamber ATP content in half was 15 s. Based on this time-constant, predicted exponential decay describing the dilution is shown in the figure (triangles), which fits very well the quantity of ATP measured during the wash period (filled circles).

Figure 2. Acute cell swelling induces transient ATP release

ATP secretion from A549, 16HBE14o⁻ and NIH/3T3 cells was markedly enhanced for a short period when fluid tonicity was acutely reduced by 50%. The peak rate of ATP release was many-times above its basal level (see Table 1 for details). It was reached in less than 2 to 3 min, and returned to baseline after 15 min. INSET: ATP secretion from NIH/3T3 cells is shown on an expanded *y*-axis to better visualize the transient nature and similarity of ATP release with the other cell types.

Figure 3. Hypotonic stress- induced volume changes of substrate-adherent cells

A: Examples of single A549, 16HBEo14o⁻ and NIH/3T3 cell volume changes induced by 50% hypotonic shock (representative of 5 independent experiments for each cell type). Volume changes were evaluated as described in METHODS, and are expressed as percentage of the initial volume determined 1 min before the onset of hypotonic shock. Note that cell volume expansion was similar for all 3 cell types, but significant differences were observed in the time-course of volume restoration.

B: General pattern of cell volume changes in response to 50% hypotonic shock, which includes 3 distinct phases: swelling, plateau (invariant volume) and regulatory volume decrease (RVD).

C: The cumulative amount of ATP released during each period described in B was calculated from Figure 2 and expressed as percentages of total ATP released during 15 min post-shock. Note that very little ATP was released during cell swelling.

Figure 4. Cell swelling-induced whole-cell current in A549 cells

A: Representative whole-cell currents recorded every 15 s in response to alternate 100-ms pulses from 0 to ± 40 mV. Hypotonic shock (50%) was applied by diluting the bath medium with distilled water. This resulted in a rise of whole-cell current, which was rapidly blocked by the bath addition of NPPB (arrow).

B: The current-voltage relationship measured at the beginning of the pulses, shown in C, displays typical outward rectification as expected for volume-sensitive current.

C: Current traces in response to 2-s voltage steps from −120 mV to +120 mV in 20 mV increments. The holding potential was 0 mV, and pre-pulse, -120 mV. Note the small inactivation at high depolarizing voltages.

Figure 5. Effects of NPPB on cell volume and ATP release

This figure combines the results from 2 separate experiments. The upper curve (triangles) shows hypotonic stress-induced volume changes of a single A549 cell observed in the presence of NPPB, and after wash of the drug. The trace seen here is representative of 3 experiments. Volume changes are expressed as percentages of the

initial volume (at t = -1 min). The lower curve (open circles) indicates the rate of ATP release from a monolayer of A549 cells in the presence of NPPB and after its wash (representative of 3 experiments). Note that washing away NPPB initiated the volume restoration process, but it was not paralleled by an increase of ATP release.

Figure 6. Effect of NPPB on luciferin-luciferase luminescence

ATP (final concentration 100 nM) was added to a 50% hypotonic cell-free solution containing increasing concentrations of NPPB (10 μM to 5 mM). ATP-dependent luminescence was evaluated immediately, or 1 h later, by luciferase/luciferin-based assay, and is shown as percentages of maximal luminescence. NPPB dose-dependently inhibited luminescence, although the effect was time-independent. No inhibition was apparent below 250 μM NPPB. Data are the means of 3 independent experiments.

Figure 7. Intracellular calcium changes in response to 50% hypotonic challenge

Coverslips with Fura-2-loaded A549 cells were mounted in a modified version of the flow chamber (see METHODS). Fluorescence images were recorded every 15 s during the course of 50% hypotonic challenge. Cytosolic calcium responses are shown from 3 individual cells (fine line) in a field of view (FOV) localized in the centre of the flow chamber. It reveals variability of the response among individual cells, but when the responses were averaged for the entire FOV, a single calcium spike at 1.75 min was observed (bold line). There were approximately 600 cells in the FOV (0.2% of the total number of cells covering the coverslip).

Figure 8. Hypotonic stress-induced ATP release is synchronized with $[Ca^{2+}]_i$ changes

Peak ATP release occurred almost simultaneously with cytosolic Ca^{2+} elevations for all 3 cell lines, and the corresponding peak-times are indicated on the figure. The differences did not exceed temporal resolution of these measurements (~15 s). Graphs showing the ATP release time-course from A549, 16HBE14o⁻ and NIH/3T3 (lower

traces) are reproduced from Figure 2. Changes of $[Ca^{2+}]_i$ (upper traces) were measured in separate experiment, as described in Figure 7, and are representative of 3 experiments for each cell line.

Figure 9. Modulation of ATP release by intracellular calcium

A: In the absence of hypotonic shock, application of 5 μM ionomycin to A549 cells resulted in a robust $[Ca^{2+}]_i$ increase within 1.5 min (upper trace). In a separate experiment, ionomycin triggered transient ATP release (lower trace), which peaked at 1.5 min and vanished in less than 5 min. In this example, the peak rate of ATP secretion reached 53 pmoles/min/10^6 confluent cells, and the total amount of released ATP was 120 pmoles/10^6 confluent cells (representative of 3 independent experiments). Note the similarity in the rise of $[Ca^{2+}]_i$ and ATP secretion.

B: Loading A549 cells with the Ca^{2+} chelator BAPTA diminished hypotonic stress-induced ATP release (open circles). The peak rate of ATP secretion was 85 pmoles/min/10^6 confluent cells, while the cumulative ATP release was 370 pmoles/10^6 confluent cells. The trace showing ATP secretion from untreated cells (CTL, filled circles) is reproduced from Figure 2.

Figure 10. Hypotonic stress-induced ATP release is suppressed at low temperatures

Release of ATP from A549 cells was almost completely abolished at 10°C; the peak rate was 15 pmoles/min/10^6 confluent cells, while cumulative release was 150 pmoles/10^6 confluent cells. Perfusate temperatures was reduced from 37°C to 10°C, 5 min prior to the experiment, and hypotonic stress-induced ATP release was measured as described in METHODS (open circles). The trace showing ATP secretion from control cells (37°C, filled circles) is reproduced from Figure 2.

TABLES

Table 1. Basal, peak and cumulative ATP release from hypotonically-challenged A549, 16HBE14o⁻ and NIH/3T3 confluent cell monolayers

	Cell density at confluency	Basal release	Peak rate	Cumulative ATP released (0-15 min)
	(cells/mm²)	(pmoles/min/10⁶ cells)	(pmoles/min/10⁶ cells)	(pmoles/10⁶ cells)
A549 (n=9)	~ 500	1.77 ± 0.95 (54%)	294 ± 67 (23%)	1,002 ± 154 (15%)
16HBE14o⁻ (n=6)	~ 600	0.87 ± 0.57* (66%)	70 ± 22 (31%)	301 ± 82 (27%)
NIH/3T3 (n=6)	~ 700	0.65 ± 0.75§ (115%)	17 ± 2.8 (16%)	78 ± 20 (25%)

*: n=5; §: n=4

Table 2. Morphological parameters of A549, 16HBE14o⁻ and NIH/3T3 cells before hypotonic shock and when reaching maximal volume expansion

	A549			16HBE14o⁻			NIH/3T3		
	H(μm)	S(μm²)	V(pL)	H(μm)	S(μm²)	V(pL)	H(μm)	S(μm²)	V(pL)
Time 0	13.5	2,914	5.2	9.4	2,793	4.0	9.6	1,316	1.5
	H(μm)	S(μm²)	V(pL)	H(μm)	S(μm²)	V(pL)	H(μm)	S(μm²)	V(pL)
Maximal expansion (t=1 min 30 s or t=1 min 45 s)	16.0	3,249	9.7	12.8	3,015	7.2	11.7	1,471	2.3
	H	S	V	H	S	V	H	S	V
% increase	19	11	86	36	8	78	22	12	53
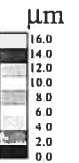
ACKNOWLEDGEMENTS

REFERENCES

Abraham, E. H., Prat, A. G., Gerweck, L., Seneveratne, T., Arceci, R. J., Kramer, R., Guidotti, G., & Cantiello, H. F. (1993). The multidrug resistance (mdr1) gene product functions as an ATP channel. *Proc.Natl.Acad.Sci.U.S.A.* **90**, 312-316.

Bankston, L. A. & Guidotti, G. (1996). Characterization of ATP transport into chromaffin granule ghosts. Synergy of ATP and serotonin accumulation in chromaffin granule ghosts. *J.Biol.Chem.* **271**, 17132-17138.

Bibby, K. J. & McCulloch, C. A. (1994). Regulation of cell volume and [Ca2+]i in attached human fibroblasts responding to anisosmotic buffers. *Am.J.Physiol.* **266**, C1639-C1649.

Birder, L. A., Barrick, S. R., Roppolo, J. R., Kanai, A. J., De Groat, W. C., Kiss, S., & Buffington, C. A. (2003). Feline interstitial cystitis results in mechanical hypersensitivity and altered ATP release from bladder urothelium. *Am.J.Physiol. Renal Physiol.* **285**, F423-F429.

Blaug, S., Rymer, J., Jalickee, S., & Miller, S. S. (2003). P2 purinoceptors regulate calcium-activated chloride and fluid transport in 31EG4 mammary epithelia. *Am.J.Physiol. Cell Physiol.* **284**, C897-C909.

Bodas, E., Aleu, J., Pujol, G., Martin-Satue, M., Marsal, J., & Solsona, C. (2000). ATP crossing the cell plasma membrane generates an ionic current in xenopus oocytes. *J.Biol.Chem.* **275**, 20268-20273.

Bodin, P. & Burnstock, G. (1998). Increased release of ATP from endothelial cells during acute inflammation. *Inflamm.Res.* **47**, 351-354.

Bodin, P. & Burnstock, G. (2001). Evidence that release of adenosine triphosphate from endothelial cells during increased shear stress is vesicular. *J.Cardiovasc.Pharmacol.* **38**, 900-908.

Boudreault, F. & Grygorczyk, R. (2002). Cell swelling-induced ATP release and gadolinium-sensitive channels. *Am.J.Physiol. Cell Physiol.* **282**, C219-C226.

Boudreault, F. & Grygorczyk, R. (2004). Evaluation of rapid volume changes of substrate-adherent cells by conventional microscopy 3D imaging. *J. Microscopy* (in press).

Brown, C. D. & Dudley, A. J. (1996). Chloride channel blockers decrease intracellular pH in cultured renal epithelial LLC-PK1 cells. *Br.J.Pharmacol.* **118**, 443-444.

Burnstock, G. (1987). Local control of blood pressure by purines. *Blood Vessels* **24**, 156-160.

Burnstock, G., Campbell, G., Satchell, D., & Smythe, A. (1970). Evidence that adenosine triphosphate or a related nucleotide is the transmitter substance released by non-adrenergic inhibitory nerves in the gut. *Br.J.Pharmacol.* **40**, 668-688.

Burnstock, G., Dumsday, B., & Smythe, A. (1972). Atropine resistant excitation of the urinary bladder: the possibility of transmission via nerves releasing a purine nucleotide. *Br.J.Pharmacol.* **44**, 451-461.

Chen, Y., Zhao, Y. H., & Wu, R. (2001). Differential regulation of airway mucin gene expression and mucin secretion by extracellular nucleotide triphosphates. *Am.J.Respir.Cell Mol.Biol.* **25**, 409-417.

Communi, D., Paindavoine, P., Place, G. A., Parmentier, M., & Boeynaems, J. M. (1999). Expression of P2Y receptors in cell lines derived from the human lung. *Br.J.Pharmacol.* **127**, 562-568.

Cotrina, M. L., Lin, J. H., Alves-Rodrigues, A., Liu, S., Li, J., Azmi-Ghadimi, H., Kang, J., Naus, C. C., & Nedergaard, M. (1998) Connexins regulate calcium signaling by controlling ATP release. Proc.Natl.Acad.Sci.U.S.A. **95**[26], 15735-15740.

Cozens, A. L., Yezzi, M. J., Kunzelmann, K., Ohrui, T., Chin, L., Eng, K., Finkbeiner, W. E., Widdicombe, J. H., & Gruenert, D. C. (1994). CFTR expression and chloride secretion in polarized immortal human bronchial epithelial cells. *Am.J.Respir.Cell Mol.Biol.* **10**, 38-47.

Darby, M., Kuzmiski, J. B., Panenka, W., Feighan, D., & MacVicar, B. A. (2003). ATP released from astrocytes during swelling activates chloride channels. *J.Neurophysiol.* **89**, 1870-1877.

Erb, L., Liu, J., Ockerhausen, J., Kong, Q., Garrad, R. C., Griffin, K., Neal, C., Krugh, B., Santiago-Perez, L. I., Gonzalez, F. A., Gresham, H. D., Turner, J. T., & Weisman, G. A. (2001). An RGD sequence in the P2Y(2) receptor interacts with alpha(V)beta(3) integrins and is required for G(o)-mediated signal transduction. *J.Cell Biol.* **153**, 491-501.

Evans, R. J., Derkach, V., & Surprenant, A. (1992). ATP mediates fast synaptic transmission in mammalian neurons. *Nature* **357**, 503-505.

Gatof, D., Kilic, G., & Fitz, J. G. (2004). Vesicular exocytosis contributes to volume-sensitive ATP release in biliary cells. *Am.J.Physiol. Gastrointest. Liver Physiol.* **286**, G538-G546.

Glass, R., Loesch, A., Bodin, P., & Burnstock, G. (2002). P2X4 and P2X6 receptors associate with VE-cadherin in human endothelial cells. *Cell Mol.Life Sci.* **59**, 870-881.

Grierson, J. P. & Meldolesi, J. (1995). Shear stress-induced [Ca2+]i transients and oscillations in mouse fibroblasts are mediated by endogenously released ATP. *J.Biol.Chem.* **270**, 4451-4456.

Grygorczyk, R. & Hanrahan, J. W. (1997). CFTR-independent ATP release from epithelial cells triggered by mechanical stimuli. *Am.J.Physiol.* **272**, C1058-C1066.

Hazama, A., Hayashi, S., & Okada, Y. (1998). Cell surface measurements of ATP release from single pancreatic beta cells using a novel biosensor technique. *Pflugers Arch.* **437**, 31-35.

Hazama, A., Shimizu, T., Ando-Akatsuka, Y., Hayashi, S., Tanaka, S., Maeno, E., & Okada, Y. (1999). Swelling-induced, CFTR-independent ATP release from a human epithelial cell line: lack of correlation with volume-sensitive cl(-) channels. *J.Gen.Physiol* **114**, 525-533.

Hisadome, K., Koyama, T., Kimura, C., Droogmans, G., Ito, Y., & Oike, M. (2002). Volume-regulated anion channels serve as an auto/paracrine nucleotide release pathway in aortic endothelial cells. *J.Gen.Physiol.* **119**, 511-520.

Homolya, L., Watt, W. C., Lazarowski, E. R., Koller, B. H., & Boucher, R. C. (1999). Nucleotide-regulated calcium signaling in lung fibroblasts and epithelial cells from normal and P2Y(2) receptor (-/-) mice. *J.Biol.Chem.* **274**, 26454-26460.

Kato, K., Evans, A. M., & Kozlowski, R. Z. (1999). Relaxation of endothelin-1-induced pulmonary arterial constriction by niflumic acid and NPPB: mechanism(s) independent of chloride channel block. *J.Pharmacol.Exp.Ther.* **288**, 1242-1250.

Lazarowski, E. R., Boucher, R. C., & Harden, T. K. (2000). Constitutive release of ATP and evidence for major contribution of ecto-nucleotide pyrophosphatase and

nucleoside diphosphokinase to extracellular nucleotide concentrations. *J.Biol.Chem.* **275**, 31061-31068.

Lazarowski, E. R., Homolya, L., Boucher, R. C., & Harden, T. K. (1997). Direct demonstration of mechanically induced release of cellular UTP and its implication for uridine nucleotide receptor activation. *J.Biol.Chem.* **272**, 24348-24354.

Li, C., Ramjeesingh, M., & Bear, C. E. (1996). Purified cystic fibrosis transmembrane conductance regulator (CFTR) does not function as an ATP channel. *J.Biol.Chem.* **271**, 11623-11626.

Light, D. B., Capes, T. L., Gronau, R. T., & Adler, M. R. (1999). Extracellular ATP stimulates volume decrease in Necturus red blood cells. *Am.J.Physiol.* **277**, C480-C491.

Maroto, R. & Hamill, O. P. (2001). Brefeldin A block of integrin-dependent mechanosensitive atp release from xenopus oocytes reveals a novel mechanism of mechanotransduction. *J.Biol.Chem.* **276**, 23867-23872.

Mitchell, C. H., Carre, D. A., McGlinn, A. M., Stone, R. A., & Civan, M. M. (1998). A release mechanism for stored ATP in ocular ciliary epithelial cells. *Proc.Natl.Acad.Sci.U.S.A.* **95**, 7174-7178.

Morse, D. M., Smullen, J. L., & Davis, C. W. (2001). Differential effects of UTP, ATP, and adenosine on ciliary activity of human nasal epithelial cells. *Am.J.Physiol Cell Physiol.* **280**, C1485-C1497.

Niggel, J., Sigurdson, W., & Sachs, F. (2000). Mechanically induced calcium movements in astrocytes, bovine aortic endothelial cells and C6 glioma cells. *J.Membr.Biol.* **174**, 121-134.

Peterson, W. M., Meggyesy, C., Yu, K., & Miller, S. S. (1997). Extracellular ATP activates calcium signaling, ion, and fluid transport in retinal pigment epithelium. *J.Neurosci.* **17**, 2324-2337.

Prat, A. G., Reisin, I. L., Ausiello, D. A., & Cantiello, H. F. (1996). Cellular ATP release by the cystic fibrosis transmembrane conductance regulator. *Am.J.Physiol.* **270**, C538-C545.

Raat, N. J., De Smet, P., van Driessche, W., Bindels, R. J., & Van Os, C. H. (1996). Measuring volume perturbation of proximal tubular cells in primary culture with three different techniques. *Am.J.Physiol.* **271**, C235-C241.

Reddy, M. M., Quinton, P. M., Haws, C., Wine, J. J., Grygorczyk, R., Tabcharani, J. A., Hanrahan, J. W., Gunderson, K. L., & Kopito, R. R. (1996). Failure of the cystic fibrosis transmembrane conductance regulator to conduct ATP. *Science* **271**, 1876-1879.

Roman, R. M., Feranchak, A. P., Davison, A. K., Schwiebert, E. M., & Fitz, J. G. (1999). Evidence for Gd(3+) inhibition of membrane ATP permeability and purinergic signaling. *Am.J.Physiol.* **277**, G1222-G1230.

Sabirov, R. Z., Dutta, A. K., & Okada, Y. (2001). Volume-dependent atp-conductive large-conductance anion channel as a pathway for swelling-induced atp release. *J.Gen.Physiol.* **118**, 251-266.

Sauer, H., Hescheler, J., & Wartenberg, M. (2000). Mechanical strain-induced Ca(2+) waves are propagated via ATP release and purinergic receptor activation. *Am.J.Physiol. Cell Physiol.* **279**, C295-C307.

Stout, C. E., Costantin, J. L., Naus, C. C., & Charles, A. C. (2002). Intercellular calcium signaling in astrocytes via ATP release through connexin hemichannels. *J.Biol.Chem.* **277**, 10482-10488.

Stutts, M. J., Chinet, T. C., Mason, S. J., Fullton, J. M., Clarke, L. L., & Boucher, R. C. (1992). Regulation of Cl- channels in normal and cystic fibrosis airway epithelial cells by extracellular ATP. *Proc.Natl.Acad.Sci.U.S.A.* **89**, 1621-1625.

Taylor, A. L., Kudlow, B. A., Marrs, K. L., Gruenert, D. C., Guggino, W. B., & Schwiebert, E. M. (1998). Bioluminescence detection of ATP release mechanisms in epithelia. *Am.J.Physiol* **275**, C1391-C1406.

Unsworth, C. D. & Johnson, R. G. (1990). Acetylcholine and ATP are coreleased from the electromotor nerve terminals of *Narcine brasiliensis* by an exocytotic mechanism. *Proc.Natl.Acad.Sci.U.S.A.* **87**, 553-557.

Van der Wijk, T., De Jonge, H. R., & Tilly, B. C. (1999). Osmotic cell swelling-induced ATP release mediates the activation of extracellular signal-regulated protein kinase (Erk)-1/2 but not the activation of osmo-sensitive anion channels. *Biochem.J.* **343 Pt 3**, 579-586.

Warburton, D., Buckley, S., & Cosico, L. (1989). P1 and P2 purinergic receptor signal transduction in rat type II pneumocytes. *J.Appl.Physiol.* **66**, 901-905.

Zhang Y & Hamill OP (2000). On the discrepancy between whole-cell and membrane patch mechanosensitivity in *Xenopus* oocytes. *J Physiol* **523 Pt 1**, 101-115.

CONCLUSION

Ce projet de doctorat a été initialement conçu pour étudier le mécanisme responsable de la sécrétion mécanosensible d'ATP par hypotonicité dans le cadre de la physiologie pulmonaire. Cela explique l'utilisation de 2 lignées cellulaires provenant du poumon et d'une lignée de fibroblastes que l'on retrouve aussi dans cet organe. Cependant les conclusions formulées dans cette thèse ont une portée qui dépasse le cadre pulmonaire et s'applique à un plus vaste ensemble de cellules eucaryotes et c'est dans cet esprit «universaliste» qu'ont été conçu l'ensemble des expériences.

La première série de ces expériences a consisté à tester, puis à rejeter, le modèle de sécrétion d'ATP par hypotonicité basé sur un canal perméable à l'ATP et supposément activé par l'étirement de la membrane plasmique. Dans la seconde série d'expérimentations, il a fallu innover dans le domaine de la mesure du volume cellulaire, en inventant une technique originale de reconstruction 3D à partir d'images obtenues grâce à une chambre de perfusion fabriquée spécialement pour visionner la variation de profil d'une cellule adhérente. Il a fallu également innover dans la dernière série d'expériences, en fabriquant une chambre de perfusion conçu pour améliorer la précision de la mesure de sécrétion d'ATP suite à un choc hypotonique. Ces innovations ont permis de proposer une alternative au modèle dominant, celle d'une sécrétion transitoire d'ATP vésiculaire par un mécanisme exocytotique dépendant étroitement du calcium intracellulaire mais, contrairement à l'opinion couramment admise, indépendant des variations de volume cellulaire. Cependant, l'identité de l'organelle qui a pour rôle de stocker et de libérer l'ATP reste encore à déterminer ainsi que le mécanisme de mécanotransdution qui précède la cascade de signalisation aboutissant à l'élévation de calcium intracellulaire, un prérequis essentiel à la sécrétion d'ATP par hypotonicité.

Il faut ajouter également trois observations originales qui concernent la variation du volume cellulaire: la découverte d'une phase plateau qui précède le RVD; l'observation qu'en réponse à un choc hypotonique de 50%, une cellule voit son volume augmenter de près de 75%, une mesure deux fois supérieure aux estimations antérieures; et finalement, que les canaux chlorure qui participent au RVD demeurent actifs tant que la cellule reste gonflée.

Avant de clore ce texte, il faut élaborer d'avantage sur un corollaire imprévu et intriguant des résultats de cette étude, tel que déjà esquissé à la fin de l'article 3, et qui concerne la nature même de la communication cellulaire par ATP. Il est curieux de constater que tous les éléments que l'on retrouve normalement à la fente synaptique de la jonction neuromusculaire sont regroupés dans le modèle standard de l'ATP comme messager extracellulaire des phénomènes de mécanotransduction. En effet, un récepteur avec une faible affinité apparente pour son ligand (EC_{50} supérieur à 1 µM), une enzyme qui coupe rapidement le signal par hydrolyse du ligand et, par dessus tout, un groupe de vésicules chargées d'ATP et prêtes à sécréter leur contenu suite à une élévation de calcium intracellulaire. Ces caractéristiques sont nécessaires à une signalisation rapide et brève telle que souvent recherchée dans une transmission synaptique. Ceci suggère que si les cellules sont équipées pour recevoir et envoyer des messages par ATP, elles ne le font pas dans le vaste espace extracellulaire qui les entoure mais plutôt dans un petit compartiment intercellulaire.

Est-ce bien surprenant? Peut-être que non. Il est difficilement concevable que la société si bien organisée qui compose l'ensemble des cellules d'un organisme ne sache, hormis le tissu nerveux, que communiquer à distance soit par l'intermédiaire d'hormones ou de cytokines. Bien que cette dernière agisse sur de plus courtes distances que l'hormone, il n'en demeure pas moins que, dans l'état actuel des connaissances, les cellule seraient «sourdes et muettes» envers leur plus proches voisines, un constat bien étonnant.

Pourtant plusieurs situations se présentent où les cellules doivent, à l'évidence, communiquer de très près. Prenons pour exemple la diapédèse par laquelle un leucocyte, en réponse à une molécule chimiotactique, doit tour à tour s'immiscer entre les jonctions serrées des cellules endothéliales, se frayer un chemin à travers les fibroblastes et parfois des cellules épithéliales pour parvenir finalement jusqu'au site d'inflammation. Comment s'adresse-t-elle à celles-ci pour qu'on lui laisse libre passage, pour qu'on lui ouvre les frontières tissulaires à elle et à elle seulement? A l'inverse, une cellule dendritique, en route pour aller présenter son antigène, doit parfois migrer du centre d'un tissu jusqu'à un noeud lymphatique; plusieurs niveaux tissulaires seront franchis durant cette migration. Quel signal utilise-t-elle pour qu'on la reconnaisse et qu'on lui permette ce

que l'on interdit aux autres – hormis les cellules métastatiques - c-à-d de quitter son poste.

Ce signal ce pourrait être l'ATP qui le communique entre cellules assez rapprochées pour permettre une communication efficace, bi-directionnelle et brève par l'entremise de petits compartiments. Et puisque l'on retrouve parfois l'ATP stockée en compagnie d'un autre neurotransmetteur, il ne serait pas étonnant aussi de découvrir que d'autres molécules participent à cette conversation intercellulaire. À l'appui de cette hypothèse, quelques études pionnières ont démontré la capacité des ostéoblastes à sécréter du glutamate par l'entremise de vésicules (Bhangu *et al.*, 2001) et également à exprimer un récepteur NMDA fonctionnel semblable à celui retrouver dans le système nerveux central (Gu *et al.*, 2002). Fait notable, ces mêmes ostéoblates sécrétent de l'ATP et ont des récepteurs purinergiques (Romanello *et al.*, 2001; Hoebertz *et al.*, 2000).

Comment est-il possible que ce mode de signalisation spécifique aux neurones se retrouve-il chez des cellules non-neuronales? Comme toutes les cellules d'un organisme possèdent le même génome, elles ont donc la capacité d'exprimer toutes les protéines de ce génome. Il serait donc permis à des cellules non-neuronales de synthétiser des protéines «neuronales», mais disons, en moindre quantité. À cet effet, on détecte de plus en plus de protéines, jusque là considéré exclusivement «réservées» au tissu nerveux, comme par exemple les protéines synapsines (Worrell *et al.*, 1989), exprimées aussi dans des tissus non-neuronaux. La lenteur de leur mise au jour tient au fait de leur faible expression dans les cellules non-neuronales en comparaison aux neurones lourdement équipés en machinerie de signalisation. Par ailleurs, on est en droit de s'interroger si les neurones ne sont pas simplement des cellules qui se sont spécialisées dans cette fonction de communication synaptique et, qu'en fait, toutes les cellules pourraient converser entre elles par cette méthode. A ce point-ci du raisonnement, il y a plus de spéculation que de solides arguments factuels mais il ne fait aucun doute que c'est une piste de recherche qui mérite d'être explorée comme interprétation alternative des observations reliées à la sécrétion mécanosensible d'ATP.

LES SOURCES DOCUMENTAIRES

Abraham, E. H., Prat, A. G., Gerweck, L., Seneveratne, T., Arceci, R. J., Kramer, R., Guidotti, G., & Cantiello, H. F. (1993). The multidrug resistance (mdr1) gene product functions as an ATP channel. *Proc.Natl.Acad.Sci.U.S.A* **90**, 312-316.

Bhangu, P. S., Genever, P. G., Spencer, G. J., Grewal, T. S., & Skerry, T. M. (2001). Evidence for targeted vesicular glutamate exocytosis in osteoblasts. *Bone* **29**, 16-23.

Birder, L. A., Barrick, S. R., Roppolo, J. R., Kanai, A. J., De Groat, W. C., Kiss, S., & Buffington, C. A. (2003). Feline interstitial cystitis results in mechanical hypersensitivity and altered ATP release from bladder urothelium. *Am.J.Physiol Renal Physiol* **285**, F423-F429.

Blaug, S., Rymer, J., Jalickee, S., & Miller, S. S. (2003). P2 purinoceptors regulate calcium-activated chloride and fluid transport in 31EG4 mammary epithelia. *Am.J.Physiol Cell Physiol* **284**, C897-C909.

Bodas, E., Aleu, J., Pujol, G., Martin-Satue, M., Marsal, J., & Solsona, C. (2000). ATP crossing the cell plasma membrane generates an ionic current in xenopus oocytes. *J.Biol.Chem.* **275**, 20268-20273.

Bodin, P. & Burnstock, G. (1998). Increased release of ATP from endothelial cells during acute inflammation. *Inflamm.Res.* **47**, 351-354.

Bodin, P. & Burnstock, G. (2001). Evidence that release of adenosine triphosphate from endothelial cells during increased shear stress is vesicular. *J.Cardiovasc.Pharmacol.* **38**, 900-908.

Burnstock, G. (1987). Local control of blood pressure by purines. *Blood Vessels* **24**, 156-160.

Burnstock, G., Campbell, G., Satchell, D., & Smythe, A. (1970). Evidence that adenosine triphosphate or a related nucleotide is the transmitter substance released by non-adrenergic inhibitory nerves in the gut. *Br.J.Pharmacol.* **40**, 668-688.

Burnstock, G., Dumsday, B., & Smythe, A. (1972). Atropine resistant excitation of the urinary bladder: the possibility of transmission via nerves releasing a purine nucleotide. *Br.J.Pharmacol.* **44**, 451-461.

Chen, Y., Zhao, Y. H., & Wu, R. (2001). Differential regulation of airway mucin gene expression and mucin secretion by extracellular nucleotide triphosphates. *Am.J.Respir.Cell Mol.Biol.* **25**, 409-417.

Communi, D., Paindavoine, P., Place, G. A., Parmentier, M., & Boeynaems, J. M. (1999). Expression of P2Y receptors in cell lines derived from the human lung. *Br.J.Pharmacol.* **127**, 562-568.

Cotrina, M. L., Lin, J. H., Alves-Rodrigues, A., Liu, S., Li, J., Azmi-Ghadimi, H., Kang, J., Naus, C. C., & Nedergaard, M. (1998). Connexins regulate calcium signaling by controlling ATP release. *Proc.Natl.Acad.Sci.U.S.A* **95**, 15735-15740.

Ferguson, D. R., Kennedy, I. & Burton, T. J. (1997). ATP is released from rabbit urinary bladder epithelial cells by hydrostatic pressure changes - a possible sensory mechanism? *J.Physiol* **505**, 503-511.

Grygorczyk, R. & Hanrahan, J. W. (1997). CFTR-independent ATP release from epithelial cells triggered by mechanical stimuli. *Am.J.Physiol* **272**, C1058-C1066.

Gu, Y., Genever, P. G., Skerry, T. M., & Publicover, S. J. (2002). The NMDA type glutamate receptors expressed by primary rat osteoblasts have the same electrophysiological characteristics as neuronal receptors. *Calcif.Tissue Int.* **70**, 194-203.

Guo, P., Weinstein, A. M., & Weinbaum, S. (2000). A hydrodynamic mechanosensory hypothesis for brush border microvilli. *Am.J.Physiol Renal Physiol* **279**, F698-F712.

Hazama, A., Shimizu, T., Ando-Akatsuka, Y., Hayashi, S., Tanaka, S., Maeno, E., & Okada, Y. (1999). Swelling-induced, CFTR-independent ATP release from a human epithelial cell line: lack of correlation with volume-sensitive cl(-) channels. *J.Gen.Physiol* **114**, 525-533.

Hisadome, K., Koyama, T., Kimura, C., Droogmans, G., Ito, Y., & Oike, M. (2002). Volume-regulated Anion Channels Serve as an Auto/Paracrine Nucleotide Release Pathway in Aortic Endothelial Cells. *J.Gen.Physiol* **119**, 511-520.

Hoebertz, A., Townsend-Nicholson, A., Glass, R., Burnstock, G., & Arnett, T. R. (2000). Expression of P2 receptors in bone and cultured bone cells. *Bone* **27**, 503-510.

Leroy, C., Dagenais, A., Berthiaume, Y., & Brochiero, E. (2004). Molecular identity and function in transepithelial transport of K(ATP) channels in alveolar epithelial cells. *Am.J.Physiol Lung Cell Mol.Physiol* **286**, L1027-L1037.

Li, C., Ramjeesingh, M., & Bear, C. E. (1996). Purified cystic fibrosis transmembrane conductance regulator (CFTR) does not function as an ATP channel. *J.Biol.Chem.* **271**, 11623-11626.

Maroto, R. & Hamill, O. P. (2001). Brefeldin a block of integrin-dependent mechanosensitive atp release from xenopus oocytes reveals a novel mechanism of mechanotransduction. *J.Biol.Chem.* **276**, 23867-23872.

Milner, P., Bodin, P., Loesch, A., & Burnstock, G. (1990). Rapid release of endothelin and ATP from isolated aortic endothelial cells exposed to increased flow. *Biochem.Biophys.Res.Commun.* **170**, 649-656.

Mitchell, C. H., Carre, D. A., McGlinn, A. M., Stone, R. A., & Civan, M. M. (1998). A release mechanism for stored ATP in ocular ciliary epithelial cells. *Proc.Natl.Acad.Sci.U.S.A* **95**, 7174-7178.

Morse, D. M., Smullen, J. L., & Davis, C. W. (2001). Differential effects of UTP, ATP, and adenosine on ciliary activity of human nasal epithelial cells. *Am.J.Physiol Cell Physiol* **280**, C1485-C1497.

Nees, S., Gerbes, A. L., Willershausen-Zonnchen, B., & Gerlach, E. (1979). Purine metabolism in cultured coronary endothelial cells. *Adv.Exp.Med.Biol.* **122B**, 25-30.

Pearson, J. D., Slakey, L. L., & Gordon, J. L. (1983). Stimulation of prostaglandin production through purinoceptors on cultured porcine endothelial cells. *Biochem.J.* **214**, 273-276.

Prat, A. G., Reisin, I. L., Ausiello, D. A., & Cantiello, H. F. (1996). Cellular ATP release by the cystic fibrosis transmembrane conductance regulator. *Am.J.Physiol* **270**, C538-C545.

Romanello, M., Pani, B., Bicego, M., & D'Andrea, P. (2001). Mechanically induced ATP release from human osteoblastic cells. *Biochem.Biophys.Res.Commun.* **289**, 1275-1281.

Sabirov, R. Z., Dutta, A. K., & Okada, Y. (2001). Volume-dependent atp-conductive large-conductance anion channel as a pathway for swelling-induced atp release. *J.Gen.Physiol* **118** , 251-266.

Sauer, H., Hescheler, J., & Wartenberg, M. (2000). Mechanical strain-induced Ca(2+) waves are propagated via ATP release and purinergic receptor activation. *Am.J.Physiol Cell Physiol* **279**, C295-C307.

Stout, C. E., Costantin, J. L., Naus, C. C., & Charles, A. C. (2002). Intercellular calcium signaling in astrocytes via ATP release through connexin hemichannels. *J.Biol.Chem.* **277**, 10482-10488.

Stutts, M. J., Chinet, T. C., Mason, S. J., Fullton, J. M., Clarke, L. L., & Boucher, R. C. (1992). Regulation of Cl- channels in normal and cystic fibrosis airway epithelial cells by extracellular ATP. *Proc.Natl.Acad.Sci.U.S.A* **89**, 1621-1625.

Taylor, A. L., Kudlow, B. A., Marrs, K. L., Gruenert, D. C., Guggino, W. B., & Schwiebert, E. M. (1998). Bioluminescence detection of ATP release mechanisms in epithelia. *Am.J.Physiol* **275**, C1391-C1406.

Unsworth, C. D. & Johnson, R. G. (1990). Acetylcholine and ATP are coreleased from the electromotor nerve terminals of Narcine brasiliensis by an exocytotic mechanism. *Proc.Natl.Acad.Sci.U.S.A* **87**, 553-557.

Van der Wijk, T., De Jonge, H. R., & Tilly, B. C. (1999). Osmotic cell swelling-induced ATP release mediates the activation of extracellular signal-regulated protein kinase (Erk)-1/2 but not the activation of osmo-sensitive anion channels. *Biochem.J.* **343 Pt 3**, 579-586.

Worrell, R. T., Butt, A. G., Cliff, W. H., & Frizzell, R. A. (1989). A volume-sensitive chloride conductance in human colonic cell line T84. *Am.J.Physiol* **256**, C1111-C1119.